PRELIMINARY INVESTIGATION INTO ELECTRON BEAM LENSING UTILIZING BEVELED CERROBEND GEOMETRIES

By

Harrison D. Ludewig

A THESIS

Presented to the Department of Medical Physics
and the Oregon Health & Science University
School of Medicine
in partial fulfillment of
the requirements for the degree of

Master of Science

June 2019

School of Medicine

Oregon Health & Science University

CERTIFICATE OF APPROVAL

This is to certify that the Master's thesis of

HARRISON DREW LUDEWIG

Has been approved

_____
Mentor/Advisor

_____
Member

_____
Member

_____
Member

Table of Contents

List of Tables and Figures

Tables

Figures

Acknowledgements

I would like to express my sincerest gratitude to the faculty and staff here at Oregon Health & Science University. This work could not have been completed without the knowledge and expertise of the people whom I have grown to know here. In particular, I would like to thank Dr. Ross Brody, Dr. Lindsey DeWeese, Kyle Gallagher, Dr. Thomas Griglock, Dr. Krystina Tack, Dr. Malcolm Heard, Dr. James Tanyi, Dr. Shannon Voss, and all those who have helped form my knowledge on the application of ionizing radiation to medicine.

My advisor, Dr. Richard Crilly, has earned my deepest respect and appreciation. It has been a pleasure learning from a man with such deep knowledge and experience in this field. The breadth of his knowledge is only surpassed by his superb sense of humor. It was his intuition into the nature of electron beams which lead to the investigation presented here.

Finally, I would like to thank my friends and family for always being supportive and caring.

Abstract

Purpose: To investigate the feasibility of beveling the edges of small Cerrobend electron beam cutouts to provide clinically preferable dose distributions for small-size superficial lesions. This technique may be further developed in the future to create a device applicable for clinical use.

Methods: The ability for Cerrobend to be melted and poured allows for the creation of cut outs with any arbitrary geometry. Utilizing the Ultimaker 2 3D-printer and ABS red material, the molds for the linear beveling angles of 0, 5, 10, 12.5, 15, 17.5, 20, 22.5, 25, and 30 degrees were investigated for 2 cm diameter circular electron fields. These molds were used to generate 6 cm by 6 cm Cerrobend cutouts. An Elekta Versa HD was used to investigate the dose distributions of 6 and 8 megaelectronvolts (MeV) electron beams. The dose was recorded on Gafchromic™ EBT3 film in a Nomos™ solid water phantom. Calibration films were shot along with known electron dose distributions to confirm the conversion of film intensity to absorbed dose in tissue was correct.

Results: The dose distributions from the various Cerrobend geometries and electron beam energies were recorded and analyzed for clinical advantages. The dose distributions were normalized to their peak doses. The area of 90% of the max dose was investigated for use as the treatment region of the field for superficial lesions with diameters of 2 cm or less. Calculations for dose prescriptions along with treatment field dimensions with depth are given for the various cut outs.

Conclusions: All beveling angles displayed an increase in the maximum dose in the field when compared to the standard 0 degree, straight-neck, cut out used currently for small field electron beams. The large angle beveled edges lead to a decrease in the clinically useful portion of the field. This result is nonoptimal for clinical implementation. This study acts as a proof of concept. Future work may be done to generate preferable Cerrobend geometries. This study shows that future work should focus on narrow Cerrobend neck geometries.

1. Introduction

Every year, in the United States of America, more people are diagnosed with skin cancer than the combined number of all other cancers [1]. There are many treatment options for these patients, with one of them being electron beam radiation therapy [2]. Should large field electron beams be used as a treatment for these diseases, large areas of healthy tissue adjacent to the target would receive doses equivalent to the treatment doses. Small size electron beams are characteristically difficult to predict, and individual calibrations must be performed to adequately characterize the dose distribution in tissue [2,3,4]. Generating a device which shields the normal tissue and more evenly distributes dose into treatment region would be preferable to either the small or large field electron beam therapy options available today.

This thesis provides data from a preliminary investigation into the use of beveled Cerrobend cut out holes to generate more conformal small sized electron fields. The goal of a continuation of this research would be to generate a 3D-printed mold which would be filled with Cerrobend and placed on the patient's skin during treatment. These devices are termed electron beam lenses, as they focus the electron fluence of the electron beam into the treatment region. This is accomplished with electron scatter off the upper portion of the Cerrobend cut out which is beveled or flared outward. Like a magnifying glass and light, the electrons are focused into the desired region.

The beveling geometries investigated were linear angles off of the typical straight-necked Cerrobend cut out. The final device shape will most likely be a

continuous function. The angles investigated in this study were used to illuminate whether a large or small mouthed Cerrobend cut out would be preferable for the final device. This paper is written with the intent to inform future investigations into this behavior, as this experiment acts as a feasibility study into the phenomenon. The technique described in this paper requires further investigation before clinical application.

This thesis will describe the comparative results between typical straight-hole Cerrobend cut outs to various linear beveling angles for 6 megaelectronvolt (MeV) and 8 MeV electron beams. The necessity for device immobilization and the reproducibility of the fields is also briefly investigated. Methods of dose calculations and field coverages are briefly discussed. Confounding factors are discussed along with possible directions for future studies.

2. Background

2.1 Relativistic Electron Energy Transfer

Electrons are subatomic elementary particles with a rest mass much less than the mass of an atom and an electric charge equal to that of a proton. These particles may be accelerated up to relativistic speeds using a modern linear accelerator (LINAC). The potential for treatment utilizing electron beams has been well demonstrated [2,3,4]. Electron beams offer certain clinical advantages over other forms of radiotherapy. This includes high superficial dose deposition and rapid dose fall-off.

Electrons follow ‘tortured paths’ while traversing through material. This means that the path the electron travels is longer than the distance it is displaced from its source. Relativistic electrons continuously transfer energy from themselves to their environment, approximately 2 MeV/cm in water equivalent materials [3]. Two main processes are responsible for electron energy loss: collisional and radiative losses. The prevalence of either type of energy loss is dependent on the energy of the electron and the material it is traversing.

Collisional energy transfers occur when the passing electron interacts with an electron bound to a nucleus. The result from this energy transfer leads to either excitation or ionization of the bound electron. The electric force is dominant over the magnetic force for this interaction. This is due to the electric force falling off inversely with the square of distance and the magnetic force falling off with the cube of distance. When excitation occurs, an electron bound to the atom is raised to a higher energy state while remaining bound to the atom. Only a few eV are transferred from the electron to the atom. The excited electron will deexcite and release a characteristic photon which is typically dissipated into the environment as heat [3,4].

Should the impinging electron approach closer to the atom, within the atomic orbitals, it may experience a knock-on collision with a bound electron. In this case the bound electron becomes freed by the interaction; the atom becomes ionized. This secondary electron may have sufficient energy to cause further ionizations and excitations. These interactions can typically be treated as free

electron collisions, as the binding energy is negligible when compared to the energy transferred from the impinging electron to the secondary electron [3].

Radiative losses occur when the impinging electron passes within the atomic radius. The nuclear coulombic field will interact with the electron and deflect the primary electron's trajectory. The atom will also experience a recoil; however, this is very slight due to the vastly different mass of an atom and a single electron. The loss of energy from the electron will be emitted as a bremsstrahlung photon. Bremsstrahlung production is more common in high atomic number materials. The angular distribution of the bremsstrahlung photons is dependent on the energy of the impinging electron. Lower energy electrons, with kinetic energies much lower than the rest mass of an electron, experience the maximum intensity of bremsstrahlung in the perpendicular direction to the path of the incident electron. As electron energy increases, the angle of bremsstrahlung becomes increasingly directed forward [3]. Relativistic electrons will also experience energy loss due to Cerenkov emissions, should the electron velocity exceed the speed of light in the medium in which it travels. This effect is negligible for the electron beam energies of 6 MeV and 8 MeV investigated in this report. [4].

2.2 Electron Dose Deposition

Electron beams experience a buildup region from the surface of the material to the depth of maximum dose. This is due to a balance between two effects as the electrons penetrate deeper into the material. The smaller of the two effects is the buildup of secondary electrons due to knock-on collisions. As the impinging

electron travels through the material, it will generate a series of ionizations which continue on to produce their own ionizations. Thus, the number of electrons impinging on areas perpendicular to the beam direction increases as one moves from the surface of the material to the depth of maximum dose [3].

The effect most responsible for dose build up region is the increased obliquity of the electrons as they penetrate materials. Electrons entering perpendicular to a surface will undergo scattering interactions which lead their paths to diverge from their initial trajectory. Higher atomic number materials lead to a higher typical scattering angle. Higher kinetic energy electrons undergo lower scattering angles than lower energy electrons. The depth of maximum dose occurs at the point in which the knock-on build-up of electrons balances with the increasing obliquity of the electron paths. The increased obliquity of electron paths is also responsible for the increasing radius of dose deposited with depth [3,4].

The practical range of an electron beam is the average penetration depth of the most probable energy in an electron beam. The most probable energy of an electron beam is the most common energy for the electrons to have when leaving the gantry head. This differs slightly from the average energy of the electron beam. The electron beam percentage depth-dose (PDD) curve displays a Bremsstrahlung tail at depths beyond the practical range of the electrons. This is due to bremsstrahlung photons generated by radiative losses of energy. This bremsstrahlung tail remains fairly constant and depends on the energies of the photons generated. The bremsstrahlung tail for 6 MeV to 12 MeV electron beams

is typically 0.5% to 1% of the maximum dose respectively. Higher energy electron beam energies correspond with higher bremsstrahlung tail intensity [6].

2.3 Dose Prescription and Lateral Scatter Equilibrium

Due to the low penetration depth of electron beams when compared to photon beams, electron beams are preferable in the treatment of superficial lesions. Electron beams are typically prescribed to the 90% dose line. This allows for rapid dose fall-off outside of the treatment region and a relatively homogenous dose distribution inside of the treatment region. Energies and field sizes are determined with this consideration in mind when prescribing dose.

In the case of broad electron field sizes, in which the radius of a circular field exceeds the practical range of the electron beam, any electron which is scattered latterly is replaced by another electron scattered laterally from an adjacent region. This process of having laterally scattered electrons be replaced with laterally scattered electrons is called lateral scatter equilibrium (LSE). This leads to a constant PDD curve for the center of the field and all areas of the field in which LSE exists. In other words, increasing the field size beyond this point will not lead to an increase in the PDD curve along the central axis of the field. Electrons scattered laterally at the edges of the field are not replaced. This leads to a dose fall off in the region between the field edge and the practical range of electrons within the field.

Should the electron field size be less than the required radius for LSE along the central axis, the beam is considered a small or narrow field electron beam.

Small electron fields exhibit less predictability and lower max doses than large fields for the same energies. Small field electron cut outs should be individually measured for output factors, useful field size, and PDD curves, as small electron fields behave far less predictably than broad electron fields. Small field size electron beams exhibit more rapid dose build-up and more rapid dose fall off than broad electron fields [3,4,5].

2.4 Cerrobend Utilization in Electron Beam Shaping

Cerrobend, also known as Lipowitz metal, Woods metal, and Ostolloy 158, is a eutectic alloy comprised of 50% bismuth, 27% lead, 13% cadmium, and 10% tin by weight. The defining property of this material is its low melting point at 70 degrees Celsius. Cerrobend also has a high effective atomic number due to the prevalence of bismuth, with 83 protons per atom, and Lead, with 82 protons per atom. This makes it ideal for shielding electrons and the high energy Bremsstrahlung photons given off by inelastic radiative energy losses. A thickness of 2.8 mm and 4.7 mm of Cerrobend is sufficient to shield 95% of a 6MeV and 9 MeV electron beams respectively [6]. This was considered in the design of the beveled Cerrobend cut outs. A straight neck of 5 mm of Cerrobend was determined to be appropriate to avoid unwanted bremsstrahlung from entering the patient.

2.5 Skin Anatomy and Response to Irradiation

The most superficial layer of the human skin is the stratum corneum. This is a dead skin layer which continuously desquamates from the skin surface. Inferior

to this layer is the epidermis, which contains keratinizing epithelial cells, Langerhans, and Merkle cells. The Merkel cells are responsible for transmitting sensory information such as temperature, pressure, and texture from the skin to the nervous system. The Langerhans cells are immune cells located in the epidermis. The keratinizing epithelial cells work their way to the surface at which point they become the part of the stratum corneum. These layers typically range from 30 to 300 micrometers in depth. The keratinizing epithelial cells originate from the stem cells just inferior of the epidermis in the basal layer. The basal layer is a single cell thick. These cells have infinite proliferation potential; allowing for the healing of damage to the higher layers. It typically takes an epidermal cell approximately 14 days from generation in the basal layer to be sloughed off from the body [5].

Inferior to the basal layer lies the dermis. This is a 1-3mm thick layer of connective tissue. The dermis contains the vasculature of the skin. The epidermis relies on nutrients to be passed up through the epidermis. This causes the upper layers to die due to lack of nutrients. The basal layer also contains the lymphatic system of the skin, hair follicles, and the sensory neurons connected to the Merkle cells. Inferior to the dermis lies the hypodermis which primarily consists of adipose tissue and blood vessels [5].

Following irradiation, the skin displays both early and late responses dependent on which layers of skin underwent damage and the extent of the damage. Within hours of the irradiation the skin may present with localized erythema, or dermatitis. The radiation results in an inflammatory response similar

to the one presented during sunburns. More severe responses during the acute stage of the response to irradiation typically present after a latency period of 10 days and results from damage to the dermis. Sterilization of the basal layer will cause the skin in an area to come off without being replaced. This is worsened still by the destruction of vasculature in the dermis. Should the damage not be too severe, the area will present with dry desquamation of cells. Late responses typically manifest months after the irradiation and are resultant from damage to the vasculature in the dermis. The late response to radiation is the dose limiting reaction for the skin. Moist desquamation, the sloughing off of significantly large moist areas of skin, can occur of acute doses in excess of 30 Gy. These can leave large ulcerations on the patient, which could result in infection. The human skin can tolerate doses of 60 Gy when fractionated over 6 to 8 weeks [5]. These gaps allow for adequate stem cell proliferation to occur between irradiations. In the cases of superficial radiation damage, both early and late reactions will present themselves. In the case of deeper penetrating ionizing radiation, it is possible for only late effects to present themselves. Telangiectasia can occur over a year post irradiation without any of the other reactions being present. Telangiectasia is evidence of damage to the vasculature in dermis or hypodermis [5,7].

2.6 Small Size Superficial Tumors

There exists a number of cancers that present with superficial primary or metastatic tumors. The most common of these is basal cell carcinoma. This cancer typically presents in the basal layer at a depth between 0.03 cm and 0.3 cm below

the surface. Exposure to ultraviolet light from the sun is the primary risk factor for the development of basal cell carcinoma. The most prominent regions of occurrence, 80% of documented cases, are on the head and neck. Tumor diameters of greater than 2cm present a substantive risk factor for metastatic spread of the disease; however, metastatic spread is rare, only occurring in 0.0028% to 0.55% of cases [8].

Squamous cell carcinoma is the second most prevalent form of skin cancer and presents with tumors in the epithelial layer of the skin. More than 250,000 new cases of squamous cell carcinoma are diagnosed in the United States every year. This disease, like cutaneous basal cell carcinoma, is believed to primarily be caused by exposure to ultraviolet light from the sun. Unlike basal cell carcinoma, squamous cell carcinoma presents a significant risk of metastasizing. The most common areas of occurrence for invasive squamous cell carcinoma are the head and neck, followed by the trunk. Risk factors which increase the likelihood of recurrence or metastasis include tumor sizes of greater than 2 cm diameter, tumor depths deeper than 4 mm (reticular dermis and or subcutaneous fat involvement), poorly differentiated appearance, previous presentations of squamous cell carcinoma, and perineural invasion (neoplastic invasion of nerves as a means of metastatic spread). Surgical evaluation of the disease is recommended for presentations with these risk factors [9].

The third most common and singular most deadly skin cancer in the United States is malignant melanoma, responsible for 6 out of every 7 skin cancer deaths and 4% of all cancer deaths. Like all of the skin cancers mentioned thus far,

populations with blond or red hair and fair skin are at an increased risk of the disease. Exposure to ultraviolet radiation is believed to be the primary risk factor for the development of this disease. Malignant melanoma exhibits a much higher likelihood of metastasizing than basal cell carcinoma [10].

Mycosis Fungoides is the most common form of cutaneous T-Cell lymphoma and presents with superficial skin lesions such as flat patches, thin plaques, or tumors. This disease is still fairly uncommon with an incidence rate of approximately 0.36 per 100,000 person-year. The cancerous T-cells are typically behaving in a manner that healthy T-cells do. They become activated, persist in this activated state and achieve clonal dominance. These colonies typically form on the skin of the patient; however, this can occur in the lymphatic tissue or peripheral blood. The skin plaques of mycosis fungoides typically appear in regions of low sun exposure. The tumors typically display a phase of exaggerated vertical growth. This can lead to ulceration of the region due to protruding nature of the plaque. The cancerous T-cells will form colonies around the Langerhans cells in the epidermis, and, once large enough present as a superficial lesion [11].

All of these cancers present in ways which could be treated with a small field electron beam. Metastatic spread is more likely for both basal and squamous cell carcinomas after the skin lesion exceeds 2 cm diameter. Should this be the case surgical resection, or Mohs' Surgery, and biopsy is the best course of action. It allows for the specific characterization of the cancer, and these techniques can be used to evaluate metastatic spread of the disease. Biopsies of known plaques should be performed to better characterize the subclassification of the disease.

2.7 Specific Aim of Research

This research is a feasibility study into utilizing Cerrobend cut outs with beveled top edges to create more conformal treatment regions for small size superficial lesions. Traditional electron beam treatments require a field size large enough for lateral scatter equilibrium to occur. Should sufficient electrons be scattered off the edges of the cutout into the treatment region, this would provide a sufficient dose increment such that a large field with lateral scatter equilibrium would not be necessary. This would provide significant dose sparring of the surrounding tissue, while maintaining a conformal dose to the target.

3. Materials and Methods

3.1 Generation of the Film and Solid Water Phantom

Gafchromic Film™ EBT3 was utilized for this experiment as it yields high fidelity images. This is preferable for small electron fields, as the dose may experience sharp increases or decreases over very small distances. Another advantage of film is the ability to take a cross section of any field, given the field size does not exceed the margins of the film, in a single exposure. Film also has attractive relative dosimetry features, as optical densities may be compared to determine relatively higher or lower dose regions. These features make film the ideal measurement tool for characterizing the fields relative to the typical straight-hole geometry used for small field electron beams.

There exist several draw backs with the use of film. Film may not exceed a certain temperature, or it may display artifacts. Film is particularly sensitive to physical damage such as bending, scratching, or delamination along cut edges. Any physical damage done to film will cause artifacts to appear in the images. Gloves must be worn when handling film to avoid the oils present on human skin from damaging the film. When scanning film, the orientation of the film must be maintained. Scanning the film face up as opposed to face down will cause significant differences in the resultant dose distributions. Film must also be kept away from exposure to direct sunlight or ionizing radiation. Finally, film must be left to mature over a period of hours before it may be scanned. Film continues to darken over a period following the irradiation, and this process must be complete before the film may be scanned.

The utilization of Solid Water and Film allow for dose values measured on film to be directly representative of dose in tissue with only a minor correction for Solid Water to tissue electron densities [3]. This experiment utilized Nomos™ Virtual Water blocks with thicknesses of 6 cm, 5 cm, 4 cm, 3 cm, 2 cm, 1 cm, 0.3 cm and other dimensions of 30 cm by 30 cm. Exheed® Ultra Clear Heavy Duty Plus Packaging Tape and Pro-Grade® clamps were used to hold the solid water together for the vertical scans. The blocks were stacked vertically for the calibration scans.

Two solid water phantoms of 30 x 30 x 9 cm^3 were created using packaging tape and clamps. The 5 cm thick slab was tabbed to the 4 cm thick slab to generate one of the halves. The 6 cm, 2 cm, and 1cm thick slabs were taped together to

form the second half. The thickness of this phantom ensured sufficient surrounding material around the film for accurate backscatter. The thickest slabs were placed on the inside, to provide the most homogenous medium on either side of the film. The film was placed between the two solid water phantoms, and the entire phantom was clamped together. The film was taped in place with its top edge aligned with the top edge of the solid water. The tape was placed flat against the film and solid water. No wrinkles may exist in the tape, as this would cause airgaps in the phantom and yield incorrect dose readings on the film. Care was taken to ensure the film did not peak above the top of the solid water, and no scratching of the film occurred during the clamping together and taking apart of the phantom.

The orientation of film is of great relevance, as different orientations when scanning will lead to different results. When the tab of the sleeve is opened, the face of the film facing up is considered the front for the purposes of this paper. Once the film was removed from the sleeve, a permanent marker was used to mark the bottom right corner, see figure 1. All vertical scans were shot through the top of the film. The film was cut into approximately 5 cm by 5 cm squares for the cut out exposures. A piece of film with approximate dimensions 15 cm by 7 cm was used for an open 10x10 cm^2 field to compare to the calibration scans. The lower portions of the film were cut up into approximately 4 cm by 4 cm to be used for calibration scans. All pieces of film had a permanent marker dot placed on their front face to maintain orientation. The cut pieces of film were placed into labeled envelops for protection and consistency.

The film was placed in the center of the two 9 x 30 x 30 cm^3 pieces of solid water and clamped into one for the vertical scans. The film was place parallel to the electron beam, and the phantom was centered in the field. This provides complete dosimetric data about the beam, assuming rotational symmetry of the dose distribution. Calibration films were placed on a horizontally positioned 9 x 30 x 30 cm^3 phantom, and the 1 cm and 0.3 cm thick solid water phantoms were placed on top of the film for adequate build-up for the 6 MeV electron beam.

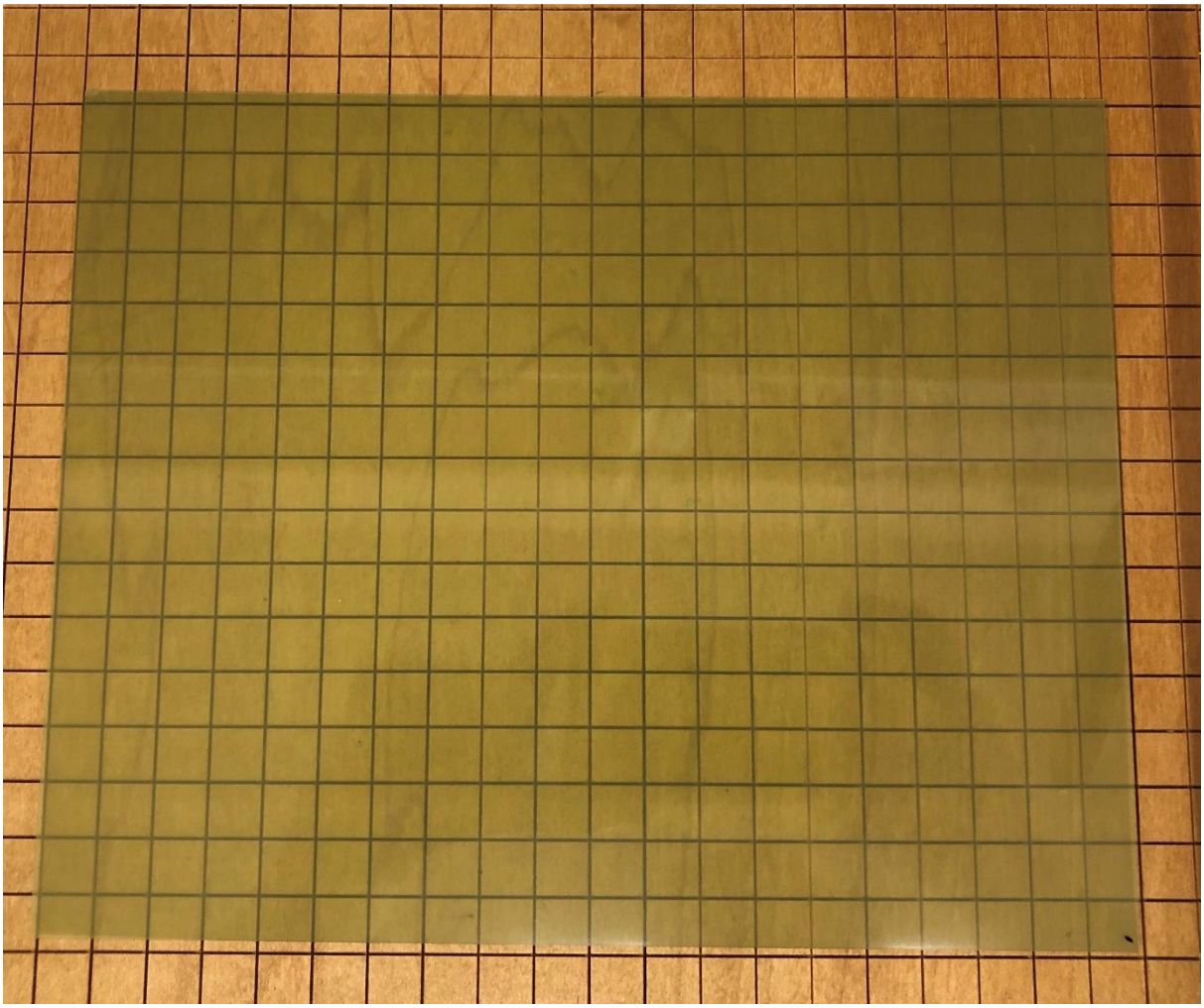

Figure 1. The film orientation as it is when first removed from the sleeve

3.2 Ultimaker2 and ABS Red

Utilizing 3D design software, AUTODEK® TINKERCAD™, ten molds were made to be used to generate the Cerrobend cut outs and printed using ABS Red material using an Ultimaker2 3D printer. These ABS molds were then placed in a Aktina Medical Corporation 6 cm by 6 cm Cerrobend mold, and Cerrobend was poured into each to generate the Cerrobend cut outs. According to the manufacturing specifications, ABS Red plastic has a melting point of 265 degrees Celsius. This is adequate for use as molds in the 96 degree Celsius Cerrobend. Figure 2 displays the 3D printer and material used to generate these molds.

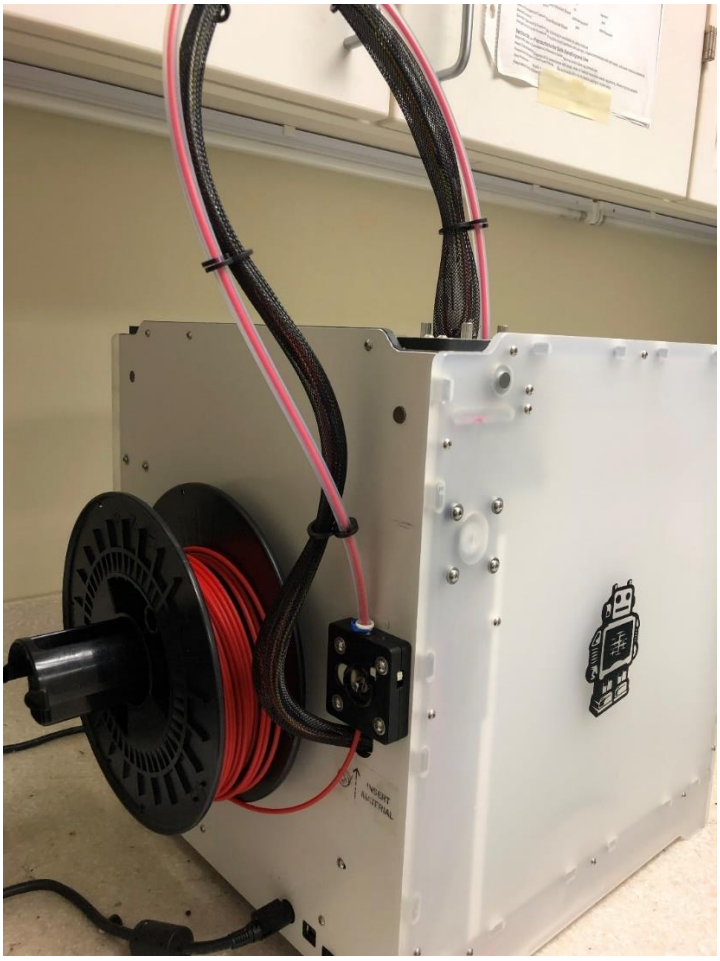

Figure 2. The ABS Red plastic being fed into the Ultimaker2 3D printer

Cerrobend is kept on site in a heating vat at 96 degrees Celsius. This ensures all of the Cerrobend in the vat is in liquid form and solid blocks added to the vat will quickly melt. It is poured from a spicket and transferred to the appropriate mold. The Cerrobend was then let to sit for at least an hour to cool before being removed from the mold. The resultant cut outs were labeled based of off their beveling angles.

Cylinders with a diameter of 2 cm and 2 cm height were generated first in the design software. The first cylinder was untouched and acts as the 0-degree or traditional straight-neck test. The remaining cylinders had cones inserted to form beveled angles into the hole. A 5 mm neck was used to prevent the Cerrobend from being too thin to adequately shield the electron beam in the portion adjacent to the treatment area. Without this 5 mm neck, the thin areas of Cerrobend would cause large amounts of bremsstrahlung photons to enter the patient. This would cause radiation to penetrate deep into the patient and negate the superficial advantages which electron beams display. Generation of the neck was accomplished by adding the cone shape in the center of the existing cylinder. The height of the cone was set to be 1.5 cm, the top diameter was set to 2 cm to match with the cylinder and the bottom diameter was set to larger values corresponding to the desired beveling angles. The beveling angles are measured off of the vertical axis of the outside of the cylinder. An infill of 20% may be used to save on material. The resulting molds can be seen in figure 3 arranged from lowest to highest beveling angles.

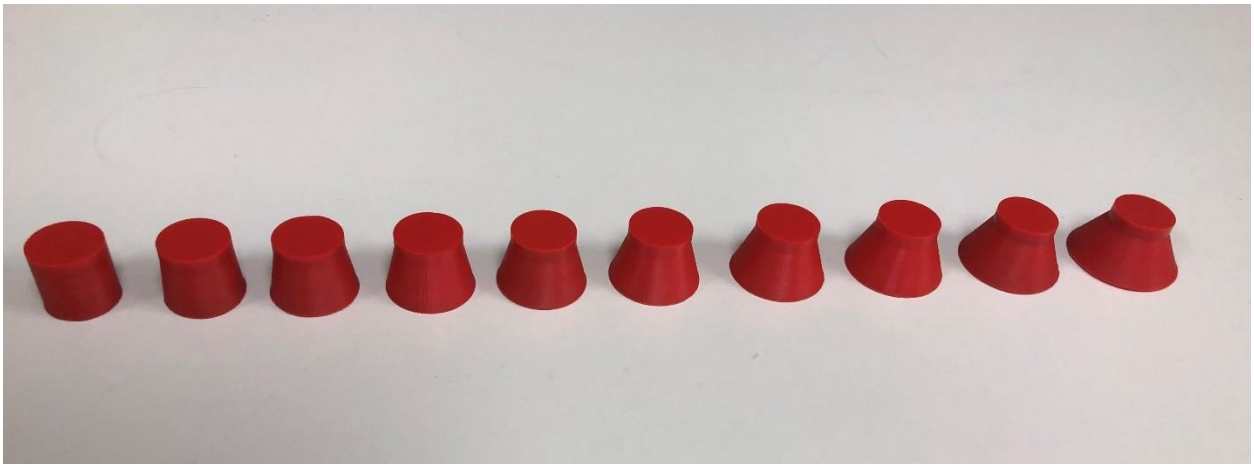

Figure 3. The 0, 5, 10, 12.5, 15, 17.5, 20, 22.5, 25, and 30 degree molds generated in TINKERCAD® and Printed on the Ultimaker2 3D-printer in ABS Red plastic

3.3 Calibration

The Elekta Versa HD located in Vault 1 at Oregon Health and Science University was used to generate the electron beams used in this study. The calibration films were shot with 6 MeV electron beams with an open 10 cm by 10 cm square field at 100 cm source to surface distance (SSD). The depth of maximum dose of 6 MeV electrons for a field size of 10 x 10 cm^2 in water equivalent material is 1.3 cm of depth. This depth was used for the calibration exposures. A 9 x 30 x 30 cm^3 block of solid water was placed under the film to provide adequate material for backscatter. The film was placed face-up in the center of the phantom and the 1 cm and 0.3 cm thick solid water slabs were placed on top of the film. The entire phantom was centered in the electron film, and the couch was raised to give a source to surface distance of 100 cm. The calibration films were exposed to fields of 100, 200, 300, 400, 500, 600, 700, and 800 Monitor Units (MU) for the 6 MeV study. This corresponds to absorbed doses to film of 1000, 2000, 3000, 4000,

5000, 6000, 7000, and 8000 mGy, as the electron beams are calibrated to deliver 10 mGy per 1 MU at the depth of maximum dose at 100 cm SSD. The 8 MeV study and the reproducibility and obliquity study had an additional 50 MU calibration sheet for better characterization of lower doses. The experimental set up utilized in the calibration shots may be seen in figure 4. A 10 x 10 cm^2 open field was shot vertically using 6 MeV electron beam for 600 MU at an SSD of 100 cm for the 6 MeV study and reproducibility & obliquity study to ensure correct calibration of the film was achieved. A 10 x 10 cm^2 open field of 8 MeV and 600 Mu at 100cm SSD for the 8 MeV study was exposed vertically to confirm proper calibration. Renormalization to the open field was performed for the 8 MeV study and reproducibility & obliquity study. The renormalization process is discussed in section 3.6.

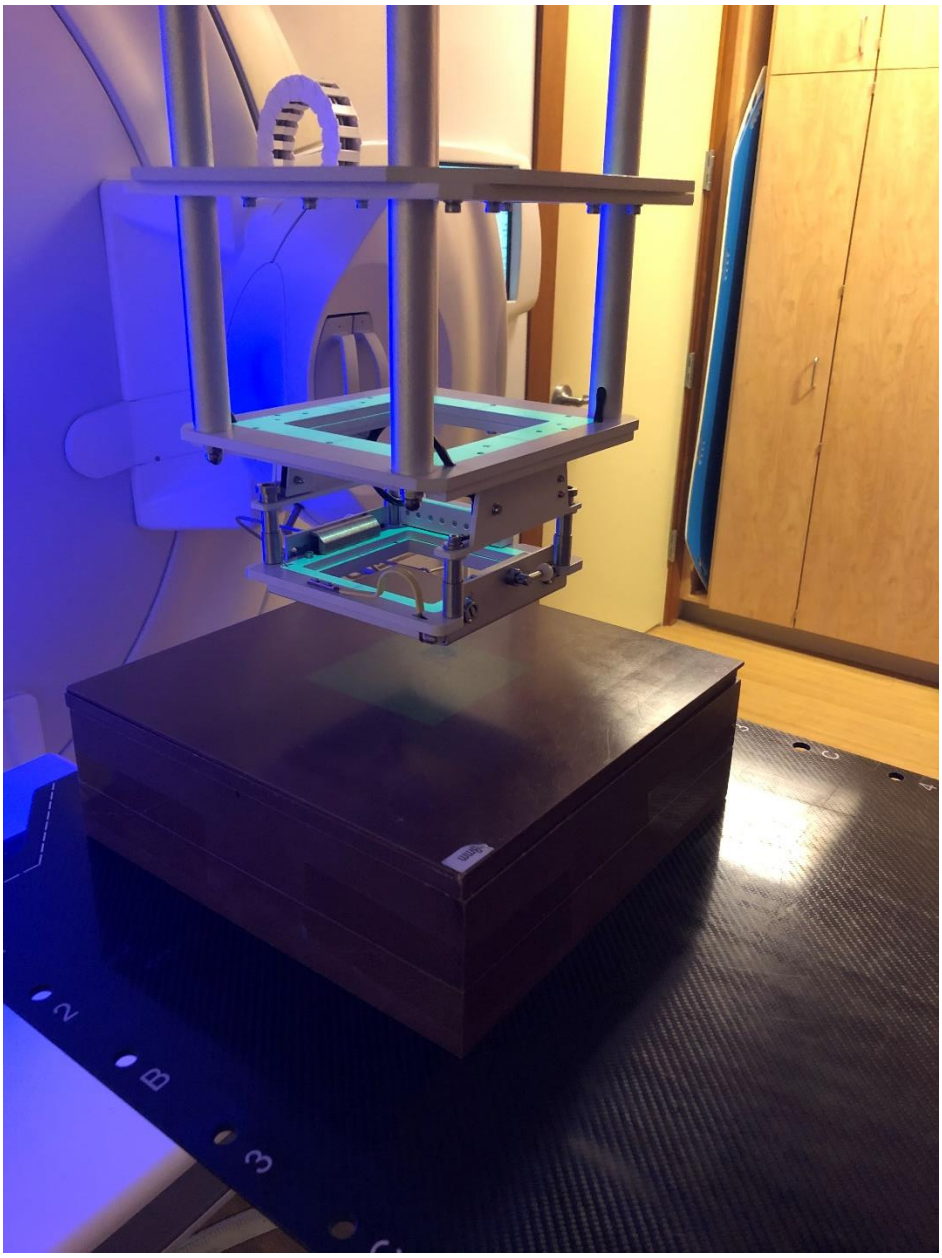

Figure 4. Experimental setup for the calibration scans

3.4 Vertical Scans

Two types of vertical scans were performed for this experiment, Head-Toe and Left-Right. For the purposes of this paper, the head side of the couch is the side closer to the linear accelerator, and the toe is the side of the couch further from the LINAC. The left and right are the left and right of an observer looking at

the linear accelerator head on. These scans allowed for cross-sectional views of the radiation dose deposited to be observed. Several vertical scans were performed for each of the 6 MeV, the 8 MeV and the reproducibility & obliquity studies.

3.4.1 The 6 MeV Investigation

The calibration sheets were shot first from 100-800 MU in 100 MU increments. The vertical solid water phantom was created using the technique described in section 4.1. The 6 x 6 cm^2 collimator was placed on the LINAC head. This was centered in the field at 100 cm SSD using the isocentric lasers in the room and the LINAC head light field. The film was sandwiched in the Head-Toe orientation in the phantom. The Cerrobend cut outs were placed in the center of the field using the rooms isocentric lasers and the light field from the gantry head. Figure 5 displays the set up for the various cut out scans done in this experiment and the 8 MeV investigation presented in the next section. Care was taken to ensure no airgaps existed between the Cerrobend cut out and the solid water phantom. Each film was exposed to 600 MU. These where left to sit at least 24 hours before being scanned using the technique described in section 3.5.

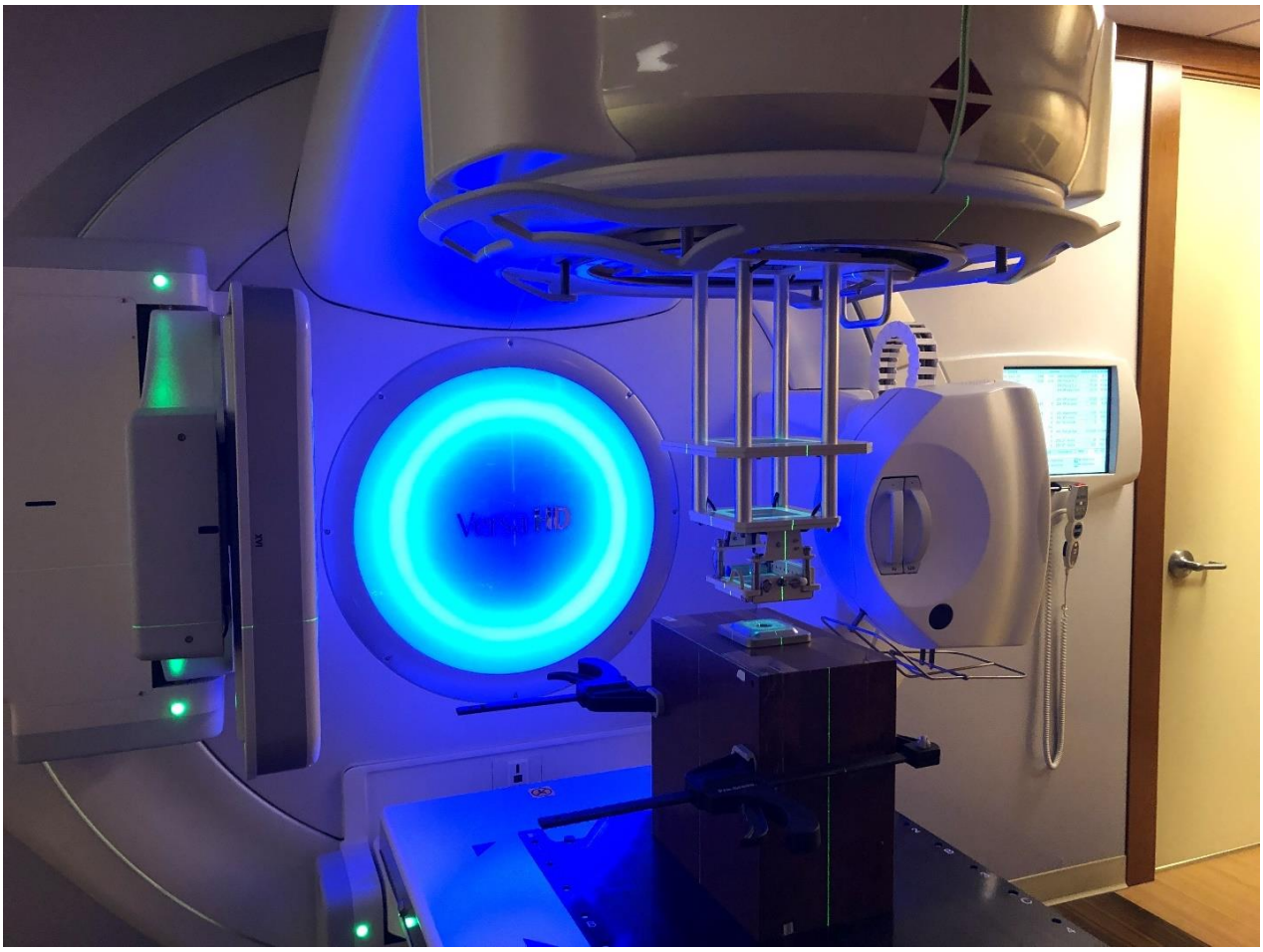

Figure 5. The experimental setup for the Head-Toe vertical scan used in the 6 MeV, 8 MeV, and Reproducibility studies

3.4.2 The 8 MeV Investigation

The same technique was used for the 8 MeV scans as the 6 MeV investigation discussed previously. An additional calibration sheet of 50 MU was shot in addition to the 100-800 MU calibration films. This was done for better characterization of low doses in the film. Specifically, for the proper calibration of the 10% of the maximum dose line. The 0 degree cut out was shot twice to ensure a proper reproducibility of the standard field.

3.4.3 The Reproducibility & Obliquity Investigation

The same technique as the 6 MeV investigation was repeated for the 0, 5, and 10 degree cut outs. Three scans of the 0 and 10 degree cut outs were taken, and five scans of the 5 degree cut out were taken. This was done to see if identical techniques corresponded to identical dose distributions. This study also utilized the 100-800 MU calibration sheets along with a 50 MU sheet.

The phantom was turned 90 degrees for the obliquity study. This put the vertical film in the Left-Right orientation seen in figure 6. These scans were done to demonstrate the necessity for the beam axis and the hole axis to be identical. The 5 degree mold was placed in the center of the field when the gantry was at 0 degrees, or straight up and down. Two scans were done at 0.00 degree obliquity. The cut out was again positioned using the light field from the 0.00 degree gantry angle and isodose lasers. Before shooting, the gantry angle was adjusted to 2.00 degrees for two shots and 5.00 degrees for two shots. The gantry head was always returned to the 0.00 degree angle for positioning of the cut out.

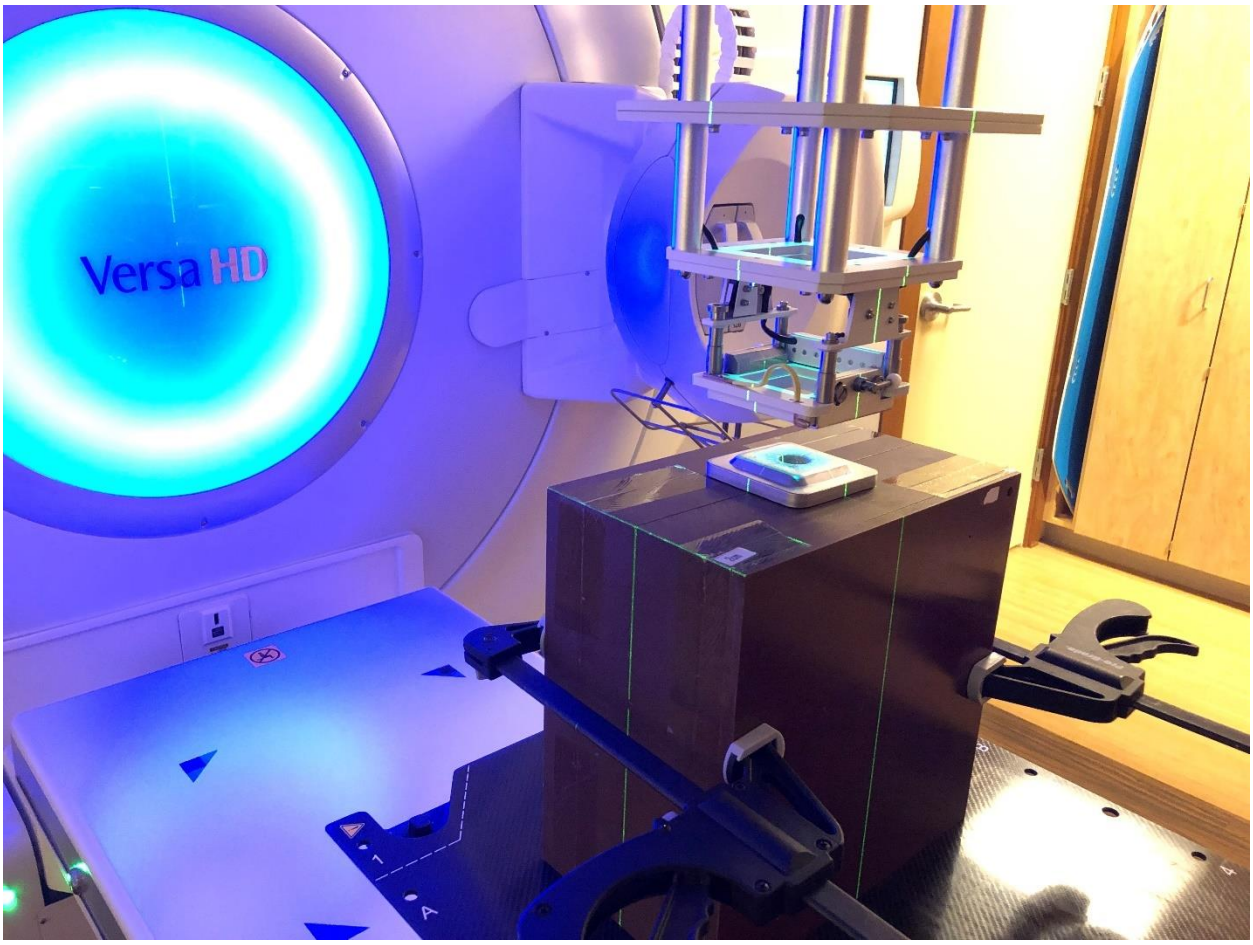

Figure 6. The experimental setup for the Head-Toe vertical scan used in the Obliquity study

3.5 Scanning the Film

The films were left to sit at least 24 hours to properly develop before scanning. An Epson Expression 10000 XL scanner was utilized for the scanning of the film. The films were placed in the top center portion face down. A sheet of glass was placed over the films in the scanner to ensure the film was flattened against the scanning surface. Care was taken to ensure no fingerprints, smudges, or stray particles were on the scanner or glass at the time of scanning. The scanner settings used can be found in table 1, below.

Epson Scan Techniques	
Document Type:	Film
Film Type:	Positive Film
Image Type:	48-bit color
Resolution:	72
Document Size:	Large enough for every film
Target Size:	Original

Table 1. Scanner Techniques Used

3.6 Creation of Calibration Curves and Manipulation in DoseLab v6.80

Utilizing the know calibration scans, a 3rd order polynomial calibration curve from optical density to absorbed dose was generated. This calibration was then applied to the open 600 MU 10 x 10 cm^2 open field at 100 cm SSD scan. The 6 MeV scans lead to a perfect calibration of the open field with maximum dose corresponding to 6000 mGy.

The 8 MeV open field did not display an accurate dose read out when the calibration was applied. The doses in the calibration curve were increased 124.22% in order to yield a dose at maximum depth equal to the predicted value of 6000 mGy. The purpose of this research is to investigate the relative difference between these different beveling angles. The doses reported in the 8 MeV scan may be used to compare the results of the different beveling angles; however, use of a second form of absolute dosimetry to confirm the film readings is recommended for future investigations.

The reproducibility & obliquity study calibration sheets did not provide an accurate calibration of the known 600 MU 10 x 10 cm^2 open field at 100 cm SSD. A correction factor 81.1% was applied to the dose values in the calibration curve to yield a proper value of 6000 mGy at the depth of maximum dose. These scans also displayed a background of 321 mGy. The purpose of this experiment was to see if using identical techniques would yield identical results. The actual dose values are not as important, as long as they are consistent between the scans. This renormalization technique is not recommended for measurements of devices intended for clinical use. Due to the background that was present, these scans were not analyzed to create diameters of clinically relevant portions of the field as a function of depth.

3.7 Generation of the Figures

3.7.1 The Isodose Images

The scanned images were analyzed in DoseLab. The profiler tool was used to find the point of maximum dose. This dose was used to generate isodose images displaying the 100%, 90%, 80%, and 10% maximum isodose lines. These correspond to the dark red, red, orange, and blue isodose lines respectively. Screenshots of the isodose images were taken. These screenshots for the 6 MeV and 8 MeV studies were opened in Microsoft Paint. Using the measurements on the side of the isodose image, a calibration from centimeters on the film to pixels in the image was formed for both the horizontal and vertical directions on the scan. An outline of the cross-section of each cut out was generated to scale in the image.

Artifacts on the image from marker dots and delamination of the edges of the film were erased. Each dose distribution was centered underneath the cut out. The isodose lines report absolute dose; however, each represents a relative dosimetric value based on the color scheme provided above. The isodose images for the reproducibility and obliquity study were not edited, as they do not reflect reality of the fields due to the high background. These shots should be only be compared for relative changes when identical techniques were implemented. These figures may be seen in Appendix A.

3.7.2 Central Axis Percentage Depth-Dose Curves

The image profiler tool was utilized in DoseLab for each of the images in the 6 MeV study, the 8 MeV study, and the reproducibility study. Vertical profiles were taken down the central axis of each film and screenshots were taken. The screenshots were then opened in Microsoft Paint. The absolute dose values along the vertical axis were erased and replaced with percentages normalized to the maximum dose along the central axis of the field. This was accomplished by calculating the maximum and minimum pixel value corresponding to the 0% and 100% dose on the image. The other percentage lines were based off of these two points, each being equidistant on the graph. The maximum dose values along the central axis as well as the maximum doses anywhere in the field are reported in the images. The dose distributions were also moved to begin right at the zero depth point. The reproducibility study displayed a background reading everywhere on the scanner. This background was normalized to 0% dose for the reproducibility percentage depth-dose curves; however, these were left in the images to show

issues with these scans. These central axis PDD curves may be found in Appendix B.

3.8 Calculating the Diameter of the Clinically Relevant Portion of the Field as a function of Depth

The 90% maximum dose is typically used as the prescription dose for electron beams. In order to characterize how this region behaves, measurements were of depth and diameter were taken in Microsoft Paint utilizing the pixel to cm scale derived earlier. Measurements of the diameter were taken in intervals exceeding one measurement per 2 mm depth in phantom. These were diameters and depths were entered into Microsoft Excel. Graphs were formed of diameter as a function of depth. Lines of best fit required 4^{th}, 5^{th}, or 6^{th} order polynomial functions to properly characterize the function. This was only performed for the 6 MeV and 8 MeV study, as the reproducibility study displayed a background. This background would lead to fictitious diameter measurements and is therefore excluded from this analysis. The results of this can be found in section 4.4 and Appendix C.

4. Results

4.1 The 6 MeV Study for Beveling Angles of 0, 15, 17.5, 20, 22.5, 25, and 30 Degrees

These initial results displayed a pinching off of the useful region, 90% isodose line, for large, greater than 15 degree, beveling angles. The maximum dose of the 5, 10, and 12.5 degree cut outs was less than the 0 degree cut out. These results are due to error in cut out positioning and have been removed from

the report to avoid confusion. The beveling angles of 15, 17.5, 20, 22.5, 25, and 30 degrees lead to a dose increment when compared with the 0 degree, standard straight hole, cut out. These results are summarized in figure 7 below. The depth of occurrence of the maximum dose, along with the depth of 90% maximum and 80% maximum dose, were driven towards the surface with increasing beveling angles. The 10% maximum dose line remained unaffected by the beveling angle. This result is presented in figure 8. Isodose images containing the 100% point, and the 90%, 80%, and 10% dose lines normalized to the maximum dose of the field can be found in the appendix A.

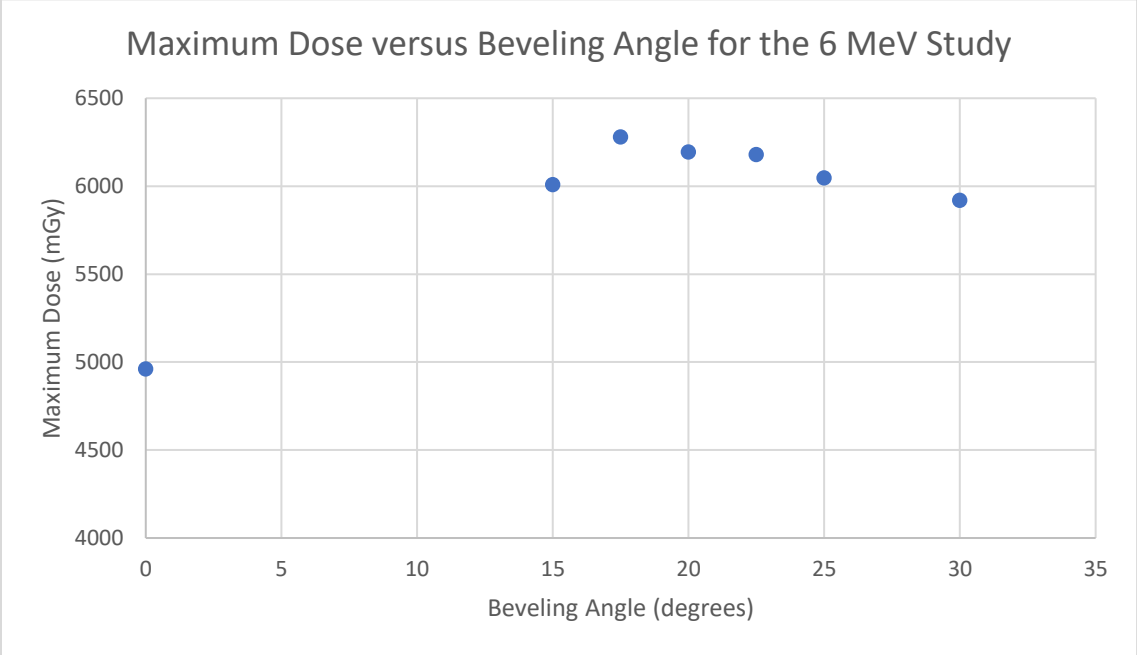

Figure 7. The Maximum Doses in each Field reported as a Function of Beveling Angle for the 6 MeV Investigation

The depth of the 100%, 90%, 80%, and 10% maximum dose for the beveling angles investigated are presented in dark red, red, yellow, and blue respectively. These depths are measured from the most inferior portion of each

field. The 10% max dose lines are unaffected by the beveling angle. This is consistent with the 6 MeV study. The depths of the 100% and 90% maximum dose were driven superiorly with increasing beveling angles. The depth of the 80% maximum dose was driven upward slightly; however, this was less pronounced than the 90% and 100% maximum dose lines.

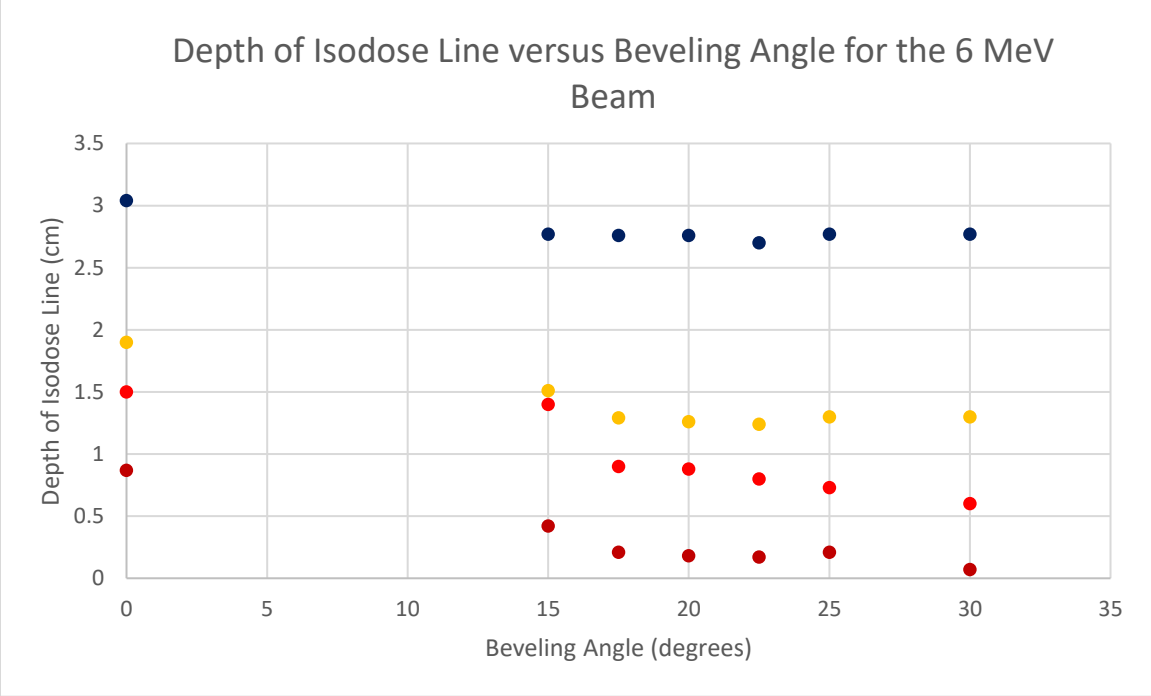

Figure 8. The Depth of Maximum Doses in each Field reported as a Function of Beveling Angle for the 6 MeV Investigation

4.2 The 8 MeV Study for Beveling Angles of 0, 5, 10, 12.5, 15, 20, 22.5, 25, and 30 Degrees

The results from the 8 MeV investigation are presented here graphically. The 17.5 degree cut out film displayed severe artifact; thus, the scan was omitted. Isodose images containing the maximum dose point, the 90%, 80%, and 10% dose lines may be found in the appendix A. The maximum dose as a function of beveling angle is displayed in figure 9. The depth of the most inferior portion of the 100%,

90%, 80%, and 10% line are presented in figure 10. These are presented as dark red, red, yellow, and blue points respectively.

The 8 MeV beam did not display the same characteristics as the 6 MeV beam. The dose increment due electron lensing is much more pronounced. The depth of maximum dose was fairly consistent as seen in figure 10. The 90% and 80% maximum dose experienced the same decrease in area with increasing beveling angle. This is undesirable for clinical applications. The 10% maximum dose, or scatter line, reached over 3.5 cm depth in the phantom for the 8 MeV fields, as opposed to the 3 cm depth reached in the 6 MeV study.

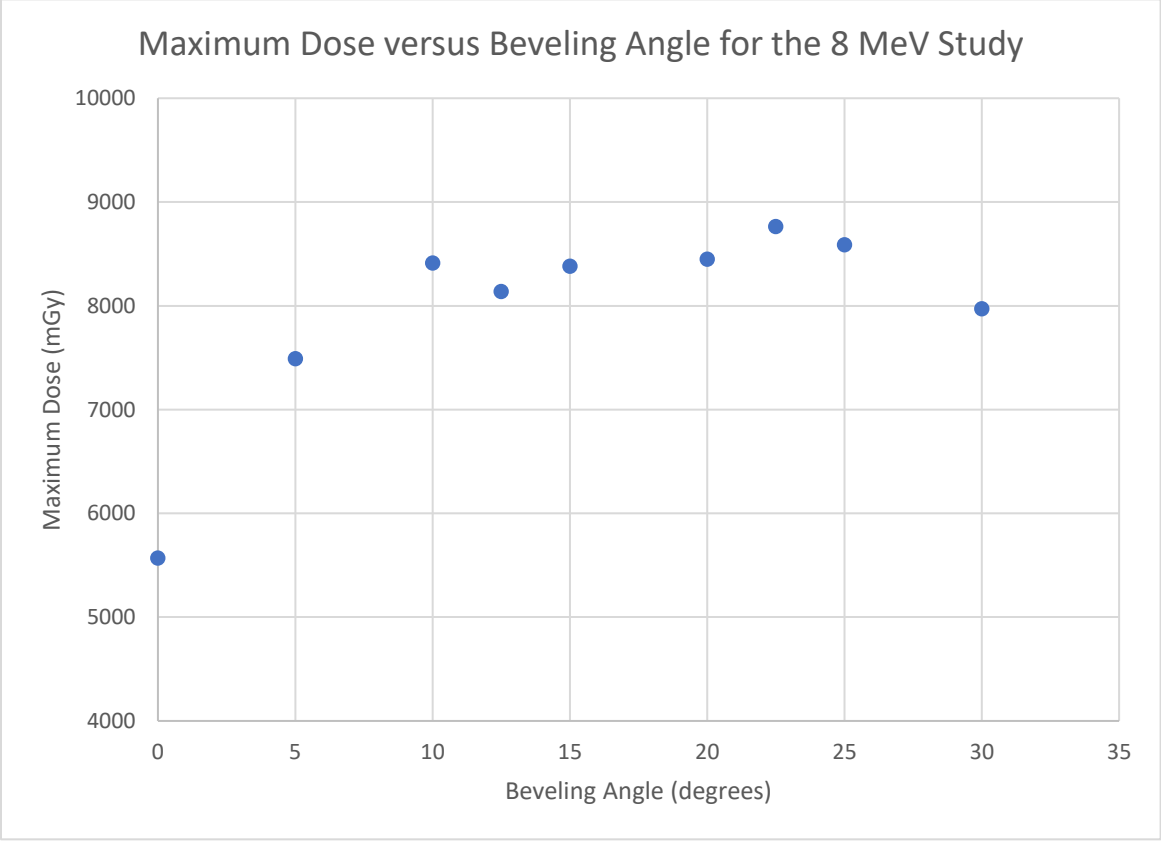

Figure 9. The Maximum Doses in each Field reported as a Function of Beveling Angle for the 8 MeV Investigation

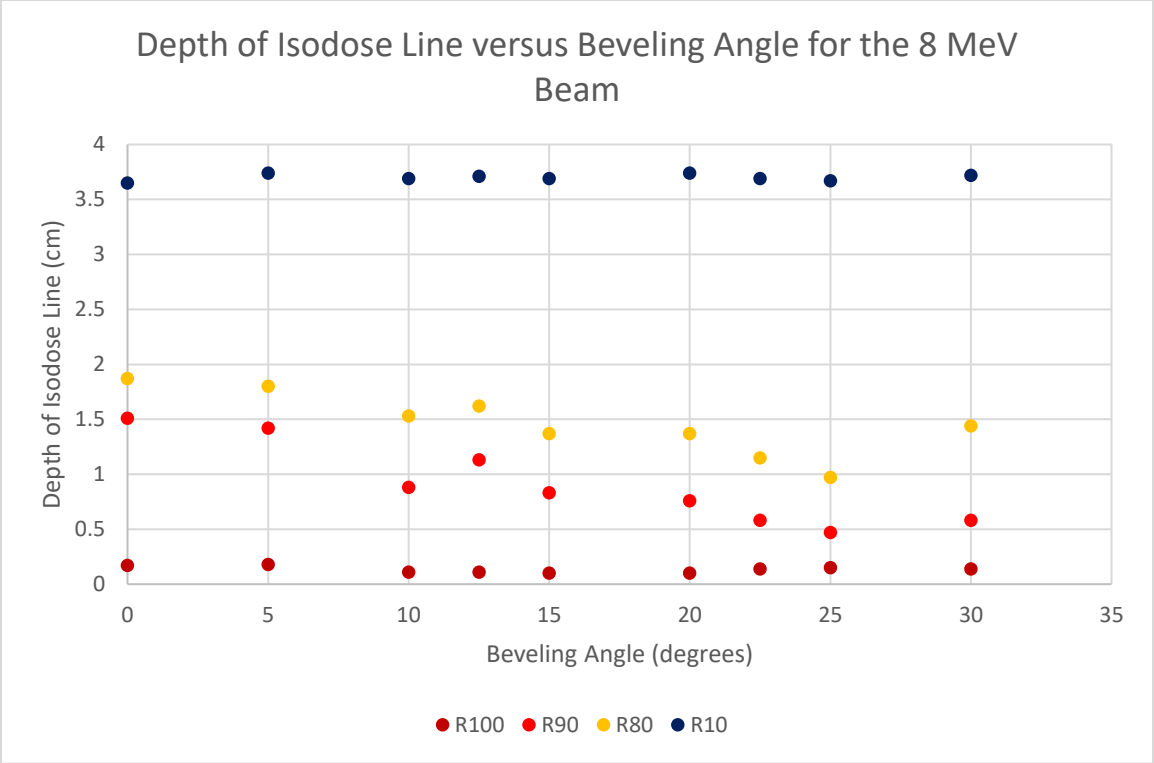

Figure 10. The Depth of 100%, 90%, 80%, and 10% Maximum Doses in each Field reported as a Function of Beveling Angle for the 8 MeV Investigation

4.3 The Reproducibility & Obliquity Study

The results from this study are summarized graphically for the maximum dose as function of the beveling angle, see figure 11. The results of depth of maximum dose versus beveling angle do not present themselves nicely graphically. This is due to the number of repeated points in the data, as well as the lack of structure to the data. Instead, table 2 was used to report these values. The central axis percentage depth-dose curves and isodose images of these films may be found in appendix B and A, respectively. The fields shot oblique angles can be found in appendix A.

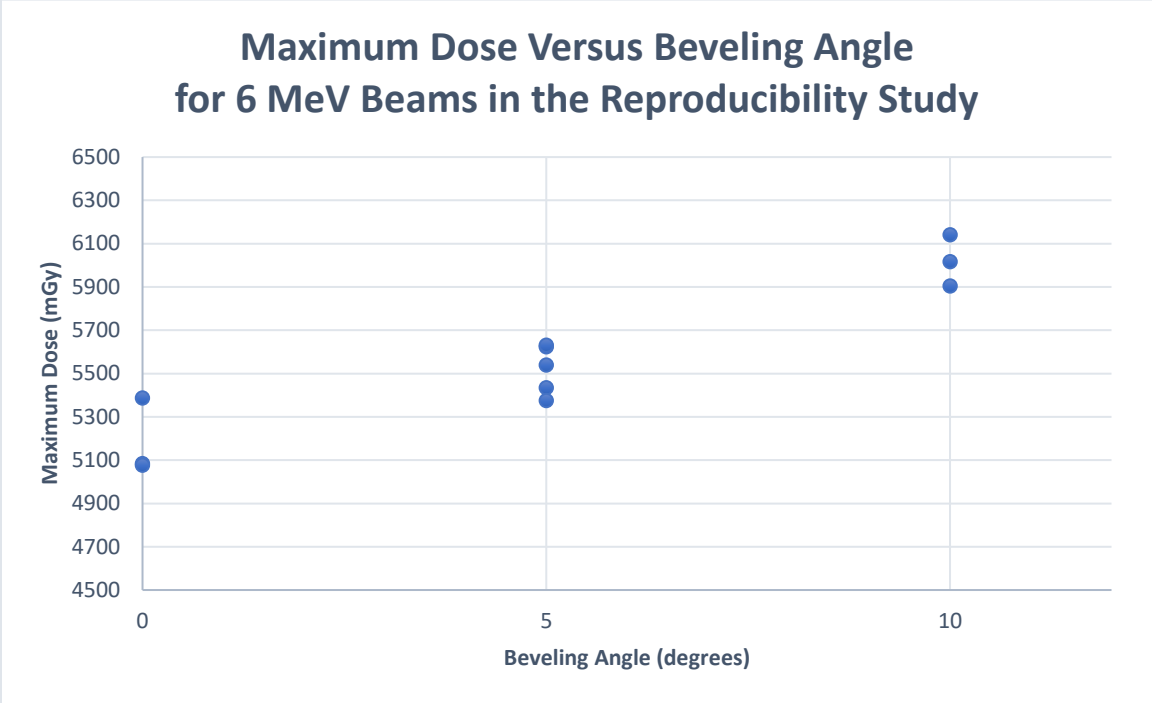

Figure 11. The Maximum Doses in each Field Reported as a Function of Beveling Angle for the 6 MeV Reproducibility Investigation

Reproducibility Study Depth of Maximum Dose Results	
Beveling Angle (degrees)	Depth of Max Dose (cm)
0	0.14
0	0.91
0	0.14
5	0.62
5	0.81
5	0.88
5	0.81
5	0.56
10	0.74
10	0.81
10	0.74

Table 2. Displays the depth of maximum dose as a function of beveling angle for the 6 MeV reproducibility study

4.4 Clinically Relevant Diameters as a Function of Depth

The clinically relevant portion of the field, or 90% maximum line, is used for the prescription of dose. It is important that lesions treated with this dose prescription technique are completely encapsulated by this portion of the field. The following equation may be used to calculate the monitor units needed to achieve the prescribe dose:

$$MU = \frac{D_{prescribed}}{0.9 * (\frac{D_{max}}{600})}$$

Where,

MU – is the monitor units needed to achieve the prescribed dose

D_{max} – is the maximum dose in the fields measured with 600 MU

$D_{prescribed}$ – is the desired prescription dose

A table of maximum dose versus beveling angle is provided below, see table 3. The values found in table 3 should not be used clinically. Every electron lens cut out should individually be measured for maximum doses. Variability was shown to exist between the same cut out shot with identical fields, see section 4.3. Better reproducibility is required before clinical implementation of electron beam lenses. Should a different dose be used to calculate the maximum dose in trials, the denominator under maximum dose in the field should be changed to reflect the monitor units used in the quantification of maximum dose.

Maximum Dose in the field (mGy)		
	Beam Energy	
Beveling Angle (degrees)	6 MeV	8 MeV
0	4961	5568
5	-	7490
10	-	8412
12.5	-	8136
15	6009	8380
17.5	6279	-
20	6194	8449
22.5	6180	8762
25	6046	8587
30	5920	7972

Table 3. Maximum dose in the field for the different energies and beveling angles investigated

The following figures display the diameter of the clinically relevant portion of the field as a function of field depth for the 6 MeV and the 8 MeV study. It should be noted that the prescription region does not begin at the surface of the phantom. The prescription field typically starts with in a depth of 2 mm in the phantom. The prescription field has a tendency to decrease in diameter and total depth with increasing beveling angles. For this reason, the author recommends that any future investigations into this effect focus around narrow beveling angles.

The 0 degree cut out shot with a 6 MeV electron beam's prescription field starts at a depth of 1 mm in water equivalent tissue. The field experiences a slight ballooning outward due to increasing electron obliquity with depth. Beyond 1.2 cm depth, the prescription dose experiences a rapid decrease in diameter. All tissue at depths greater than 1.4 cm will receive less than the prescription dose. This result is displayed graphically in figure 13.

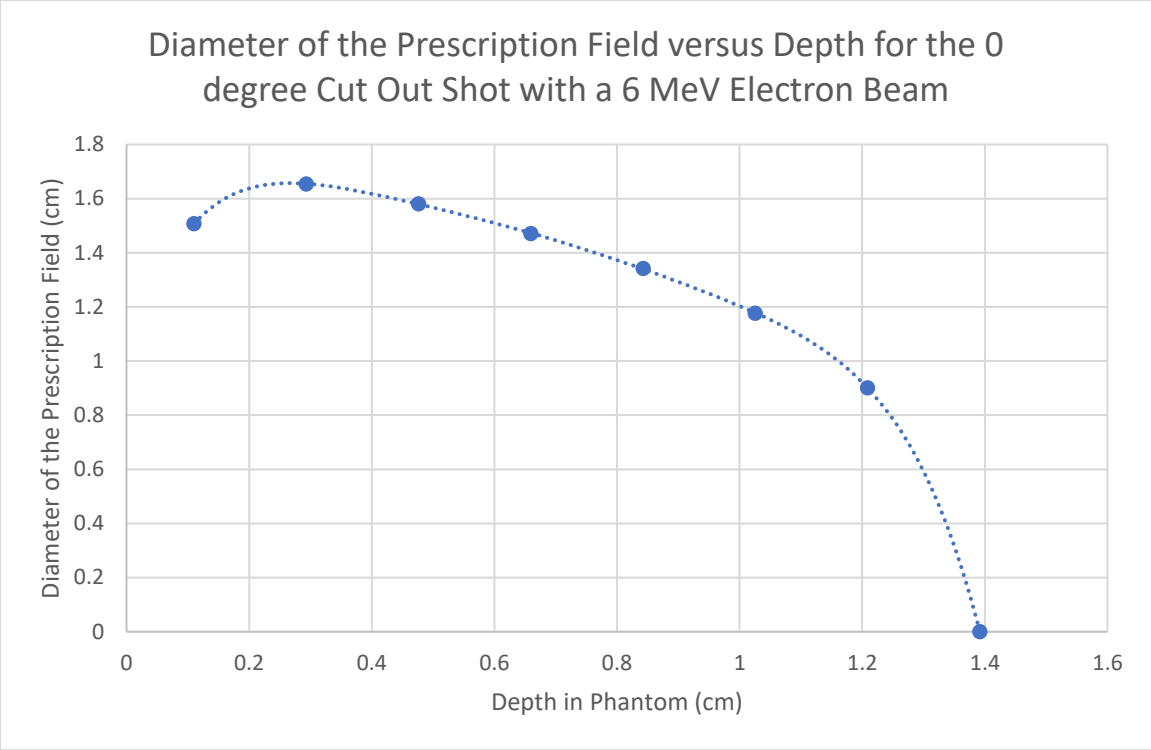

Figure 12. Graph of Diameter of the Prescription Field versus Depth for the 0 degree Cut Out Shot with a 6 MeV Electron Beam

The 15 degree cut out shot with the 6 MeV displayed a slightly larger prescription portion of the field than the open field. It also displayed a 120% higher maximum dose than the straight hole. This result may be seen in figure 12. The remaining graphs of prescription diameter as a function of depth may be found in Appendix C. The 25 degree and 30 degree cut outs had such shallow prescription regions, that this calculation was unable to be performed. The 20 degree cut out with the 6 MeV electron beam contained artifacts. This calculation was not performed for the 20 degree cut out shot with the 6 MeV electron beam field due to the artifacts present in the image. The 20 degree cut out does not appear to be preferable to the 0 or 15 degree cut out for 6 MeV electron fields.

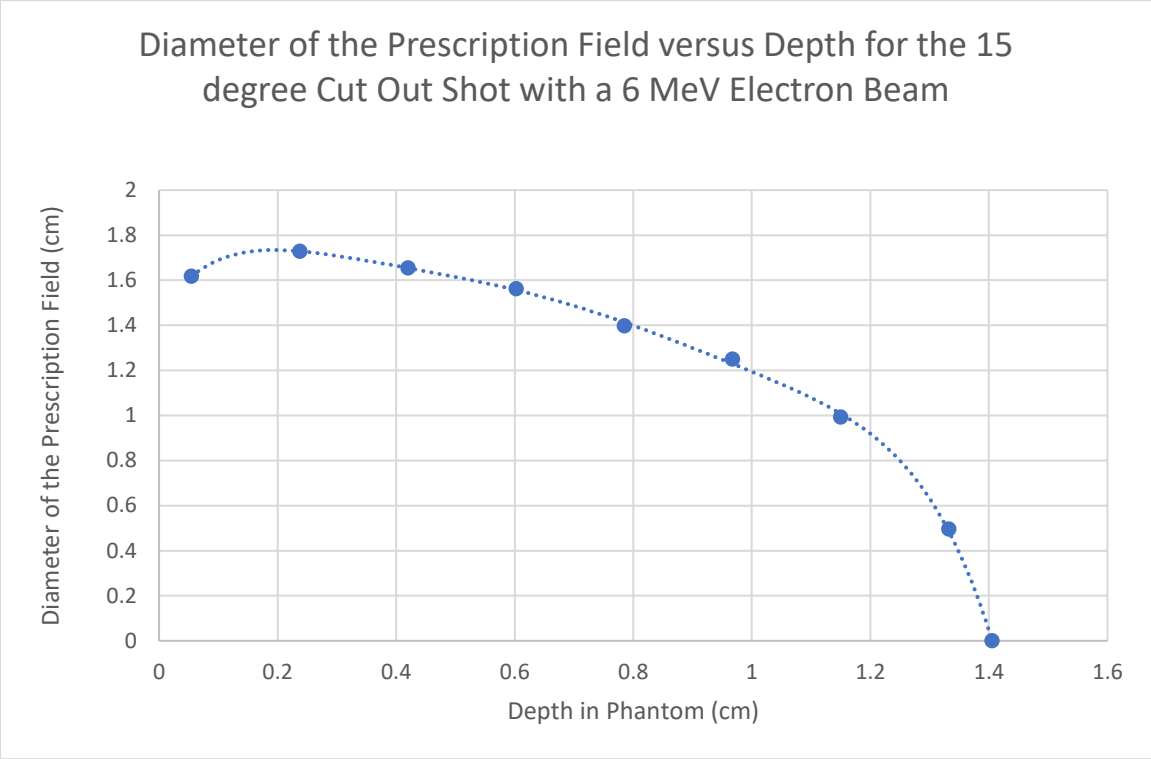

Figure 13. Diameter of the Prescription Field versus Depth for the 15 degree Cut Out Shot with a 6 MeV Electron Beam

The isodose lines seen in Appendix A may be considered plots of absolute dose, relative dose to the maximum dose in the field, or relative dose to the treatment prescription dose. The 111%, 100%, 89%, and 11% of the prescribed dose lines appear in dark red, red, orange, and blue respectively in the figures in Appendix A. These figures may be overlaid with scaled cross-sectional images of the inflicted region to ensure proper coverage of the 90% maximum dose line, also known as the prescription line.

5. Discussion

5.1 The 6 MeV Study

The 6 MeV study shows a dose increment for beveling angles of 15 degrees and above. The dose decrement witnessed for the 5, 10, and 12.5 degree molds is later contradicted in the reproducibility study. This discrepancy is due to misalignment of the cut out, film, and radiation field. These results have been omitted from the report to avoid confusion for future researchers. The decrease in the depth of maximum dose noted in figure 8 can be adequately explained by electron scattering theory. As the edges become beveled at larger angles, the electrons scattered off of those edges become increasingly obliquely incident upon the surface of the phantom. This drives the maximum dose upward in the phantom, and yields the results witnessed. The 17.5 degree cut out demonstrated the largest dose increment in this energy range; however, this did not correspond to a preferable dose distribution when compared to the standard straight-necked, or 0 degree, cut out.

5.2 The 8 MeV Study

The 8 MeV study yielded a nice graphical representation of dose increment due to beveling of the edges. The depth of maximum dose was closer to the surface of the phantom than for the 6 MeV study. The 5, 10, 12.5, and 15 degree shots displayed dose horns off of the edges of the cut out at the depth of maximum dose. This arises from electrons being backscattered into the field of off the inner edges of the cut out and entering the phantom obliquely, thus depositing much of their energy superficially. The dose horns account for the variance between

maximum dose along the central axis and the maximum dose in the field. The central axis does not receive quite as high of a dose as the adjacent off axis regions. Characterization of fields with these properties can be difficult, thus the author would recommend only the use of a 6 MeV or lower energy electron beam in future investigations.

5.3 The Obliquity and Reproducibility Study

5.3.1 The 0, 5, 10 degree 6 MeV Reproducibility Study

This study demonstrates a dose increment over the 0 degree field for the 5 and 10 degree cut outs for 6 MeV electron beams. These results are in agreement with the 8 MeV investigation, in which all beveling angles lead to some amount of dose increase. These results also display a nonnegligible amount of variation despite using the same setup techniques for all of the scans. Possible causes for reproducibility issues are discussed in section 6.4. The depths of maximum doses were reported in a table, as they were inconsistent and followed no trend.

5.3.2 Obliquity Study

This experiment demonstrated the need for device immobilization not just for the sake of reproducibility, but also the need to avoid any teetering of the device during treatment. A five degree obliquity would be generated, should one of the interior edges of the 2 cm diameter cut out be raised or lowered by 1.75 mm. This would cause large enough dose perturbation to possibly under dose a target. This can be seen dramatically in figure 47. The isodose images of this study may be found in Appendix A.

5.4 Limitations of the Study

5.4.1 Porous Nature of Superior Portions of Cut Outs

A possible confounding factor is the porous nature of the Cerrobend in the upper regions of the cut outs. The 5mm neck solidified as a smooth surface; however, the upper portions of the cut outs displayed significantly rough surfaces. Figure 14 below shows a close up of the 5 degree cut out. This could cause reproducibility errors in remakes of the mold using identical techniques. All of the cut outs tested displayed this porous feature in the upper portions of the cut out.

Figure 14. Porous nature of upper portion of 5 degree Cerrobend cut out

5.4.2 Use of Optical Systems for Cut Out Alignment

These cut outs were placed by hand for each exposure. Significant differences in cut out positioning may occur utilizing this technique. The author recommends a rigid immobilization device be used to ensure proper cut out alignment and no field obliquity. These devices could be attached to the electron beam collimator; however further investigation is required for this technique.

5.4.3 Single Point of Maximum Dose

The dose distributions were normalized to the maximum dose present in any one pixel of the field. This leaves room for noise in the images to have a significant effect on the entire distribution. It is recommended in future studies that the average of several of the highest points be utilized. This would provide more consistent results for the maximum dose of each field and make the study more robust against noise in the images.

5.5 Further Studies

Future studies could investigate continuous functions which define the geometry of the cut out hole. The use of a 3D printer allows for any shape cut out to be generated. The device should be immobilized relative to the patient and electron beam to avoid any obliquity complications. The dose horns present in the 8 MeV scans may behave unpredictably; thus, the author suggests further investigation into this effect be focused on 6 MeV and lower energy beams. Further theoretical work could be done to predict the energy spectra and obliquity of electrons scattered into the treatment region. This will determine how the lensed electron beam will deposit dose in inhomogeneous media.

6. Conclusion

This technique of electron lensing may yield clinically desirable dose distributions. The lensing effect has been demonstrated to yield a dose increment for beveled angles over traditional straight-hole cut outs. These higher maximum doses do not always correlate with preferable field geometries. Larger beveling angles lead to a constriction of the clinically useful part of the field, so narrow throat cut out geometries are recommended in the future. The results of this study also have implications outside of the intentional use of beveled edge cut outs. Any Cerrobend cut out that dose not have precisely straight edges will exhibit this effect, and further investigation could lead to a better qualification of small electron beams.

Bibliography

[1] Cancer Facts and Figures 2019. American Cancer Society. https://www.cancer.org/research/cancer-facts-statistics/all-cancer-facts-figures/cancer-facts-figures-2019.html. Accessed May 15, 2019.

[2] N. D. Tapley, “Clinical Applications of the Electron Beam” New York: *John Wiley & Sons*, 1976.

[3] F. M. Khan and J. P. Gibbons, “The Physics of Radiation Therapy, Fifth edition” Philadelphia, PA: *Lippincott Williams & Wilkins/Wolters Kluwer*, 2014.

[4] S. C. Klevenhagen, “Physics of Electron Beam Therapy” *Medical Physics Handbooks 13, Adam Higler Ltd*, 1985.

[5] E. J. Hall, A. J. Giaccia, “Radiobiology for the Radiologist, Seventh Edition” Philadelphia: *Lippincott Williams & Wilkins*, 2012.

[6] J. A. Purdy, M. C. Choi, “Lipowitz metal shielding thickness for dose reduction of 6-20 MeV electrons” *Medical Physics*, Vol. 7 No.3, pp.251-253, June 1980

[7] F. N. Bray, B. J. Simmons, A. H. Wolfson, and K. Nouri, “Acute and Chronic Cutaneous Reactions to Ionizing Radiation Therapy,” *Dermatol Ther (Heidelb)*, vol. 6, no. 2, pp. 185–206, Jun. 2016.

[8] A. I. Rubin, “Basal-Cell Carcinoma,” *The New England Journal of Medicine*, vol. 355, no, 21, pp. 2262-2269, Nov. 2005.

[9] M. Alan, D. Ratner, “Cutaneous Squamous-Cell Carcinoma” *The New England Journal of Medicine,* vol. 344, no. 13, pp. 975-983, Mar. 2001.

[10] A. I. Riker, N. Zea, and T. Trinh, “The Epidemiology, Prevention, and Detection of Melanoma,” *The Ochsner Journal*, vol. 10, no. 2, p. 10, 2010.

[11] M.Girardi, P. W. Heald, L. D. Wilson, “The Pathogenesis of Mycosis Fungoides” *The New England Journal of Medicine,* vol. 350, no. 19, pp. 1978-1988, May 2004.

Appendix A

Appendix A contains the 100%, 90%, 80%, and 10% isodose lines for the 6 MeV, the 8 MeV, and the reproducibility and obliquity studies. These correspond to 111%, 100%, 89%, and 11% of the prescription dose. These are represented in dark red, red, orange, and blue respectively. The dose distributions for the 6 MeV and 8 MeV study have been positioned under cross-sectional images of the cut outs they were shot with. The maximum dose in the field is reported for each. The reproducibility and obliquity are presented as the raw data. This is due to the background present in every image, which leads to inaccurate dose distributions. The reproducibility and obliquity study data should only be compared to one another as they do not correspond to physical reality.

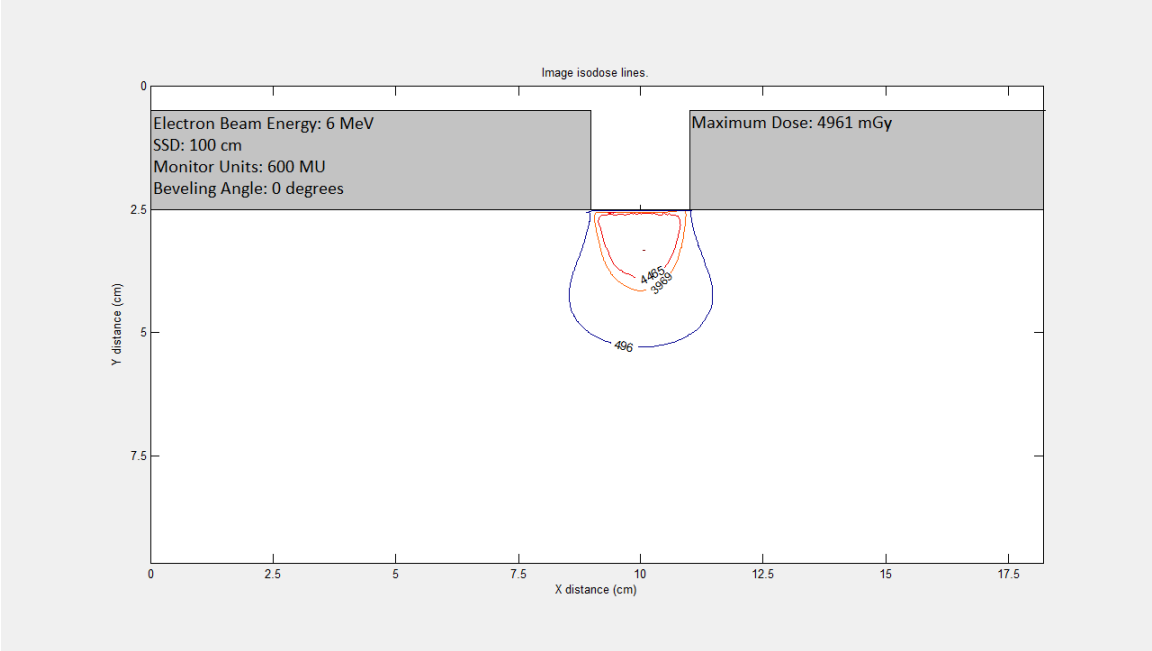

Figure 15. Isodose Lines of the 100%, 90%, 80%, and 10% Maximum Dose Under Cross-Section of the 0 Degree Cut Out Shot with a 6 MeV Electron Beam

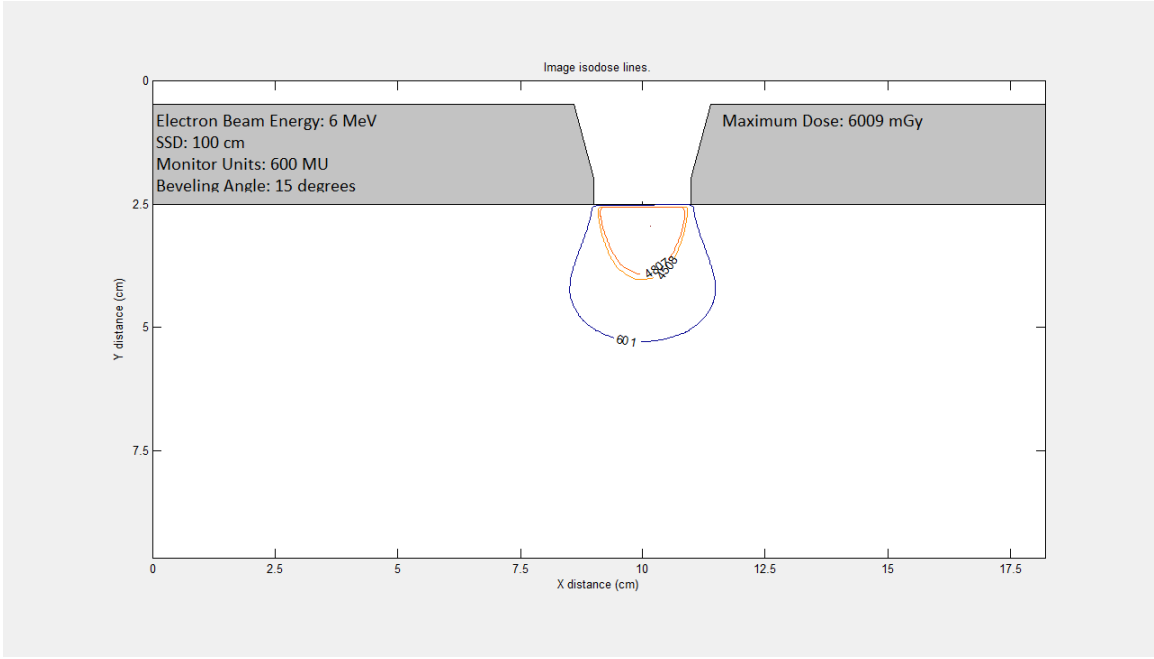

Figure 16. Isodose Lines of the 100%, 90%, 80%, and 10% Maximum Dose Under Cross-Section of the 15 Degree Cut Out Shot with a 6 MeV Electron Beam

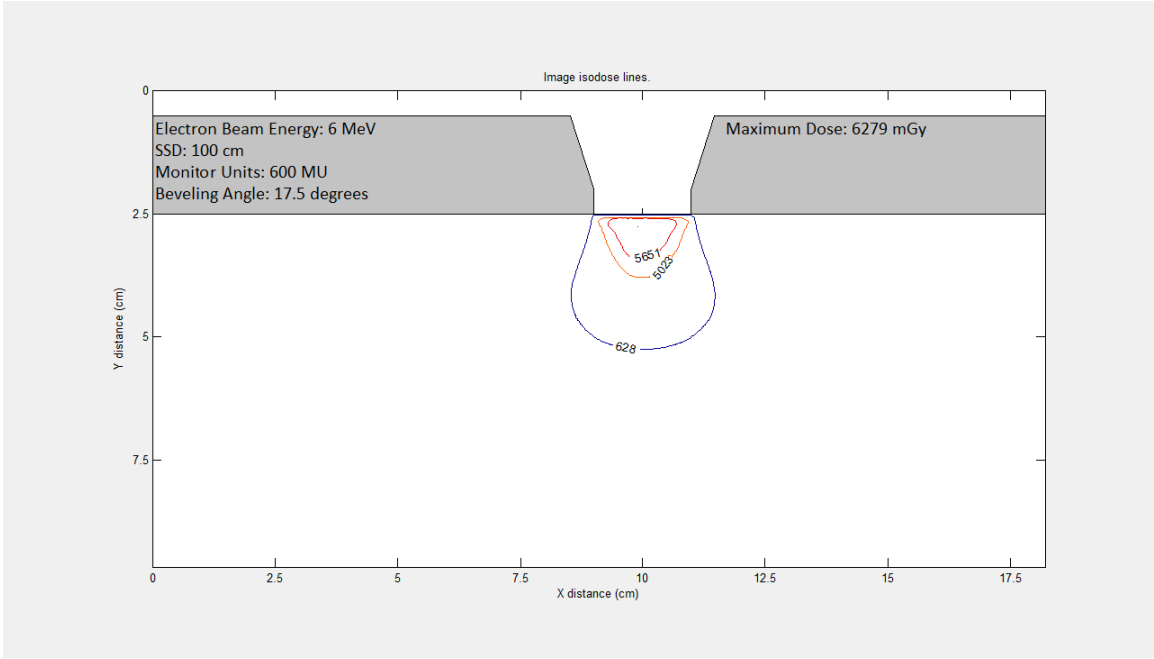

Figure 17. Isodose Lines of the 100%, 90%, 80%, and 10% Maximum Dose Under Cross-Section of the 17.5 Degree Cut Out Shot with a 6 MeV Electron Beam

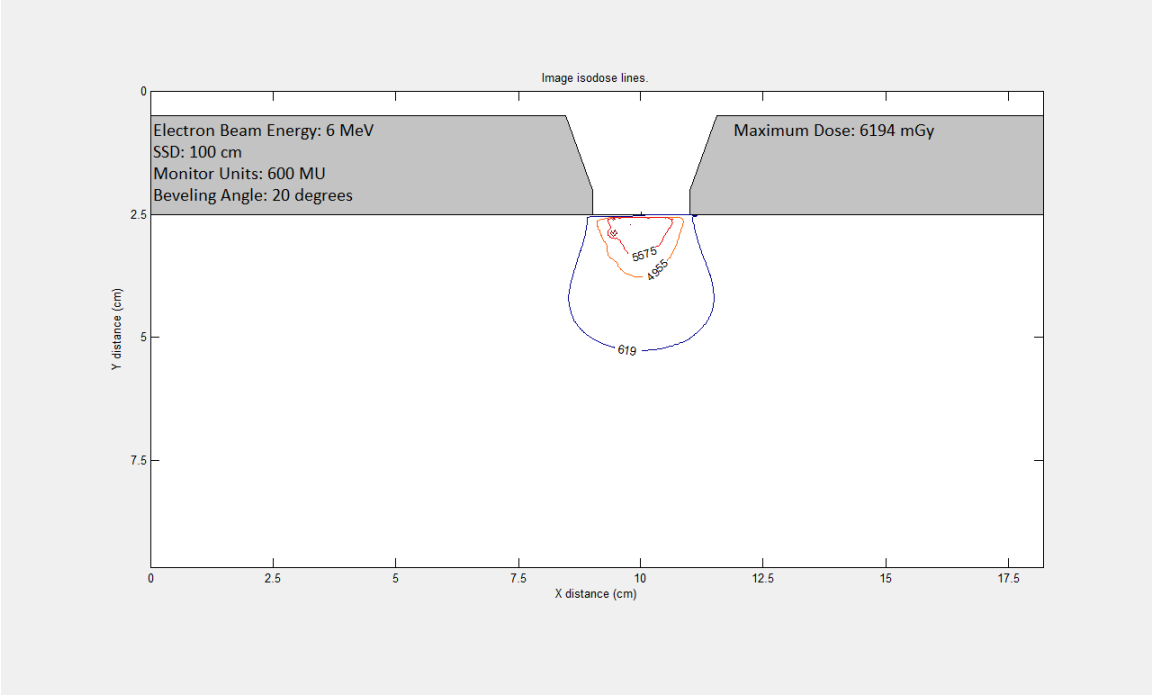

Figure 18. Isodose Lines of the 100%, 90%, 80%, and 10% Maximum Dose Under Cross-Section of the 20 Degree Cut Out Shot with a 6 MeV Electron Beam

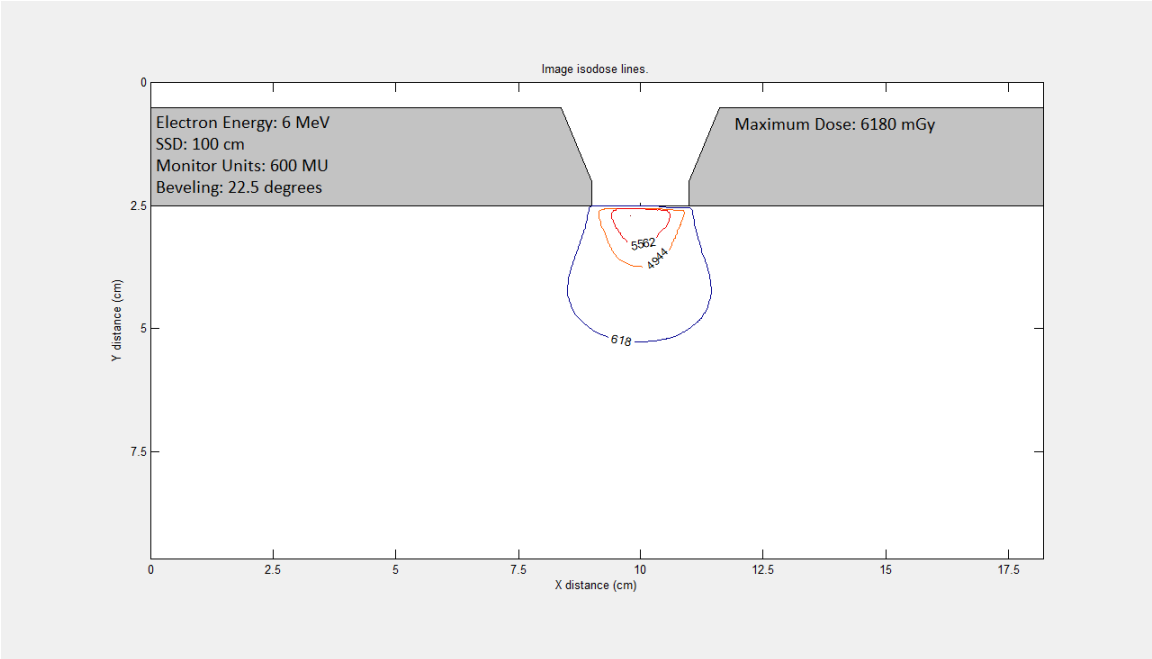

Figure 19. Isodose Lines of the 100%, 90%, 80%, and 10% Maximum Dose Under Cross-Section of the 22.5 Degree Cut Out Shot with a 6 MeV Electron Beam

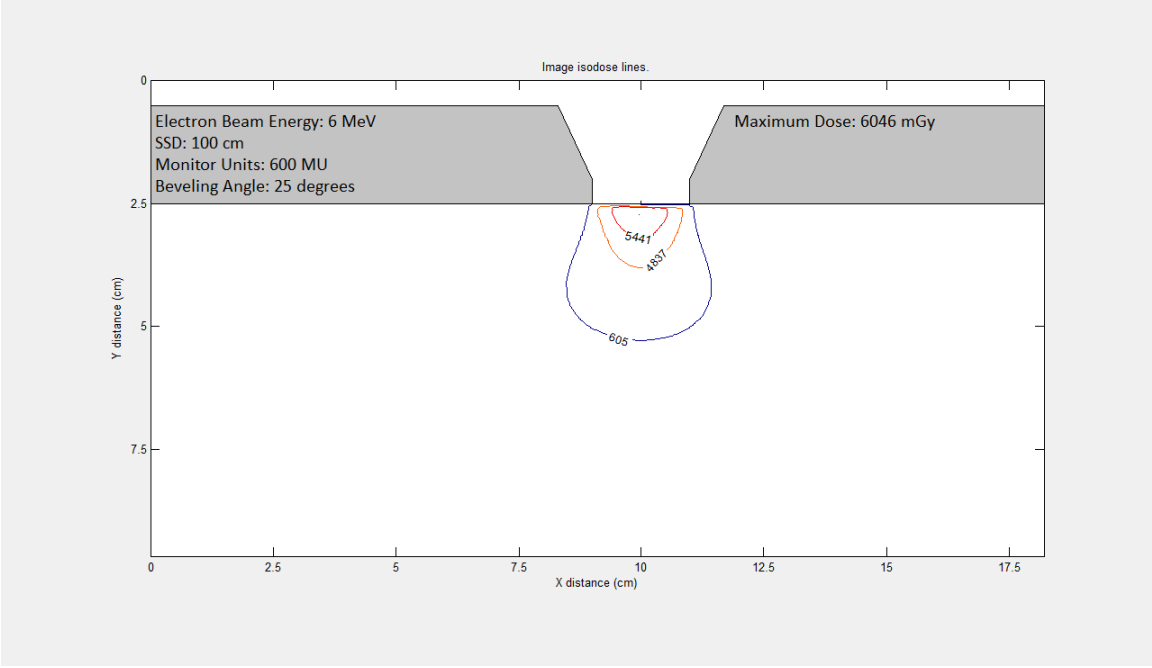

Figure 20. Isodose Lines of the 100%, 90%, 80%, and 10% Maximum Dose Under Cross-Section of the 25 Degree Cut Out Shot with a 6 MeV Electron Beam

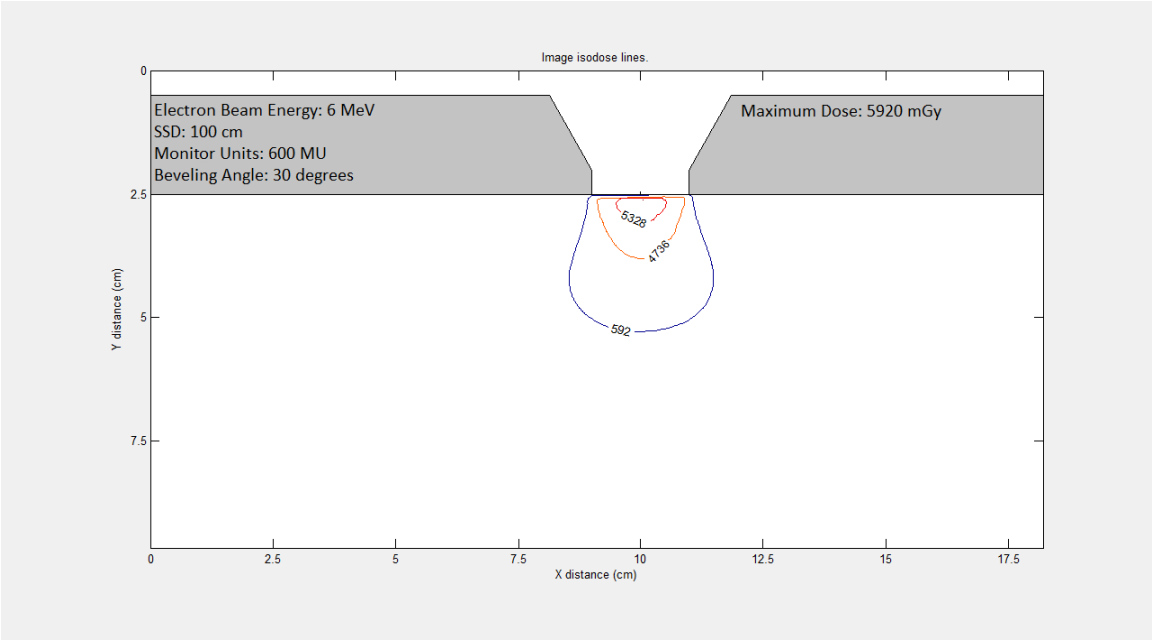

Figure 21. Isodose Lines of the 100%, 90%, 80%, and 10% Maximum Dose Under Cross-Section of the 30 Degree Cut Out Shot with a 6 MeV Electron Beam

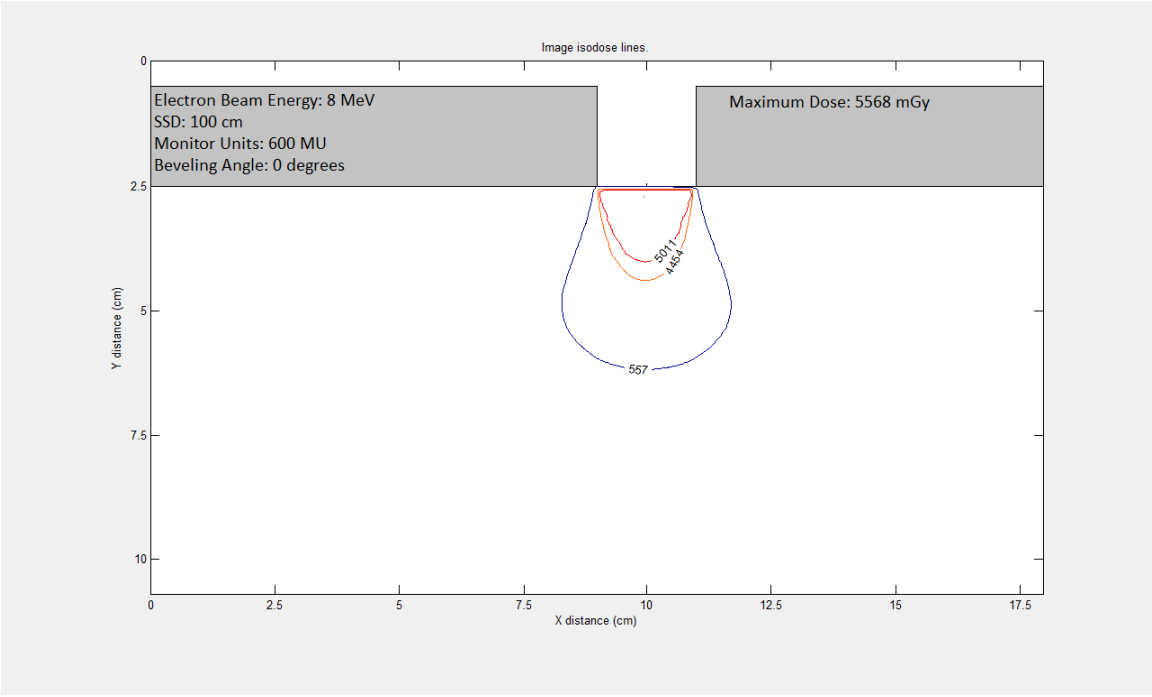

Figure 22. Isodose Lines of the 100%, 90%, 80%, and 10% Maximum Dose Under Cross-Section of the 0 Degree Cut Out Shot with an 8 MeV Electron Beam (Shot: 1 of 2)

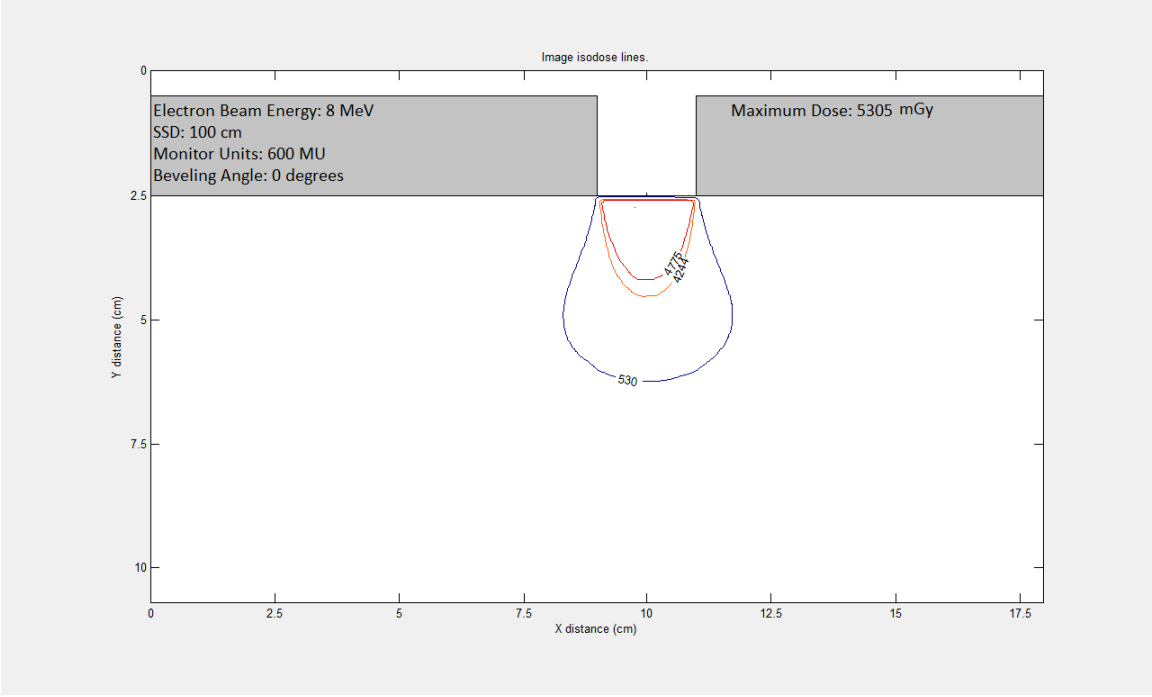

Figure 23. Isodose Lines of the 100%, 90%, 80%, and 10% Maximum Dose Under Cross-Section of the 0 Degree Cut Out Shot with an 8 MeV Electron Beam (Shot: 2 of 2)

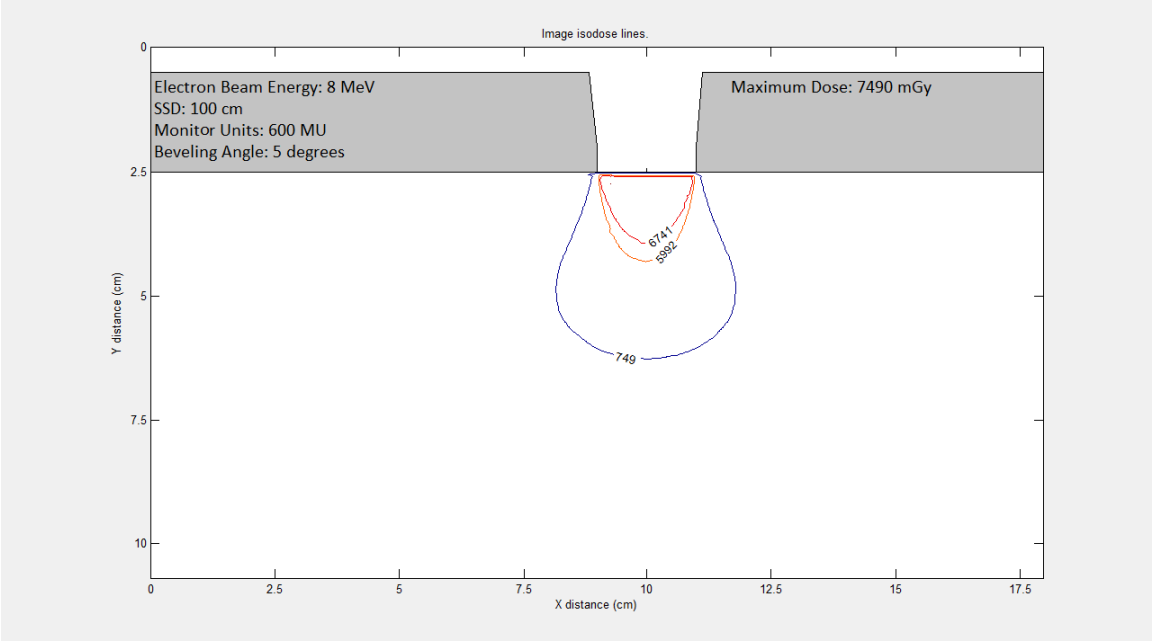

Figure 24. Isodose Lines of the 100%, 90%, 80%, and 10% Maximum Dose Under Cross-Section of the 5 Degree Cut Out Shot with an 8 MeV Electron Beam

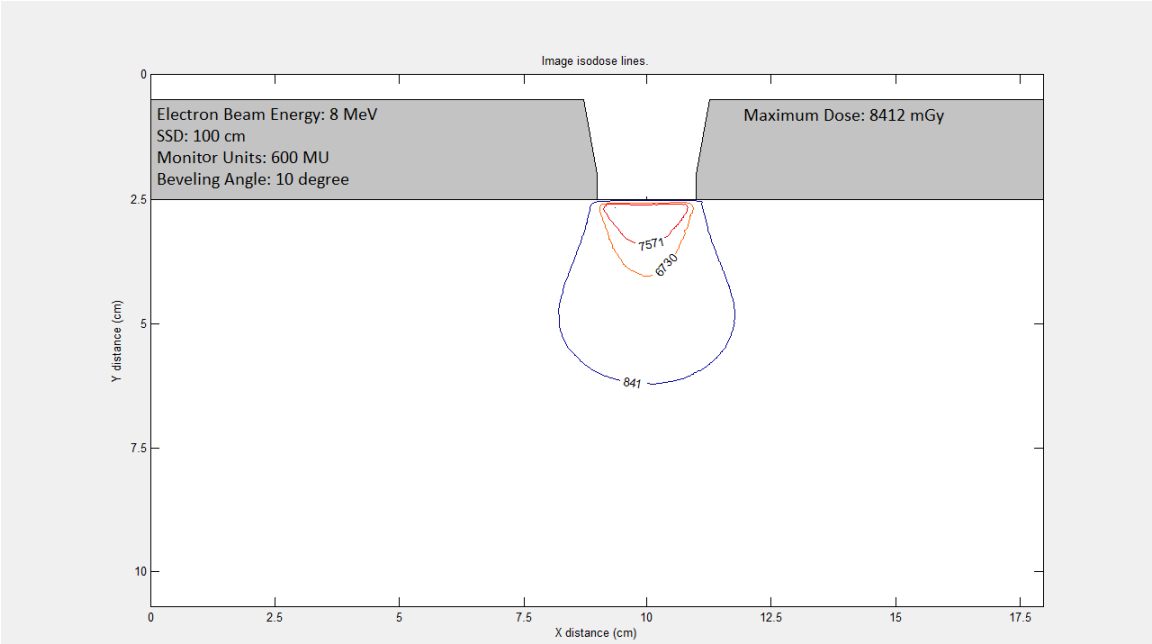

Figure 25. Isodose Lines of the 100%, 90%, 80%, and 10% Maximum Dose Under Cross-Section of the 10 Degree Cut Out Shot with an 8 MeV Electron Beam

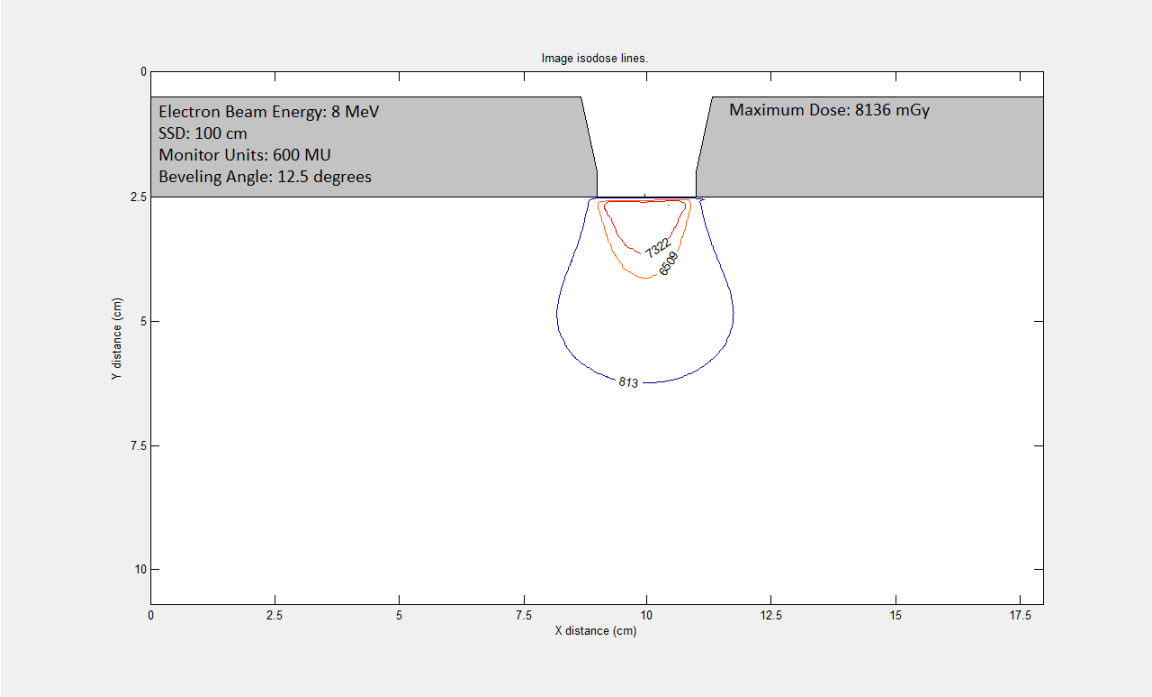

Figure 26. Isodose Lines of the 100%, 90%, 80%, and 10% Maximum Dose Under Cross-Section of the 12.5 Degree Cut Out Shot with an 8 MeV Electron Beam

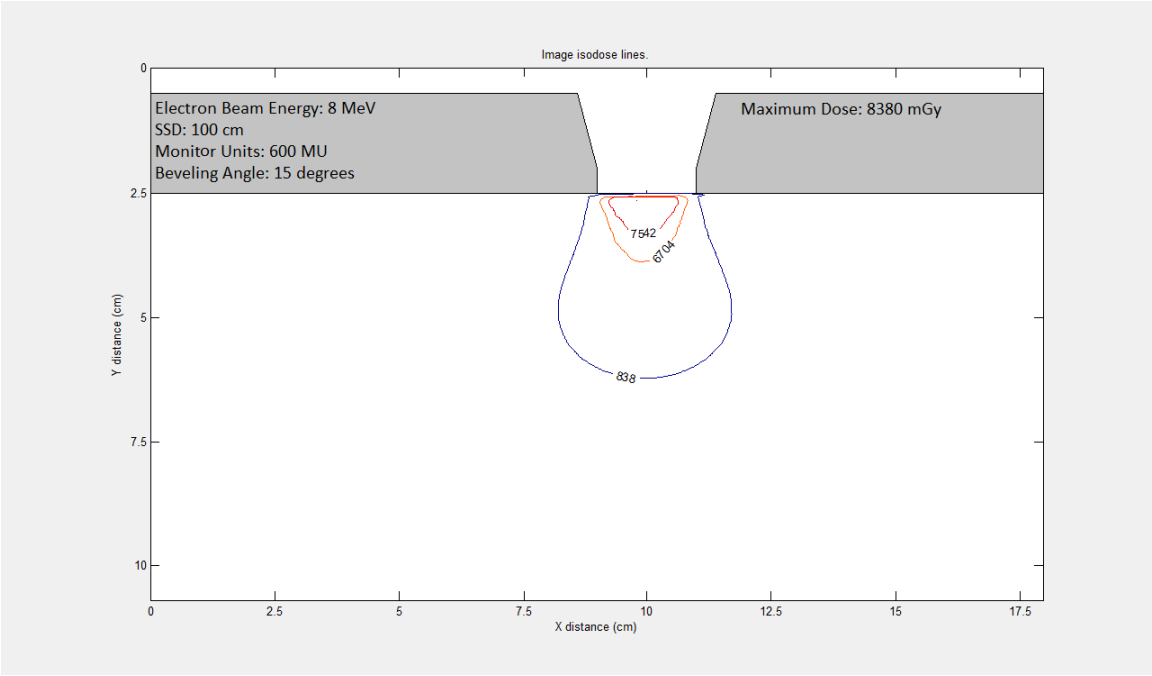

Figure 27. Isodose Lines of the 100%, 90%, 80%, and 10% Maximum Dose Under Cross-Section of the 15 Degree Cut Out Shot with an 8 MeV Electron Beam

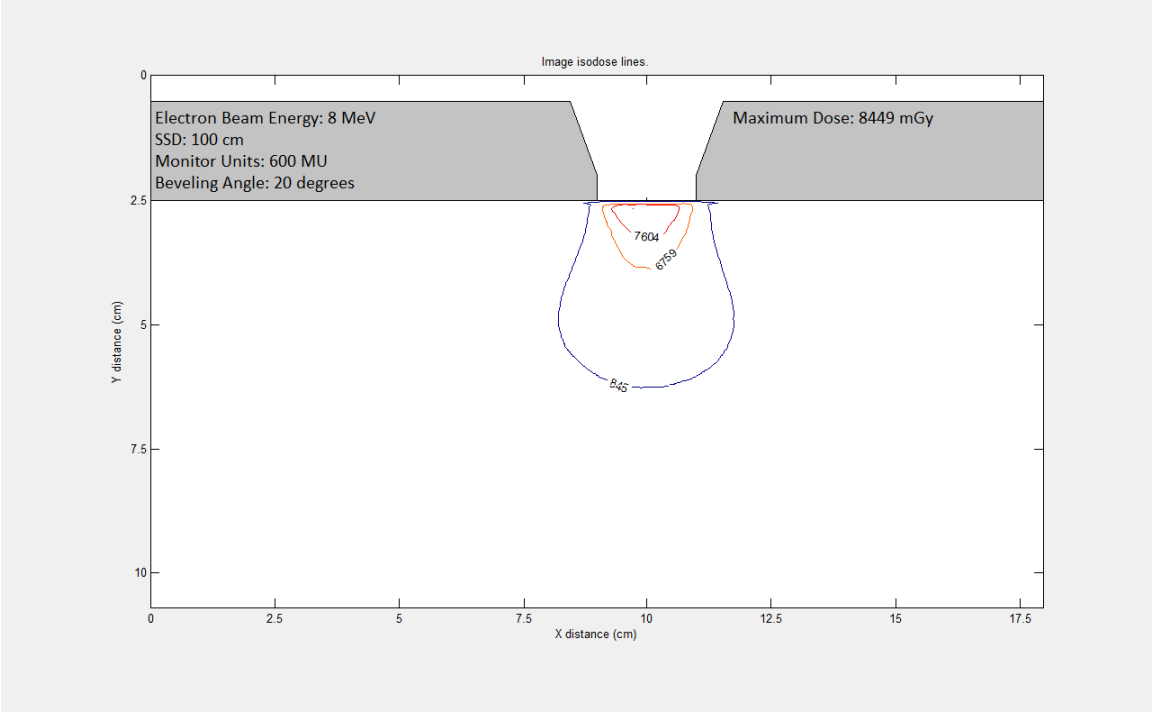

Figure 28. Isodose Lines of the 100%, 90%, 80%, and 10% Maximum Dose Under Cross-Section of the 20 Degree Cut Out Shot with an 8 MeV Electron Beam

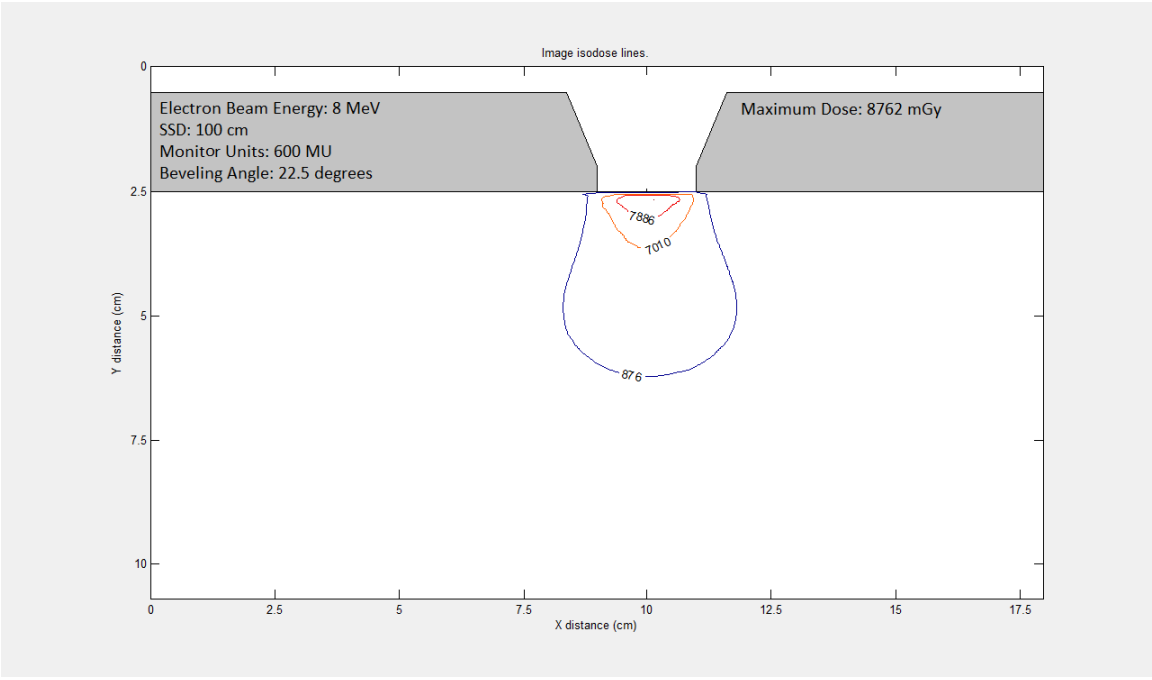

Figure 29. Isodose Lines of the 100%, 90%, 80%, and 10% Maximum Dose Under Cross-Section of the 22.5 Degree Cut Out Shot with an 8 MeV Electron Beam

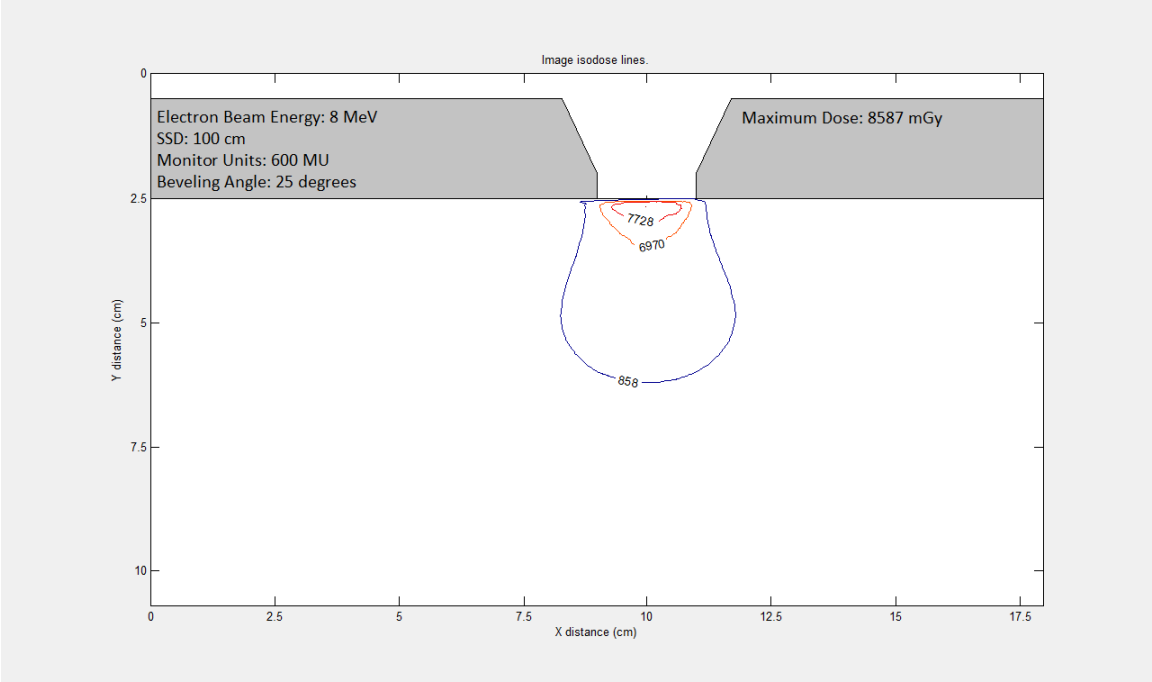

Figure 30. Isodose Lines of the 100%, 90%, 80%, and 10% Maximum Dose Under Cross-Section of the 25 Degree Cut Out Shot with an 8 MeV Electron Beam

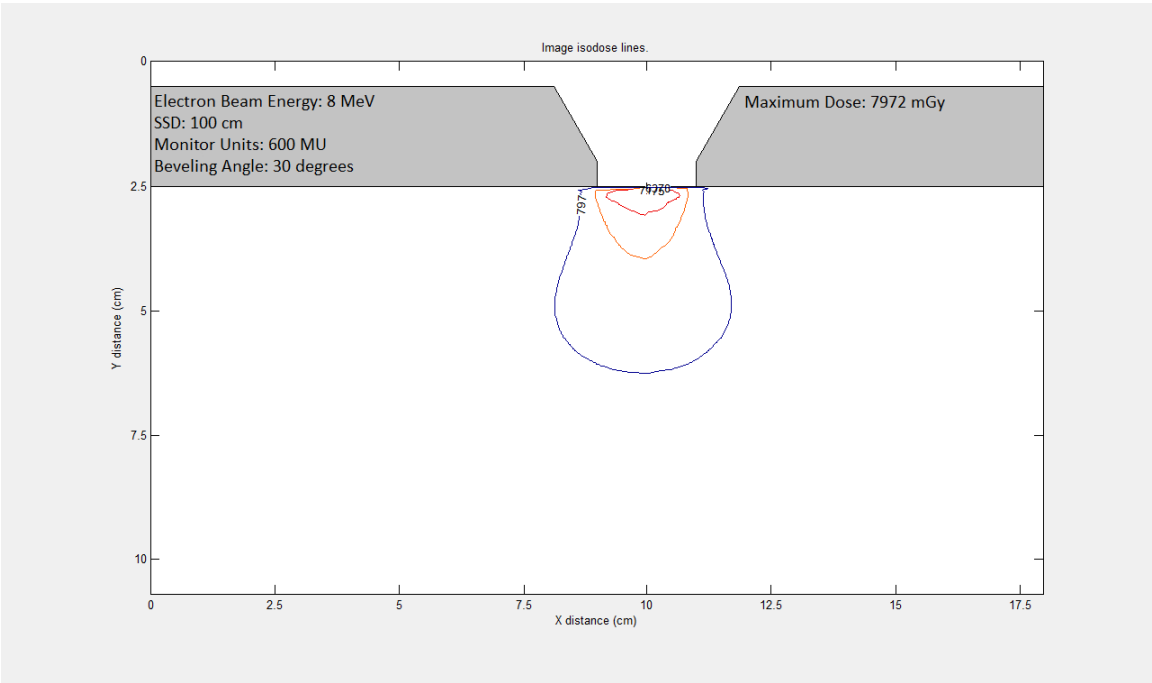

Figure 31. Isodose Lines of the 100%, 90%, 80%, and 10% Maximum Dose Under Cross-Section of the 30 Degree Cut Out Shot with an 8 MeV Electron Beam

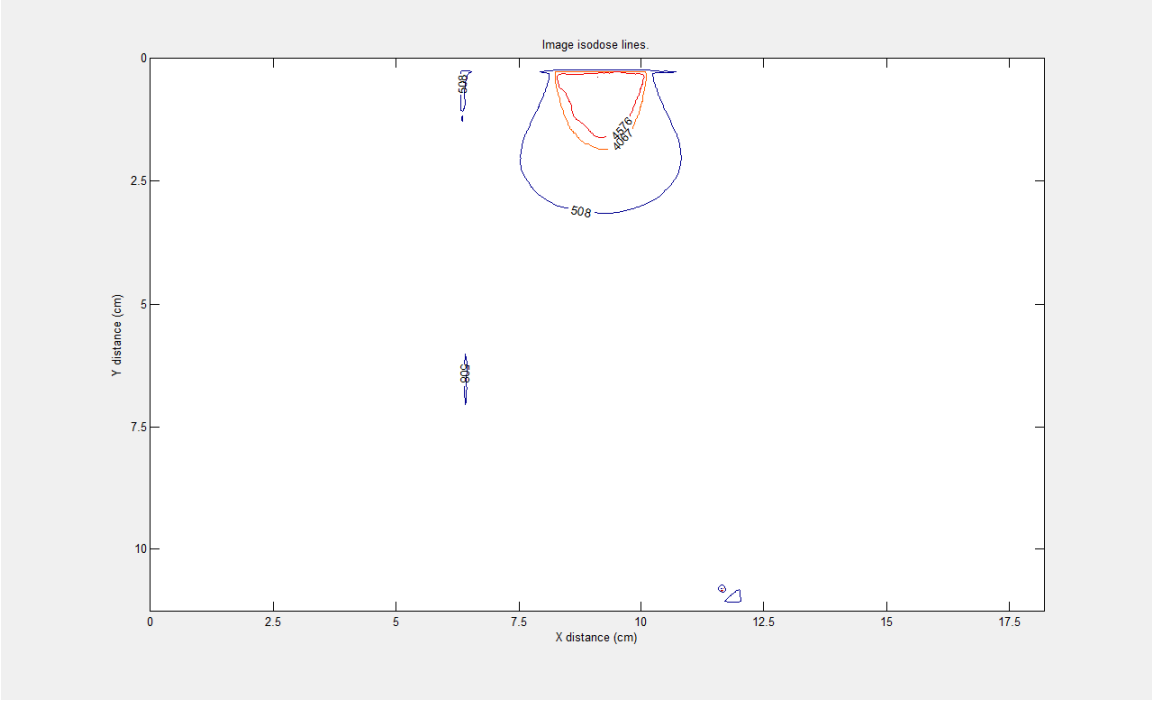

Figure 32. Isodose Lines of the 100%, 90%, 80%, and 10% Maximum Dose for the 0 Degree Cut Out Shot with a 6 MeV Electron Beam from the Reproducibility Study (Shot: 1 of 3)

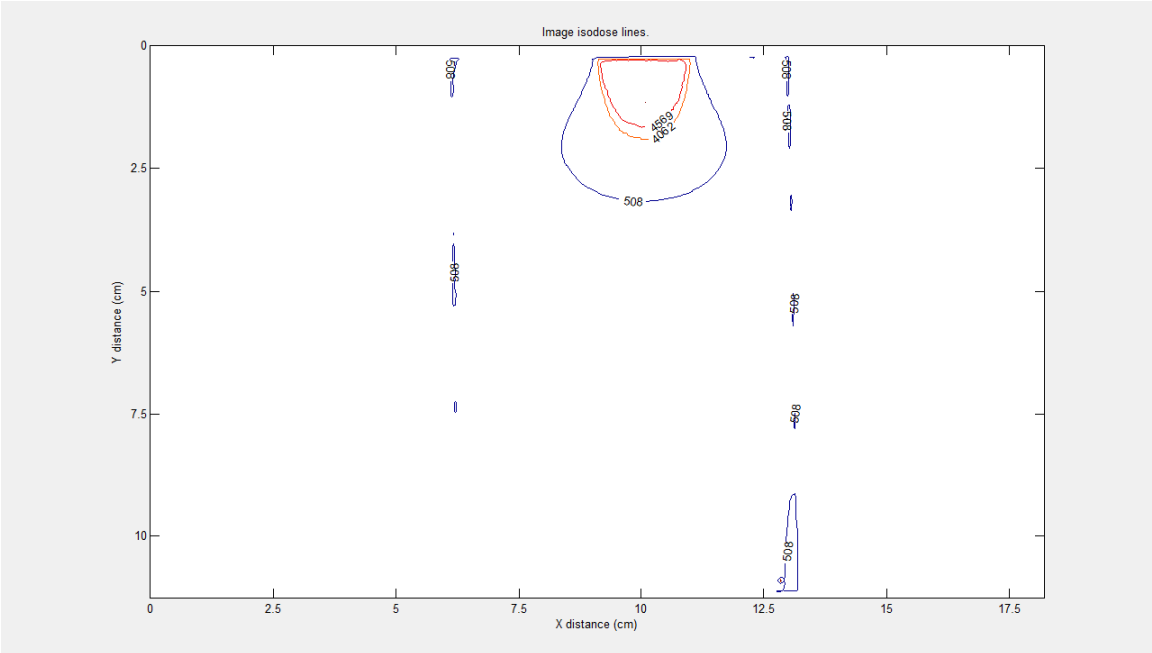

Figure 33. Isodose Lines of the 100%, 90%, 80%, and 10% Maximum Dose for the 0 Degree Cut Out Shot with a 6 MeV Electron Beam from the Reproducibility Study (Shot: 2 of 3)

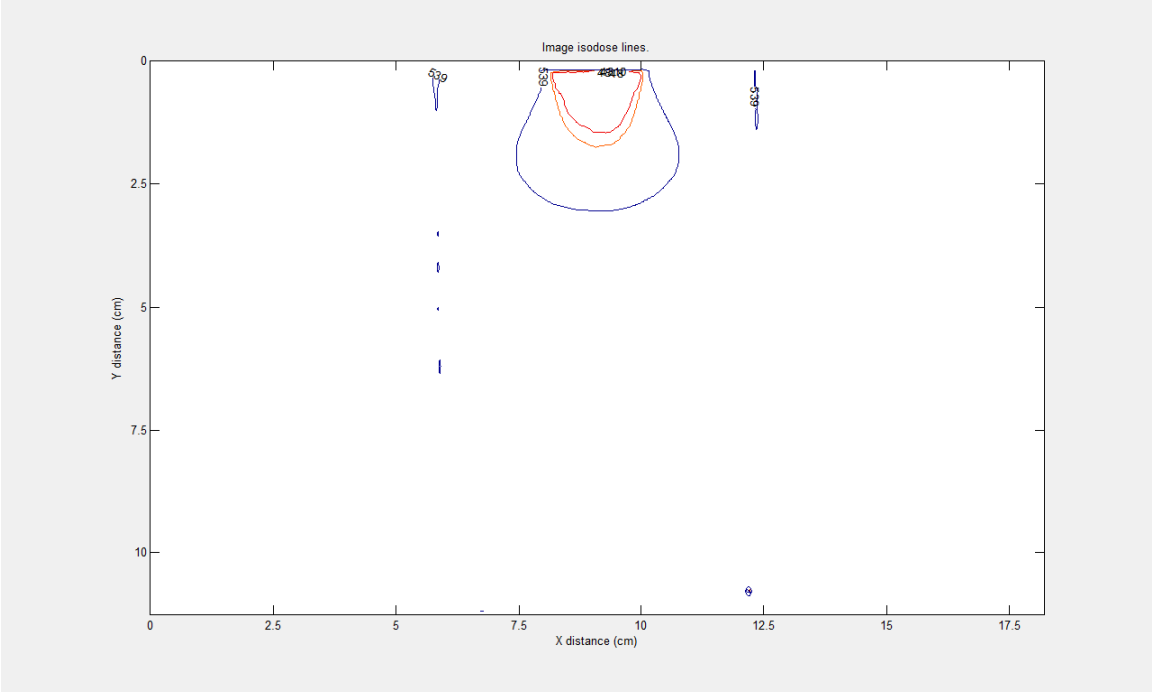

Figure 34. Isodose Lines of the 100%, 90%, 80%, and 10% Maximum Dose for the 0 Degree Cut Out Shot with a 6 MeV Electron Beam from the Reproducibility Study (Shot: 3 of 3)

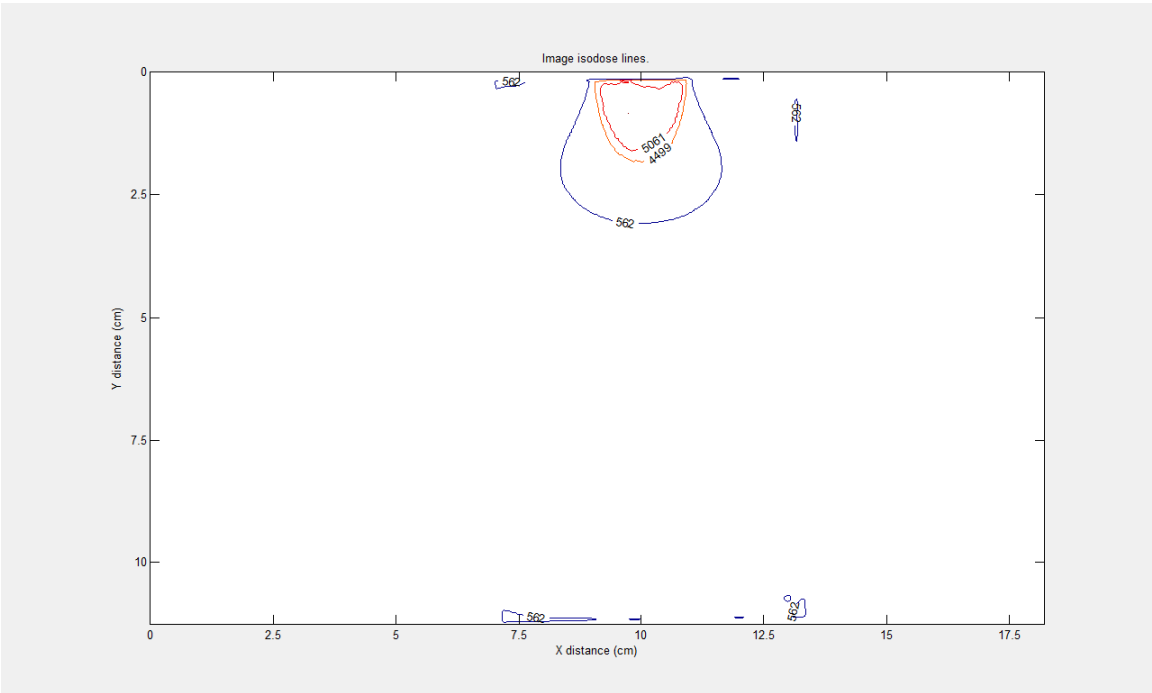

Figure 35. Isodose Lines of the 100%, 90%, 80%, and 10% Maximum Dose for the 5 Degree Cut Out Shot with a 6 MeV Electron Beam from the Reproducibility Study (Shot: 1 of 5)

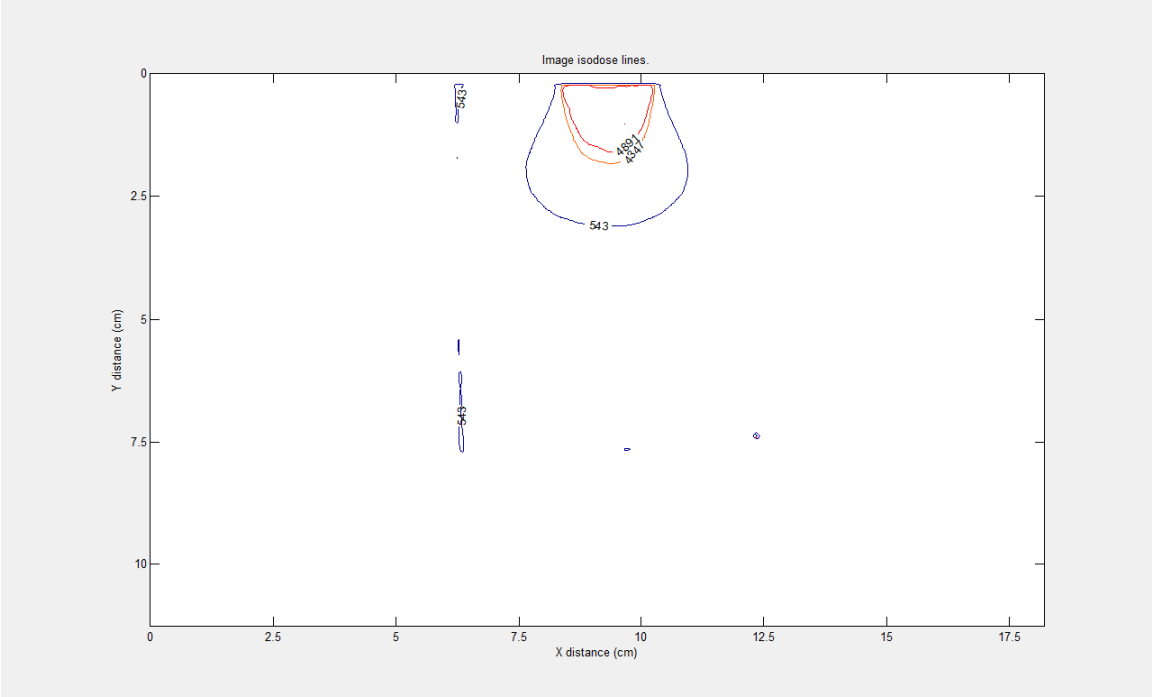

Figure 36. Isodose Lines of the 100%, 90%, 80%, and 10% Maximum Dose for the 5 Degree Cut Out Shot with a 6 MeV Electron Beam from the Reproducibility Study (Shot: 2 of 5)

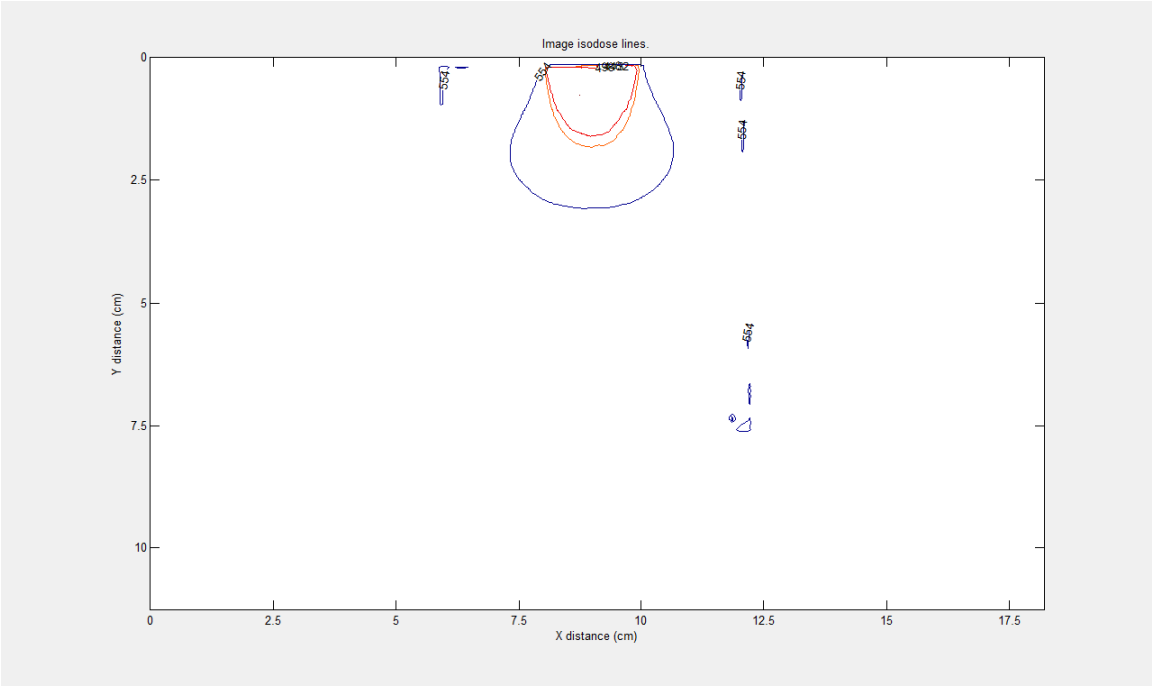

Figure 37. Isodose Lines of the 100%, 90%, 80%, and 10% Maximum Dose for the 5 Degree Cut Out Shot with a 6 MeV Electron Beam from the Reproducibility Study (Shot: 3 of 5)

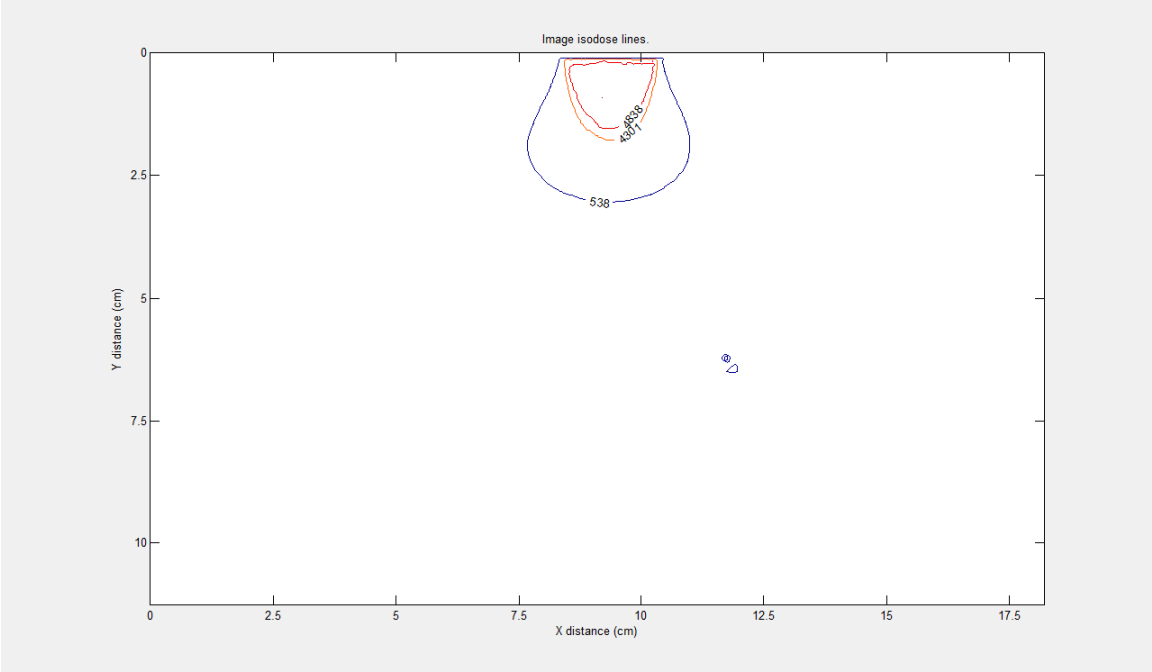

Figure 38. Isodose Lines of the 100%, 90%, 80%, and 10% Maximum Dose for the 5 Degree Cut Out Shot with a 6 MeV Electron Beam from the Reproducibility Study (Shot: 4 of 5)

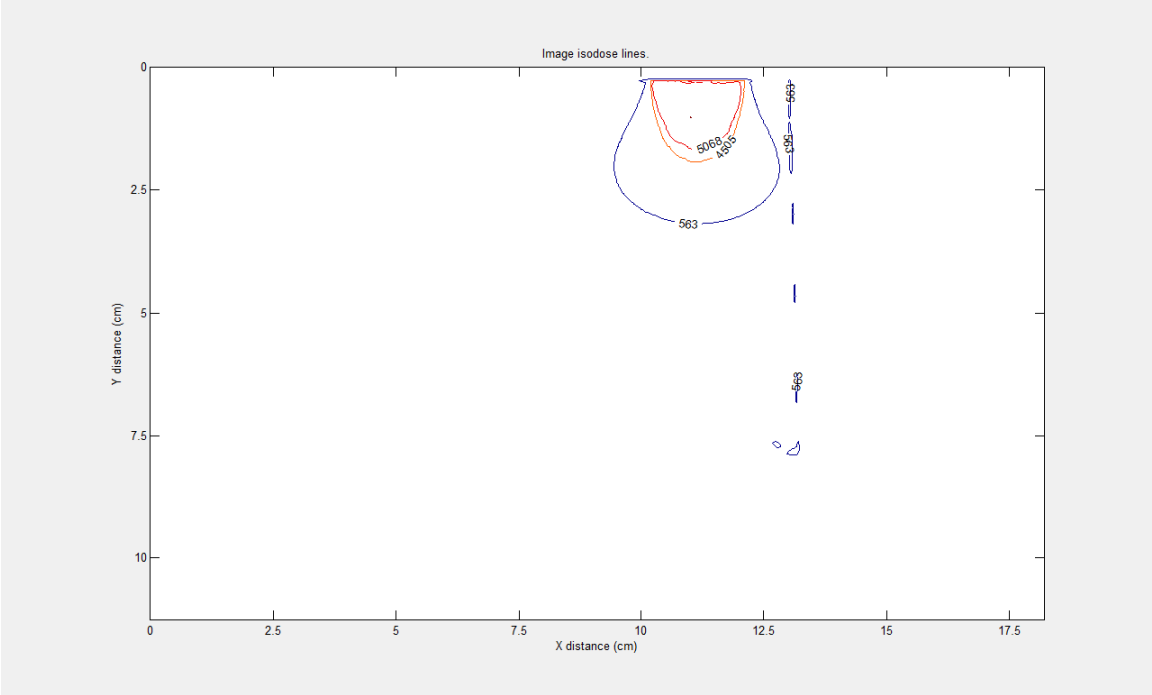

Figure 39. Isodose Lines of the 100%, 90%, 80%, and 10% Maximum Dose for the 5 Degree Cut Out Shot with a 6 MeV Electron Beam from the Reproducibility Study (Shot: 5 of 5)

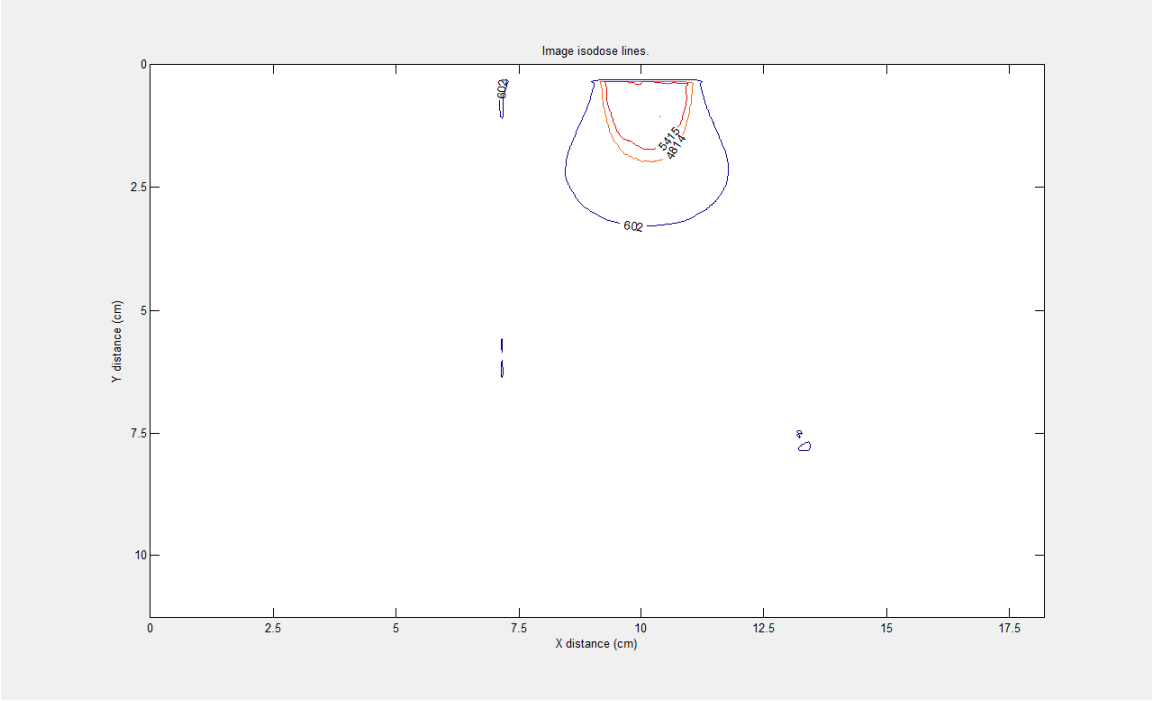

Figure 40. Isodose Lines of the 100%, 90%, 80%, and 10% Maximum Dose for the 10 Degree Cut Out Shot with a 6 MeV Electron Beam from the Reproducibility Study (Shot 1 of 3)

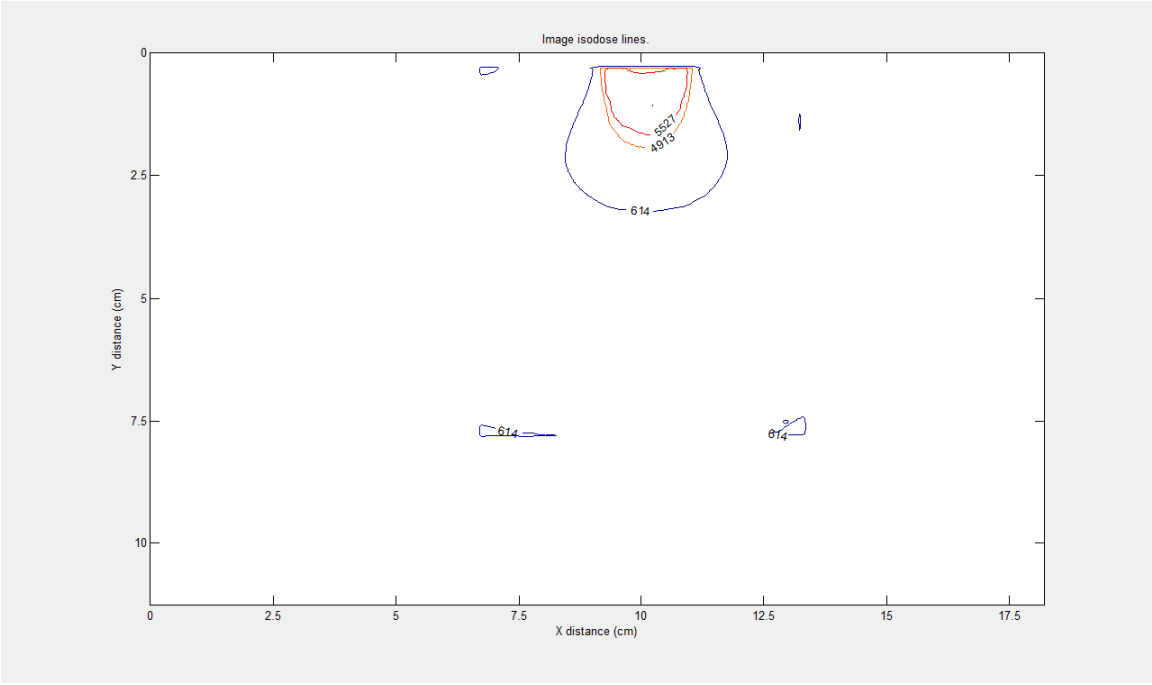

Figure 41. Isodose Lines of the 100%, 90%, 80%, and 10% Maximum Dose for the 10 Degree Cut Out Shot with a 6 MeV Electron Beam from the Reproducibility Study (Shot 2 of 3)

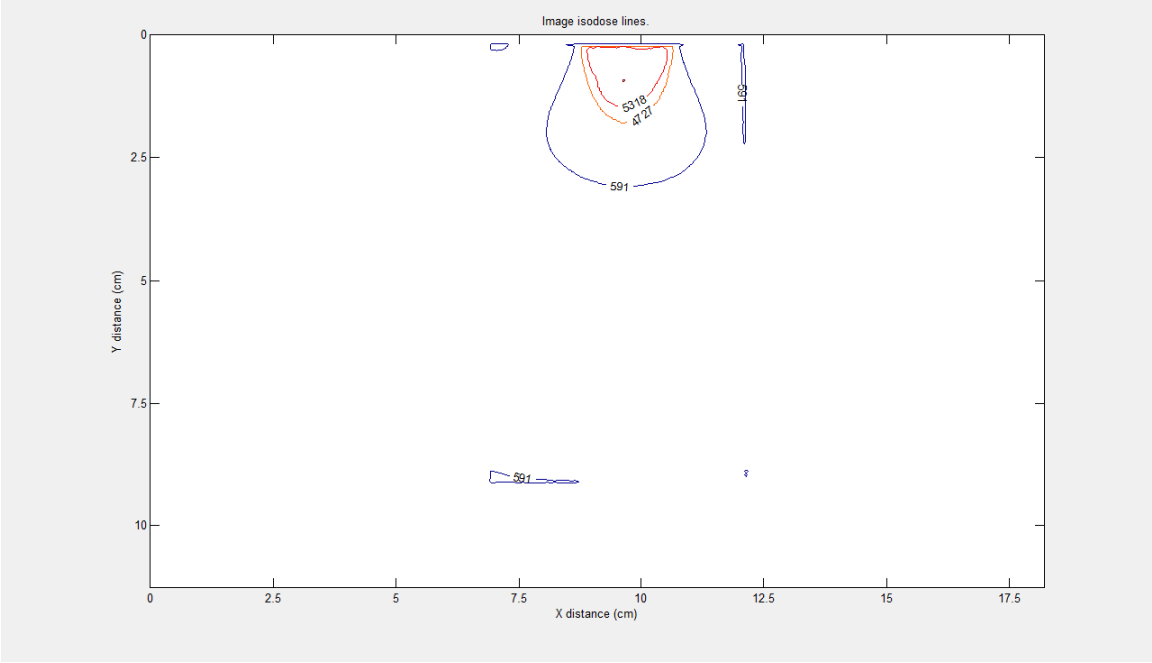

Figure 42. Isodose Lines of the 100%, 90%, 80%, and 10% Maximum Dose for the 10 Degree Cut Out Shot with a 6 MeV Electron Beam from the Reproducibility Study (Shot 3 of 3)

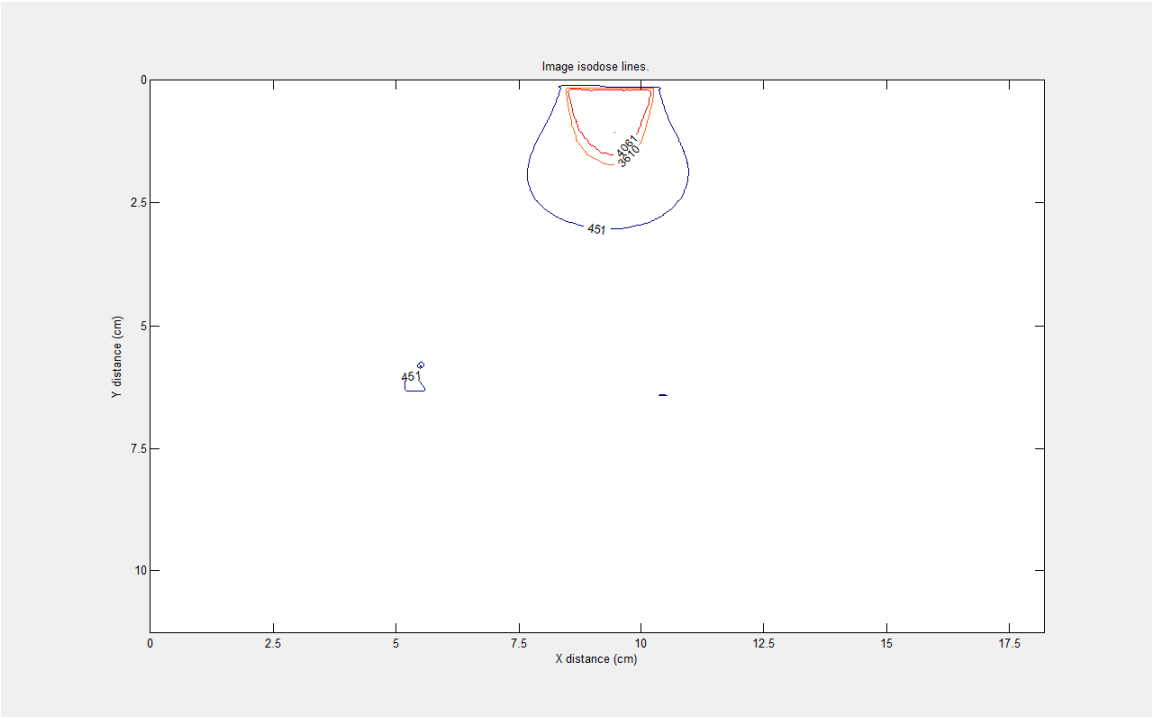

Figure 43. Isodose Lines of the 100%, 90%, 80%, and 10% Maximum Dose with the 5 Degree Cut Out Shot with a 6 MeV Electron Beam at 0.00 Degrees Obliquity from the Obliquity Study (Shot: 1 of 2)

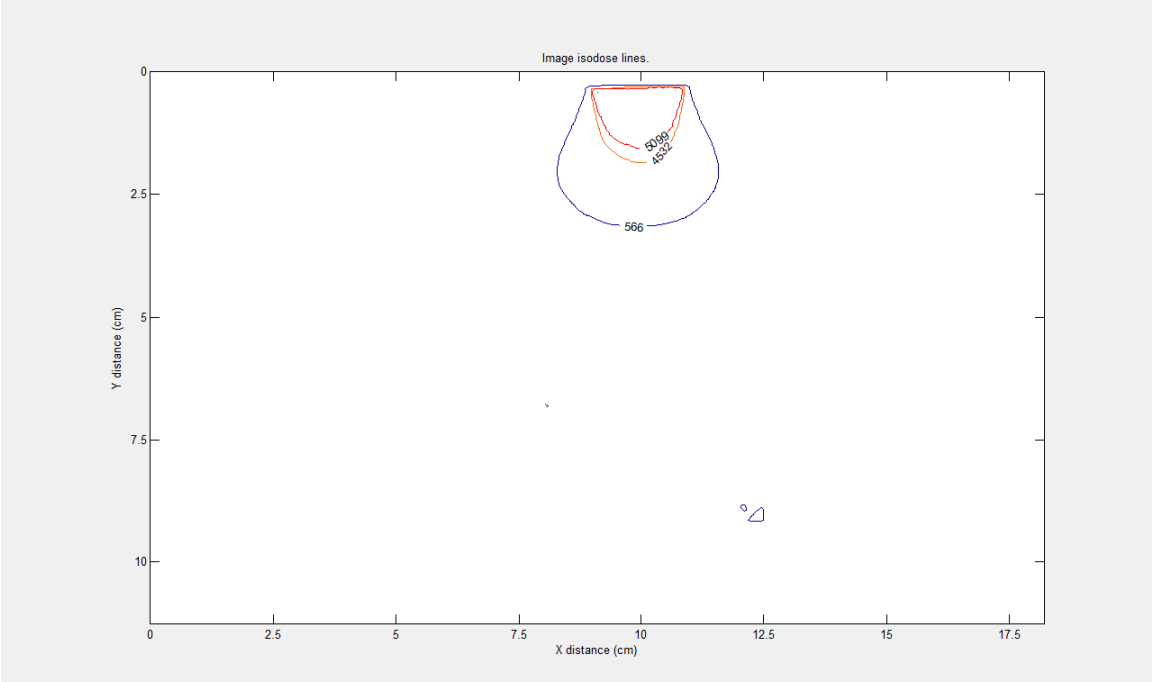

Figure 44. Isodose Lines of the 100%, 90%, 80%, and 10% Maximum Dose with the 5 Degree Cut Out Shot with a 6 MeV Electron Beam at 0.00 Degrees Obliquity from the Obliquity Study (Shot: 2 of 2)

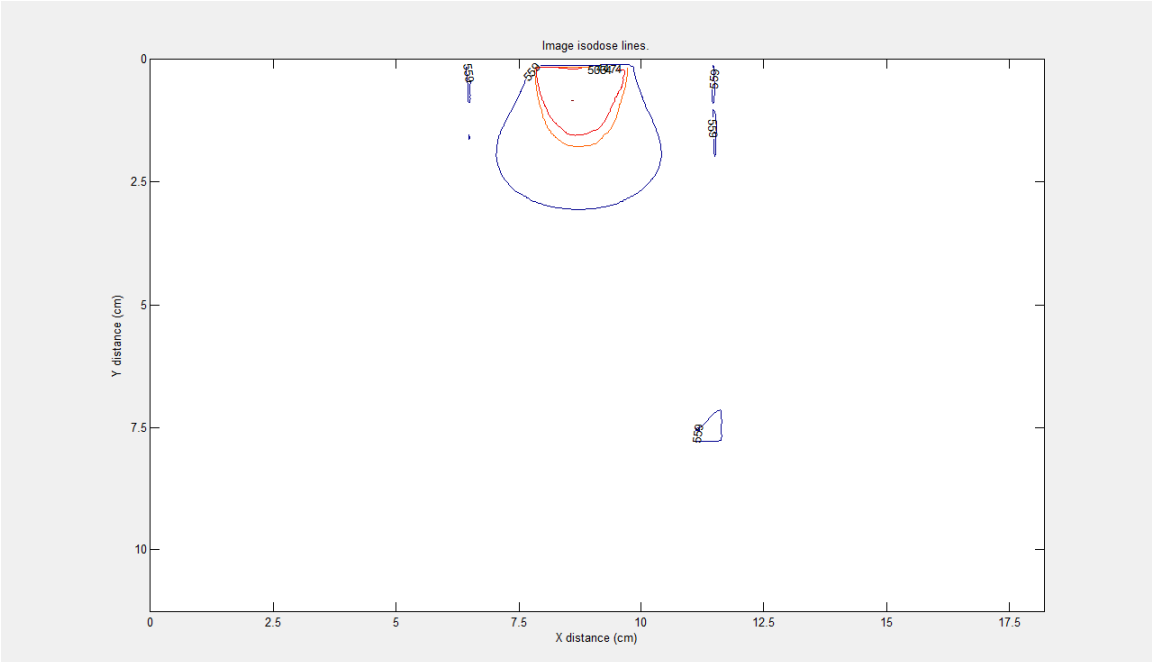

Figure 45. Isodose Lines of the 100%, 90%, 80%, and 10% Maximum Dose with the 5 Degree Cut Out Shot with a 6 MeV Electron Beam at 2.00 Degrees Obliquity from the Obliquity Study (Shot: 1 of 2)

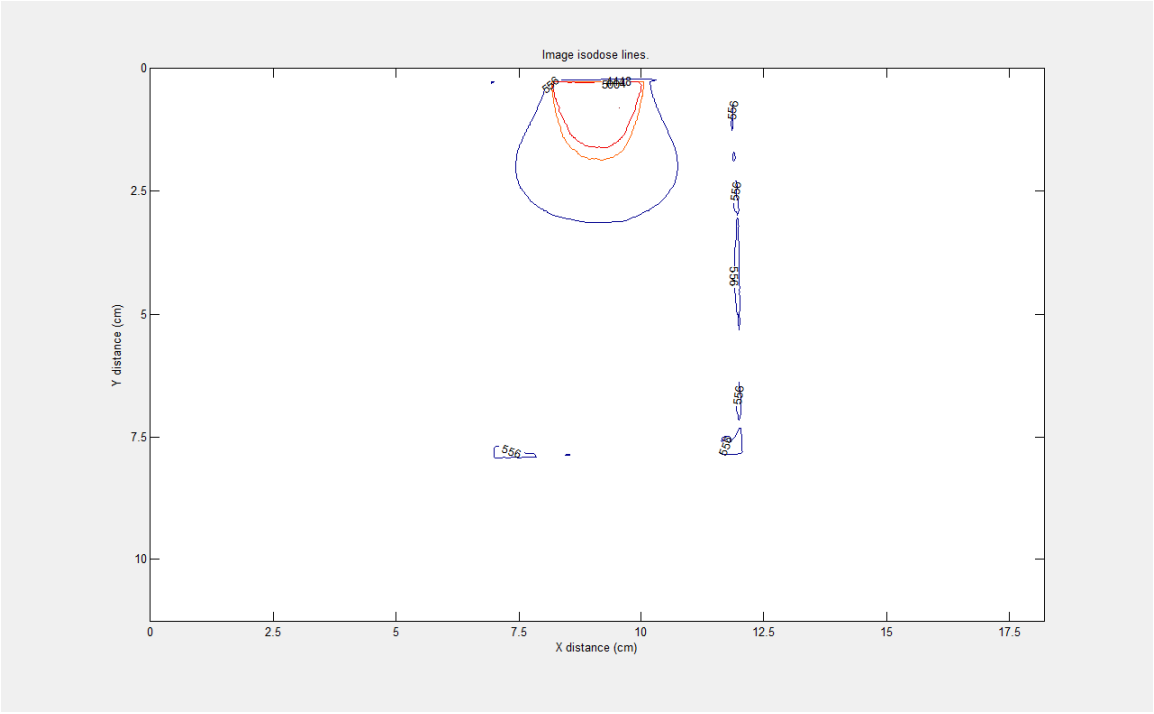

Figure 46. Isodose Lines of the 100%, 90%, 80%, and 10% Maximum Dose with the 5 Degree Cut Out Shot with a 6 MeV Electron Beam at 2.00 Degrees Obliquity from the Obliquity Study (Shot: 2 of 2)

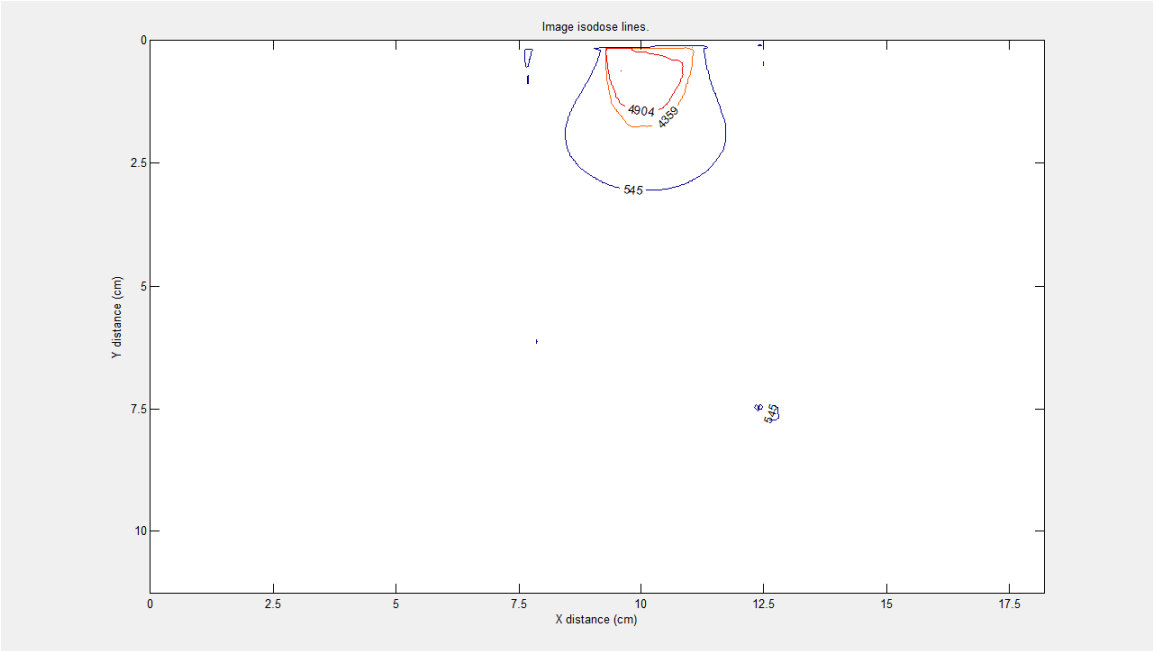

Figure 47. Isodose Lines of the 100%, 90%, 80%, and 10% Maximum Dose with the 5 Degree Cut Out Shot with a 6 MeV Electron Beam at 5.00 Degrees Obliquity from the Obliquity Study (Shot: 1 of 2)

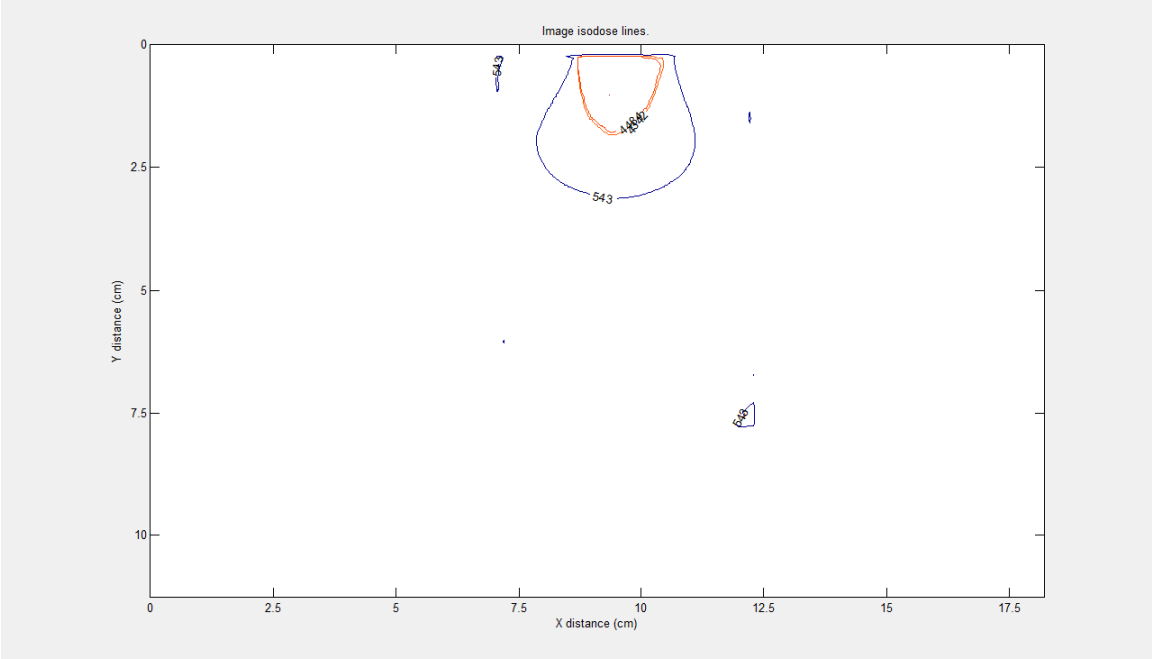

Figure 48. Isodose Lines of the 100%, 90%, 80%, and 10% Maximum Dose with the 5 Degree Cut Out Shot with a 6 MeV Electron Beam at 5.00 Degrees Obliquity from the Obliquity Study (Shot: 2 of 2)

Appendix B

Appendix B contains the central-axis percentage depth dose curves for the 6 MeV study, the 8 MeV study, and the reproducibility study. The reproducibility study contained a background in all of the images. This background is labeled as 0% as it is present everywhere. The maximum dose along the central axis is reported along with the maximum dose in the field.

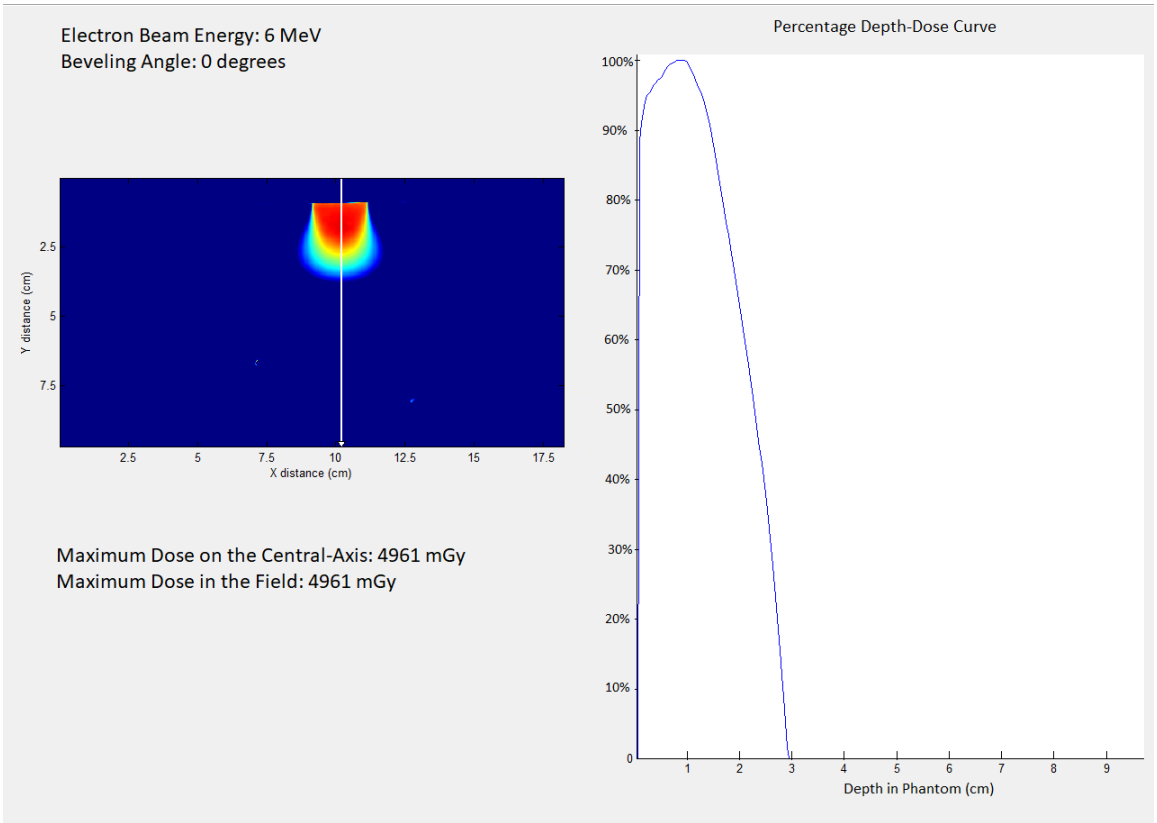

Figure 49. Central-Axis Percentage Depth-Dose Curve for the 0 degree cut out shot with a 6 MeV Electron Beam

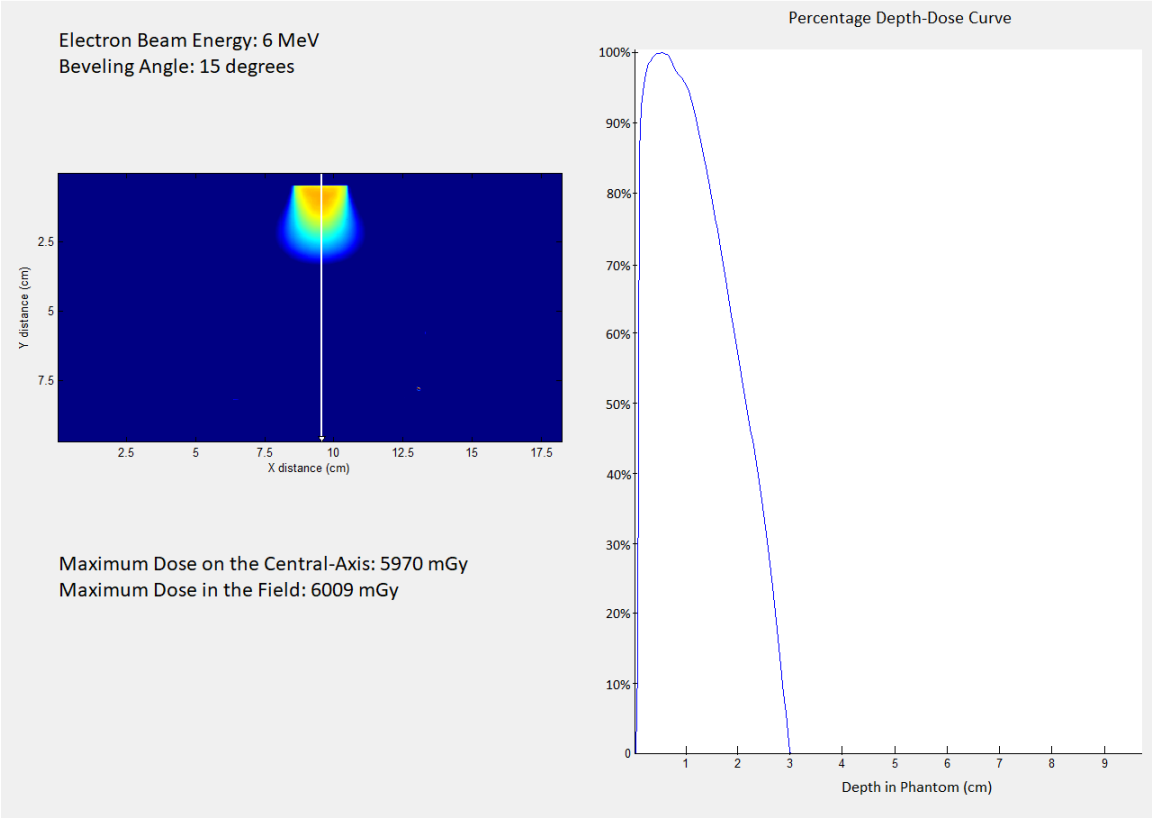

Figure 50. Central-Axis Percentage Depth-Dose Curve for the 15 degree cut out shot with a 6 MeV Electron Beam

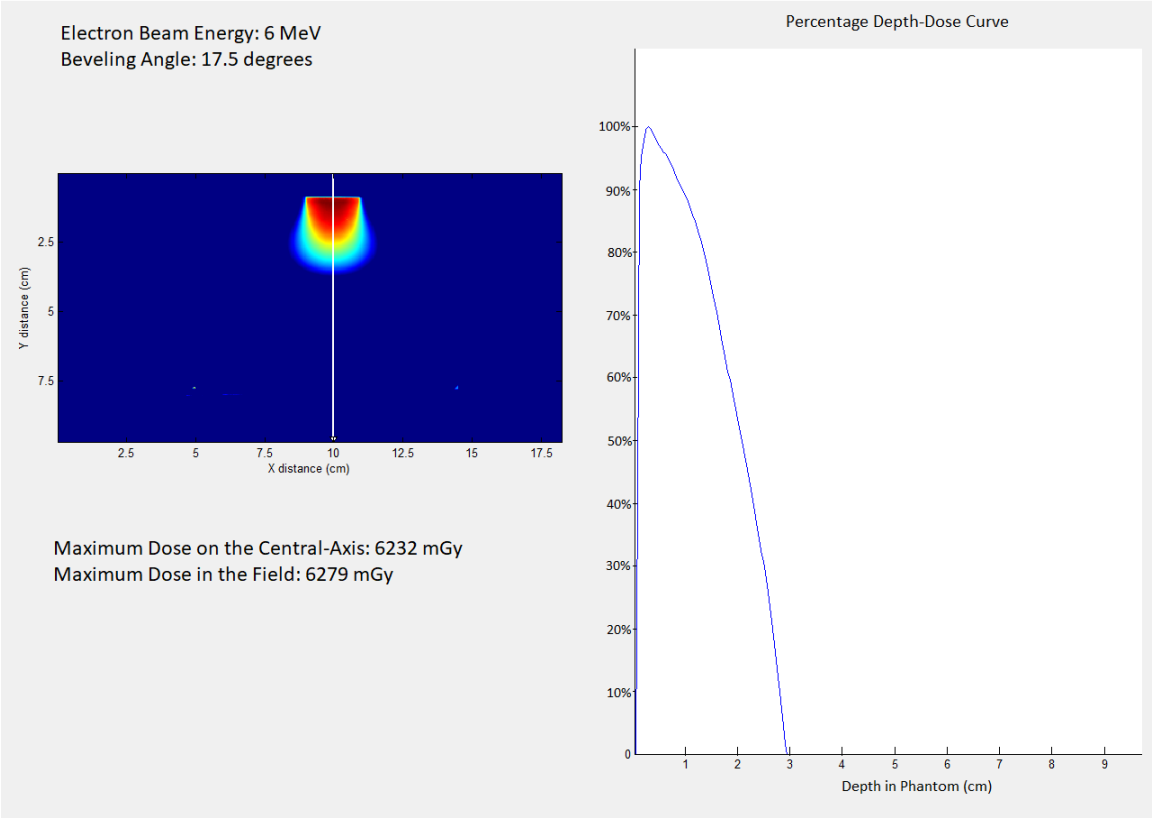

Figure 51. Central-Axis Percentage Depth-Dose Curve for the 17.5 degree cut out shot with a 6 MeV Electron Beam

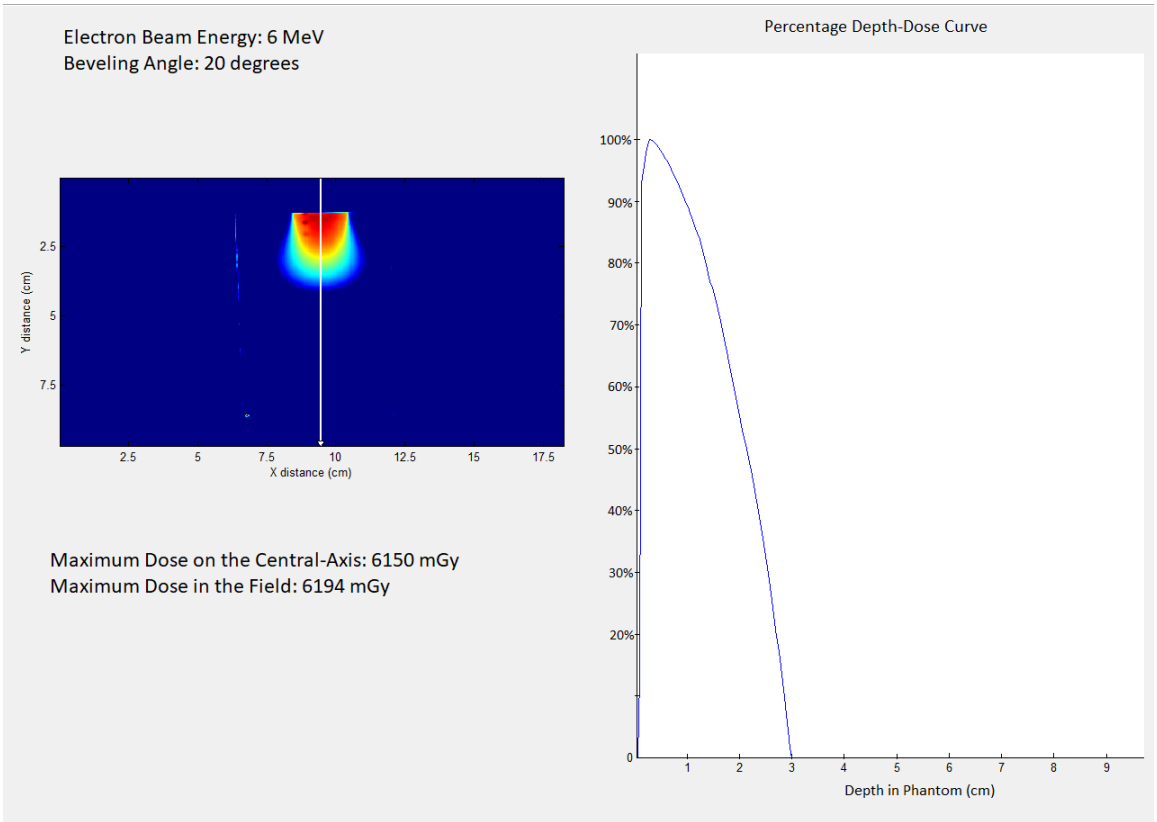

Figure 52. Central-Axis Percentage Depth-Dose Curve for the 20 degree cut out shot with a 6 MeV Electron Beam

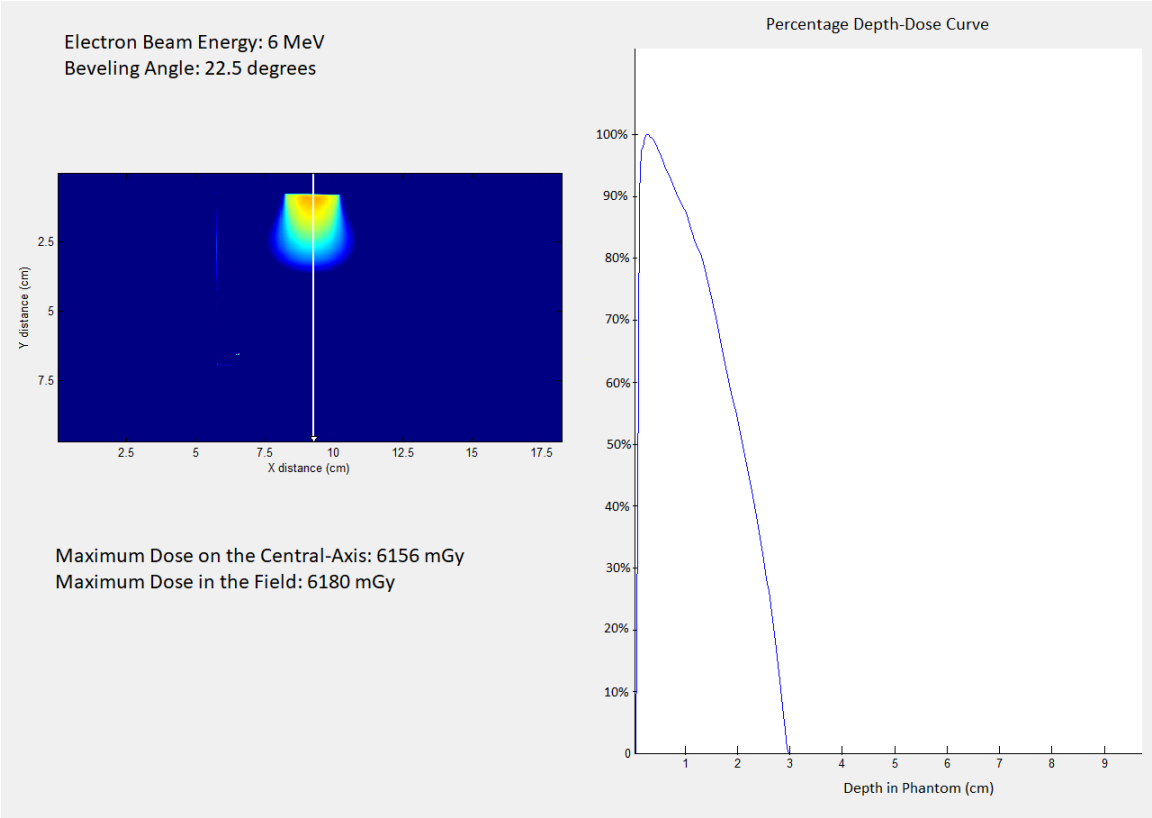

Figure 53. Central-Axis Percentage Depth-Dose Curve for the 0 degree cut out shot with a 6 MeV Electron Beam

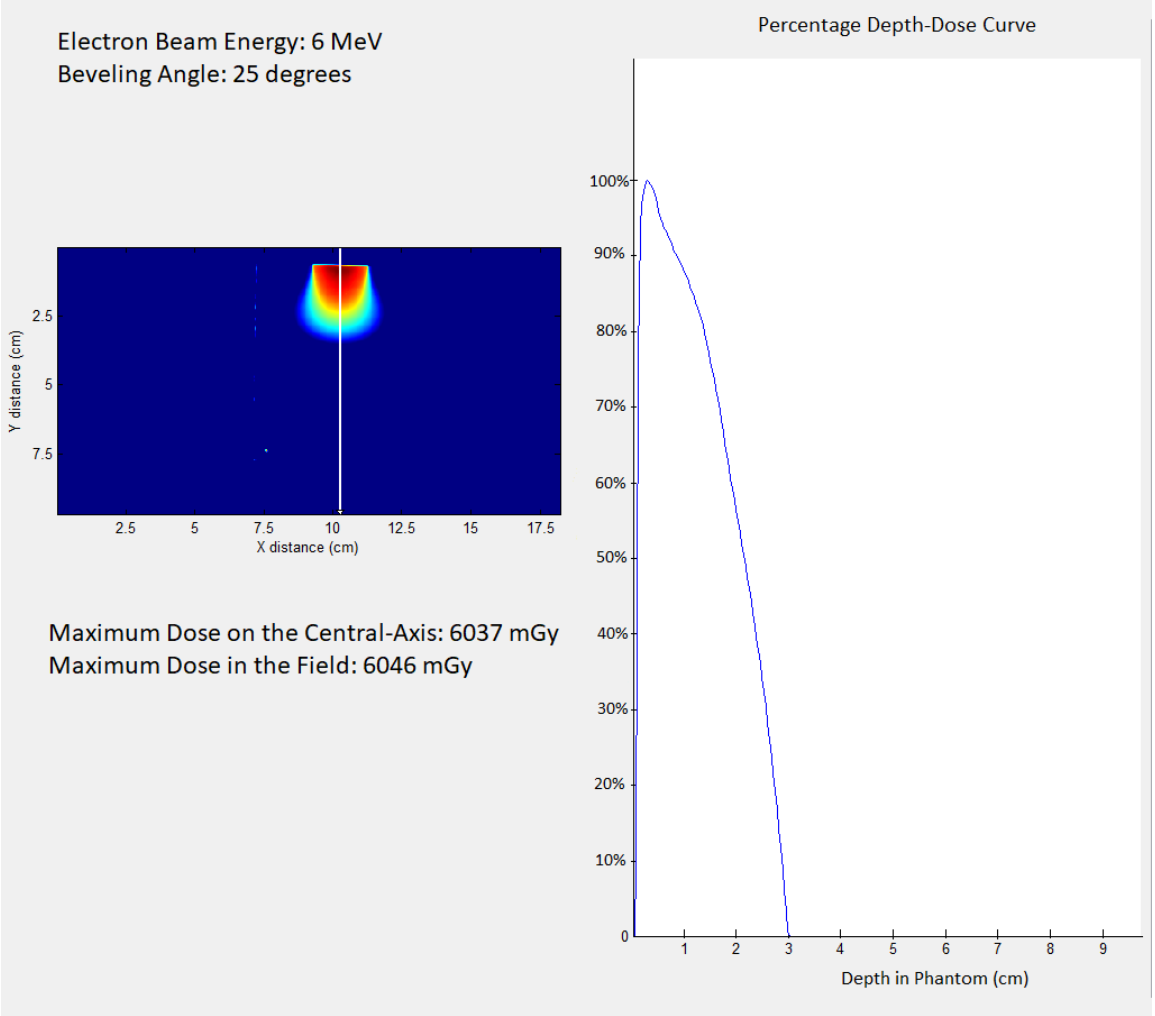

Figure 54. Central-Axis Percentage Depth-Dose Curve for the 25 degree cut out shot with a 6 MeV Electron Beam

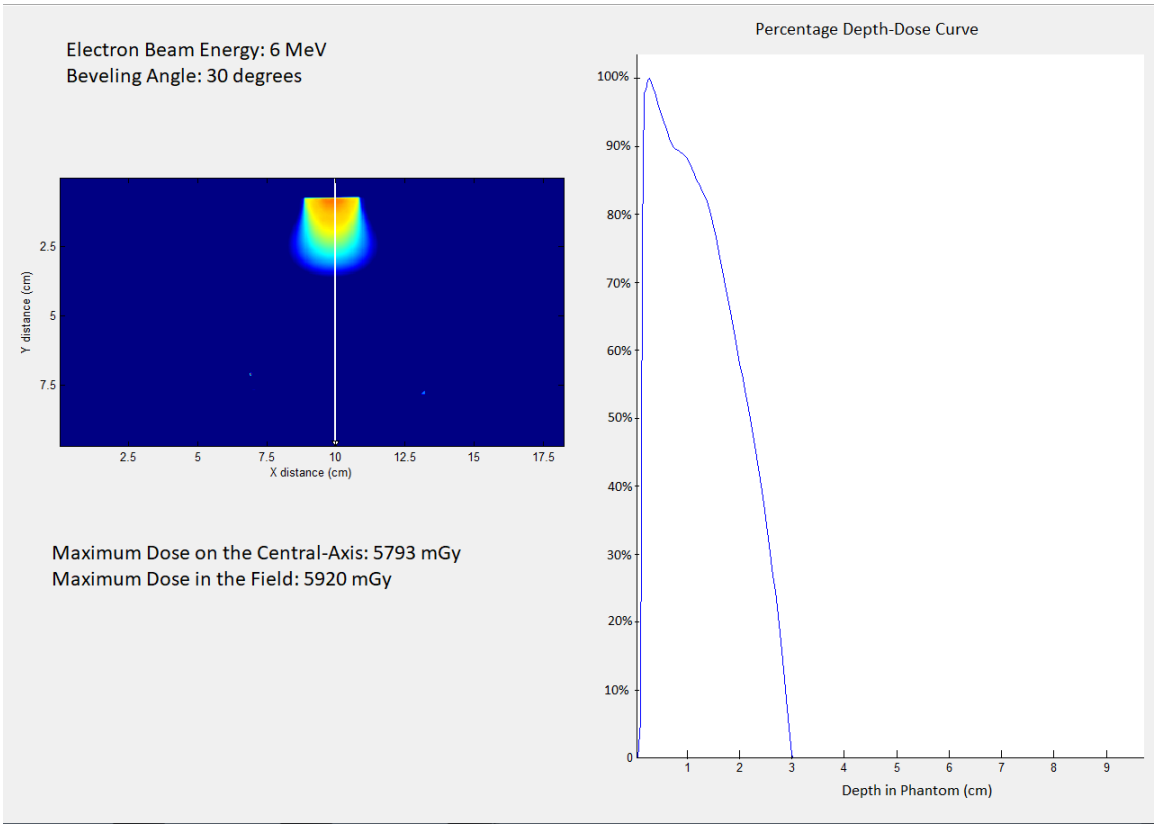

Figure 55. Central-Axis Percentage Depth-Dose Curve for the 30 degree cut out shot with a 6 MeV Electron Beam

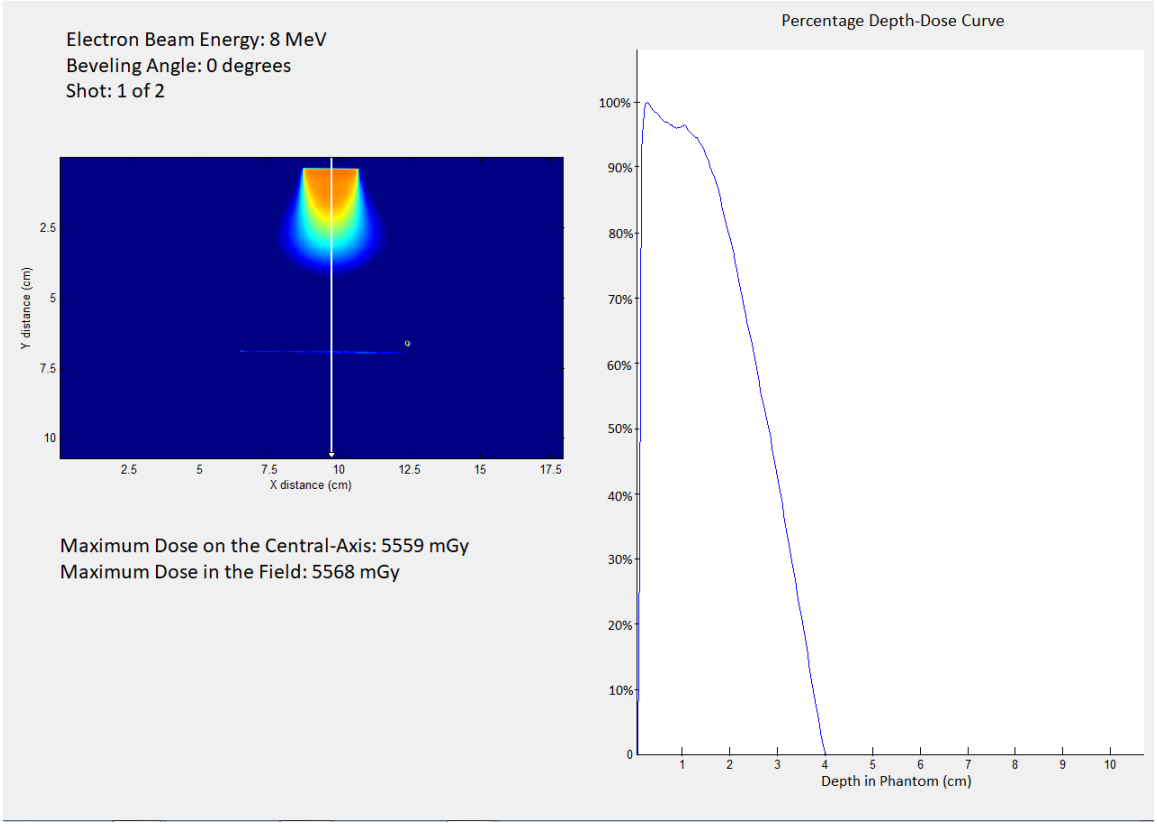

Figure 56. Central-Axis Percentage Depth-Dose Curve for the 0 degree cut out shot with an 8 MeV Electron Beam (Shot: 1 of 2)

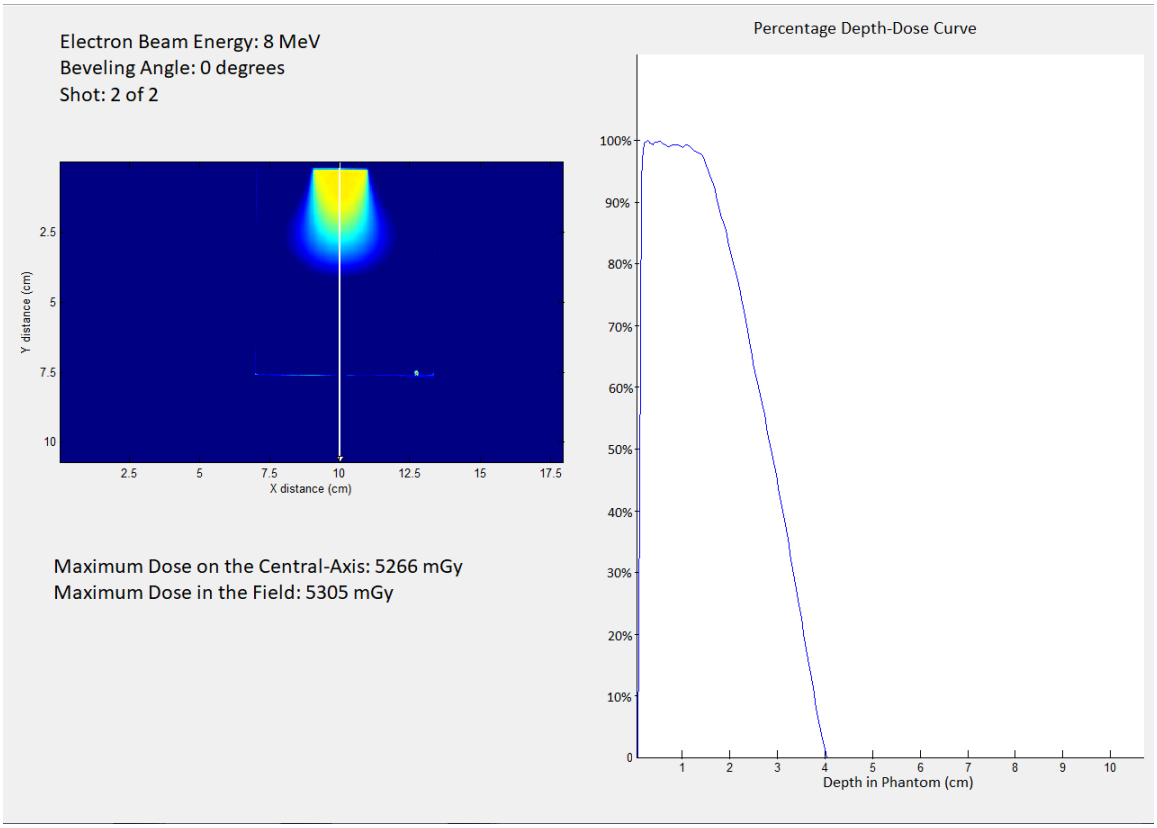

Figure 57. Central-Axis Percentage Depth-Dose Curve for the 0 degree cut out shot with an 8 MeV Electron Beam (Shot: 2 of 2)

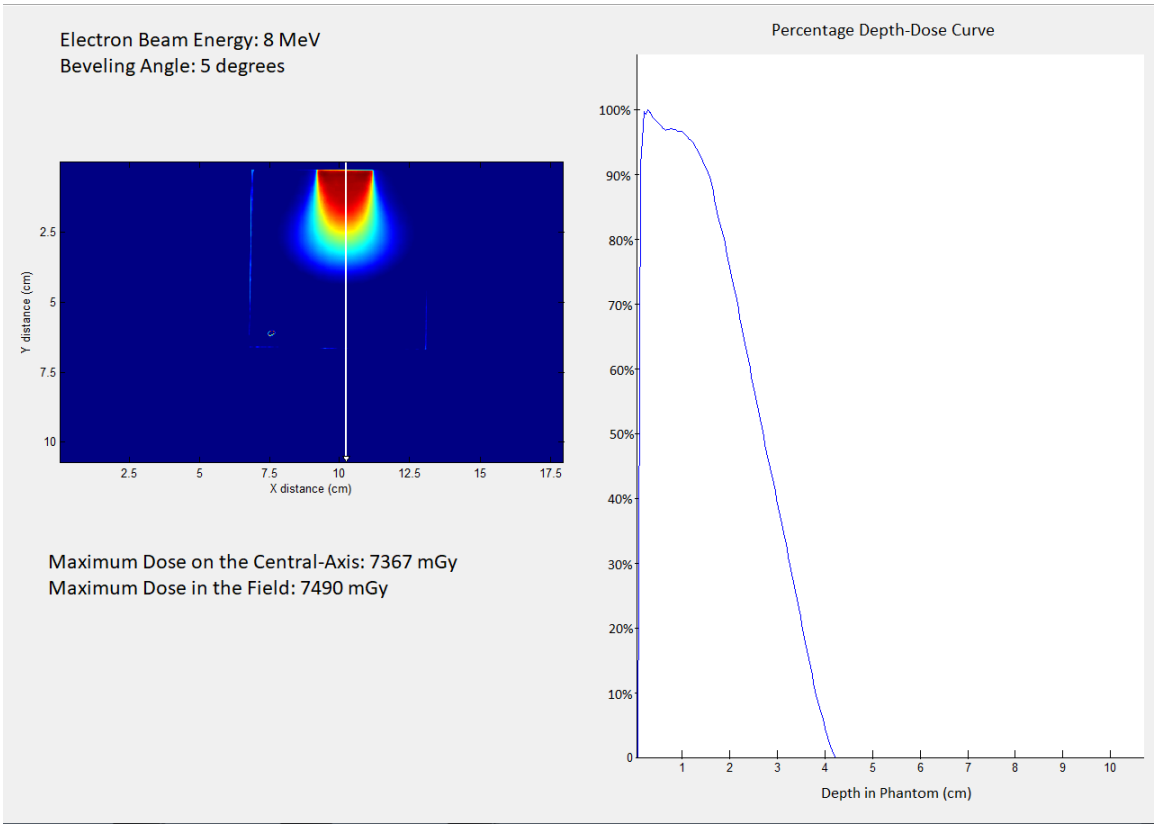

Figure 58. Central-Axis Percentage Depth-Dose Curve for the 5 degree cut out shot with an 8 MeV Electron Beam

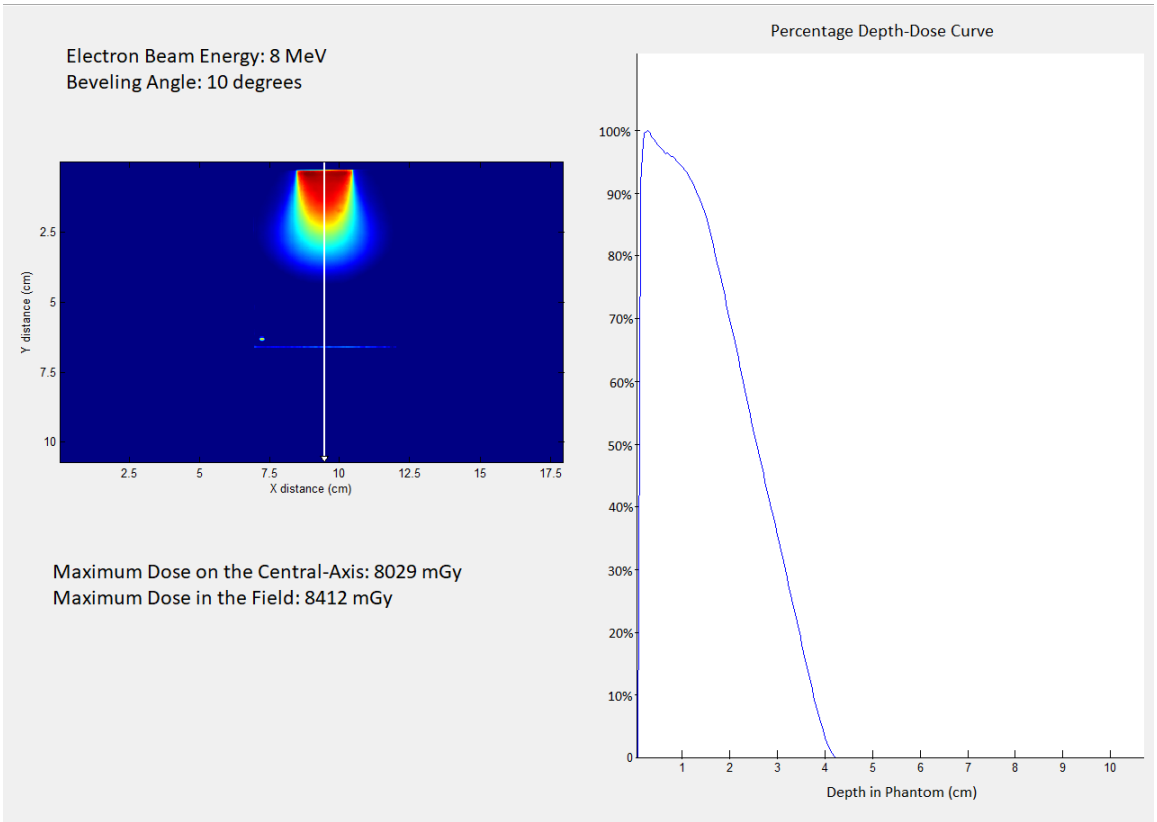

Figure 59. Central-Axis Percentage Depth-Dose Curve for the 10 degree cut out shot with an 8 MeV Electron Beam

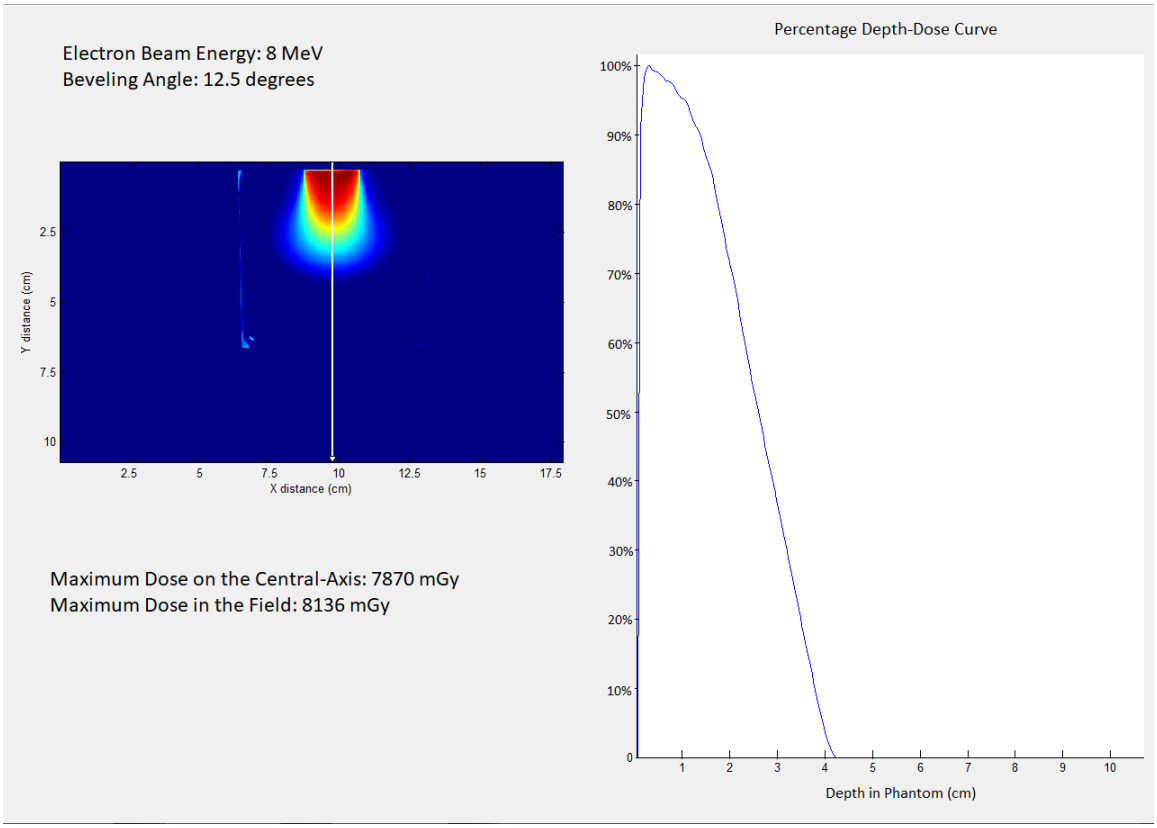

Figure 60. Central-Axis Percentage Depth-Dose Curve for the 12.5 degree cut out shot with an 8 MeV Electron Beam

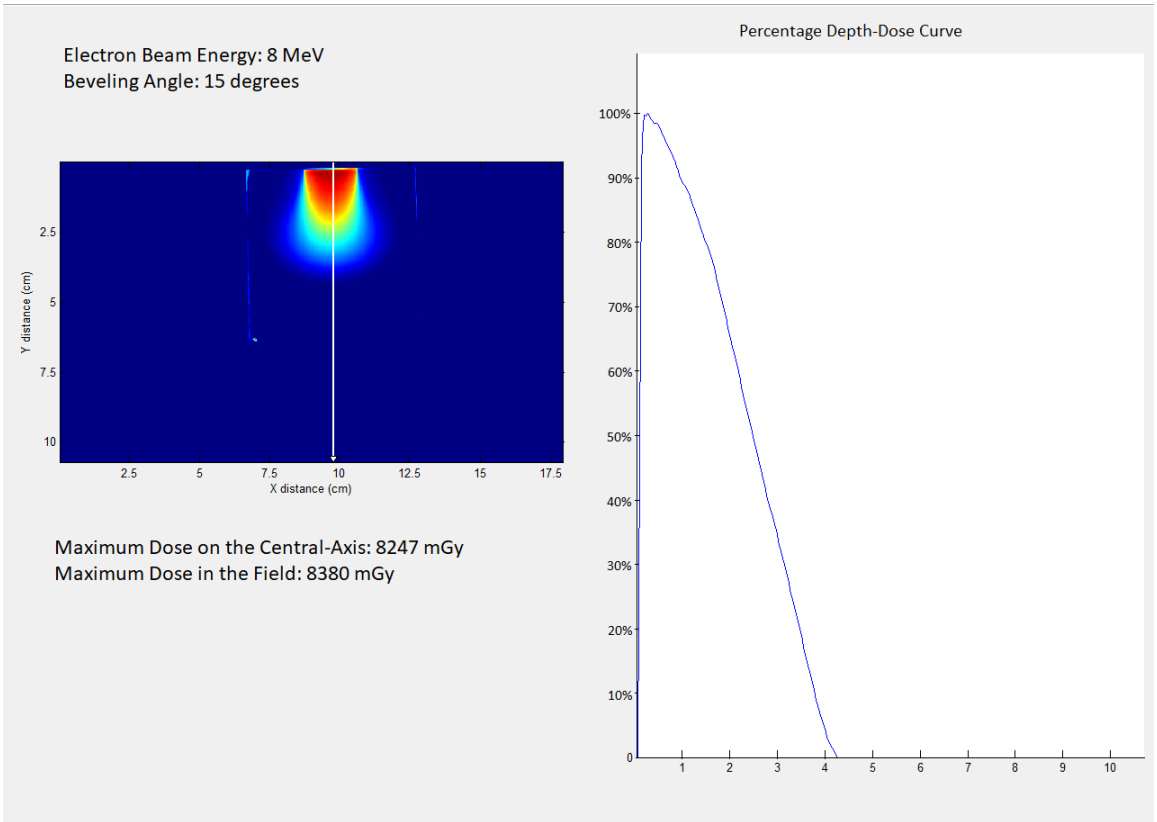

Figure 61. Central-Axis Percentage Depth-Dose Curve for the 15 degree cut out shot with an 8 MeV Electron Beam

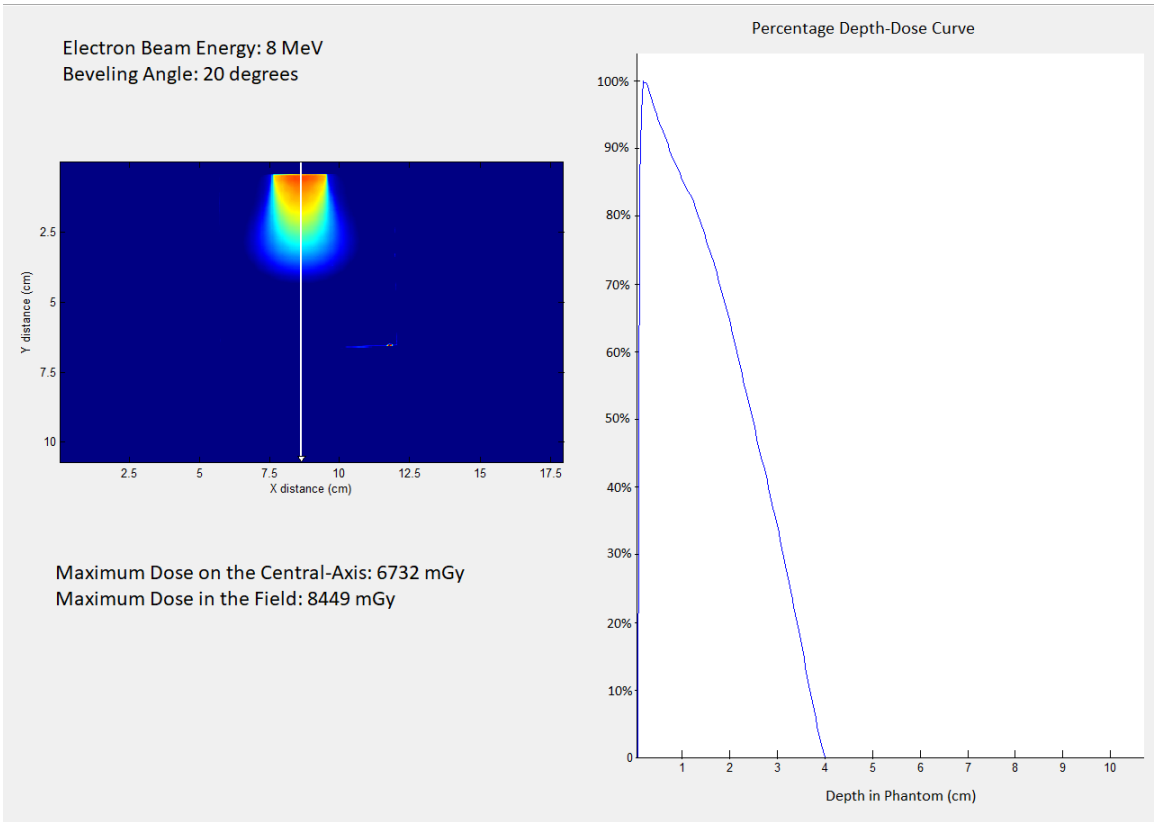

Figure 62. Central-Axis Percentage Depth-Dose Curve for the 20 degree cut out shot with an 8 MeV Electron Beam

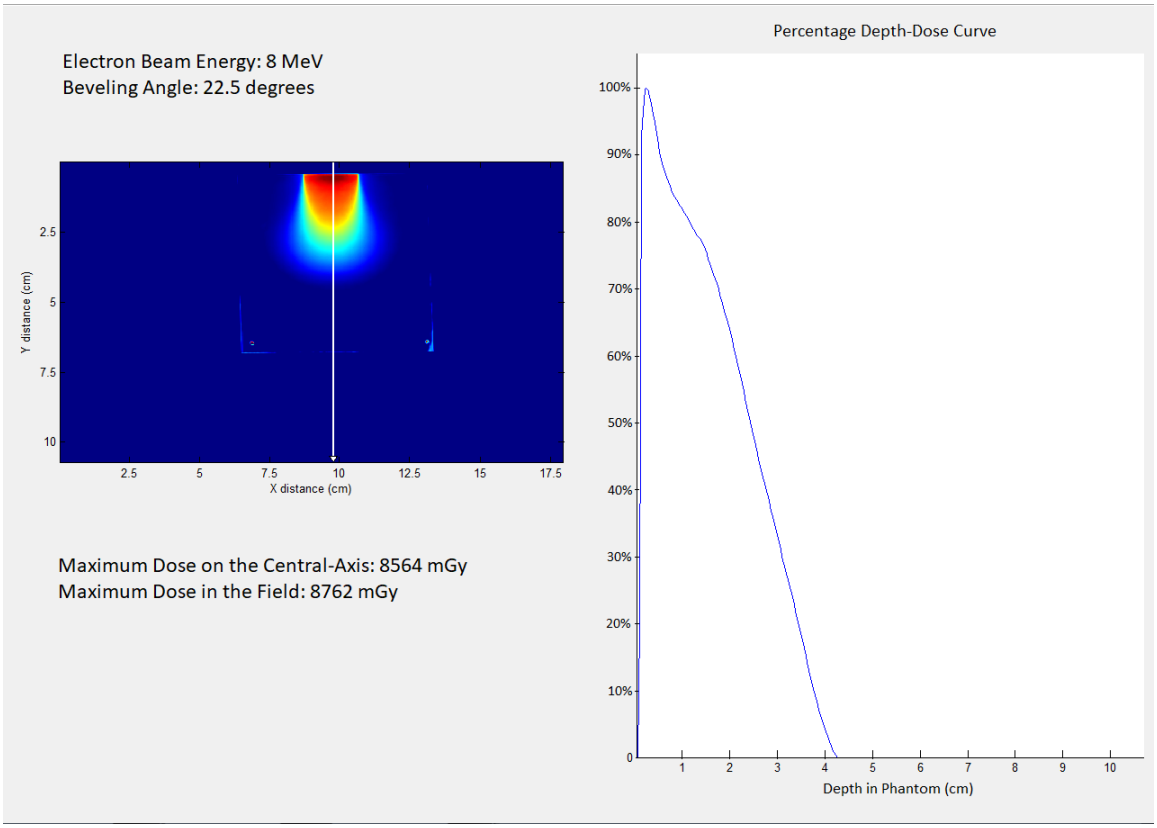

Figure 63. Central-Axis Percentage Depth-Dose Curve for the 22.5 degree cut out shot with an 8 MeV Electron Beam

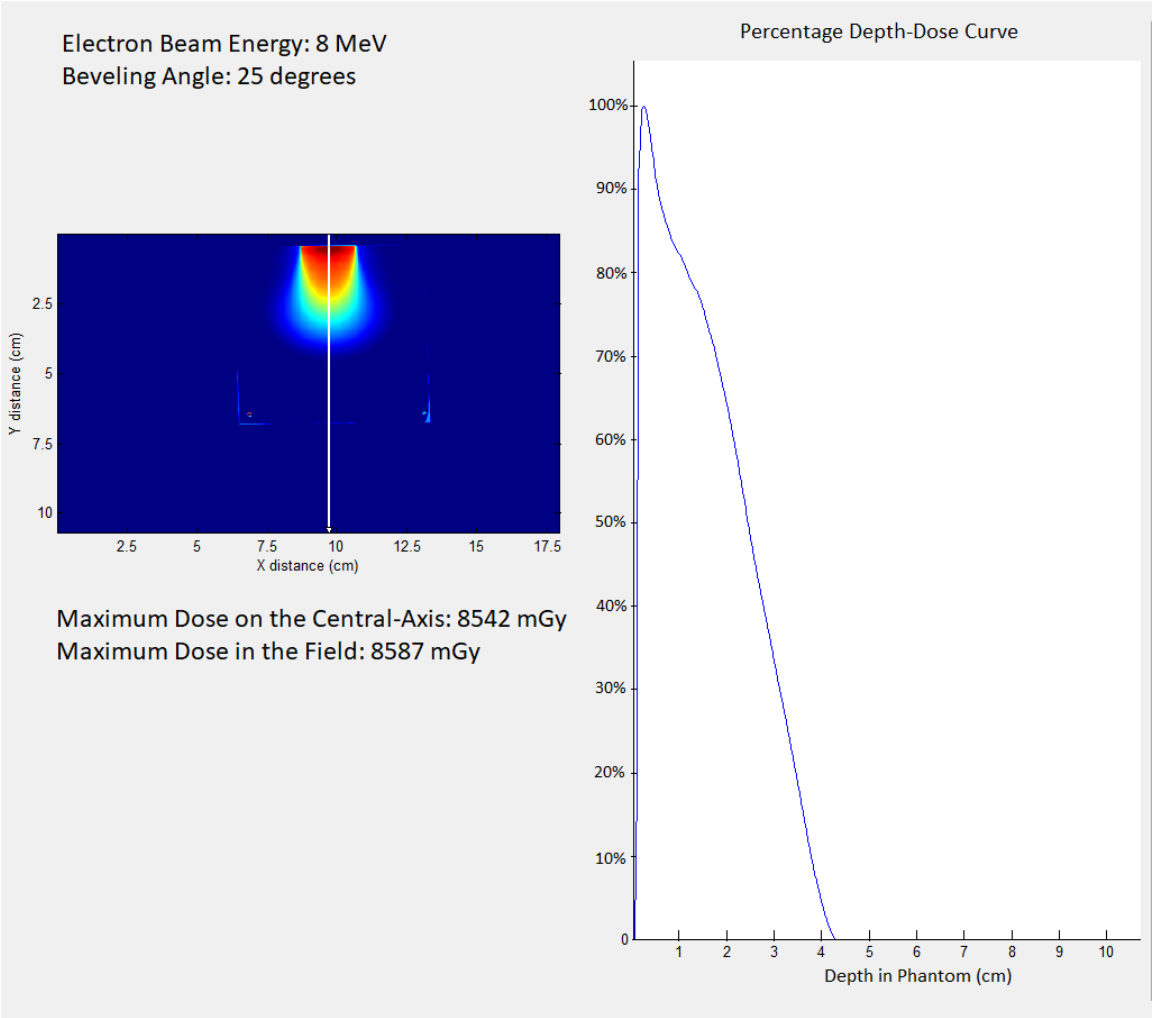

Figure 64. Central-Axis Percentage Depth-Dose Curve for the 25 degree cut out shot with an 8 MeV Electron Beam

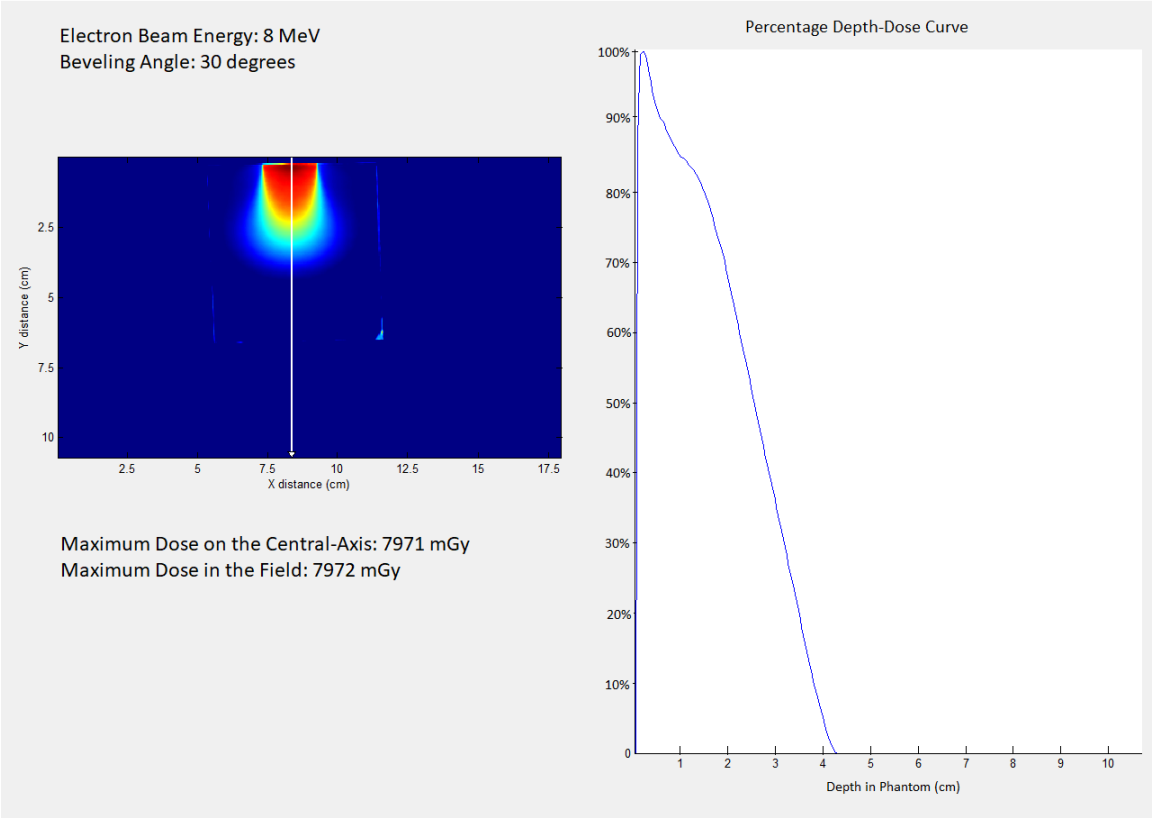

Figure 65. Central-Axis Percentage Depth-Dose Curve for the 30 degree cut out shot with an 8 MeV Electron Beam

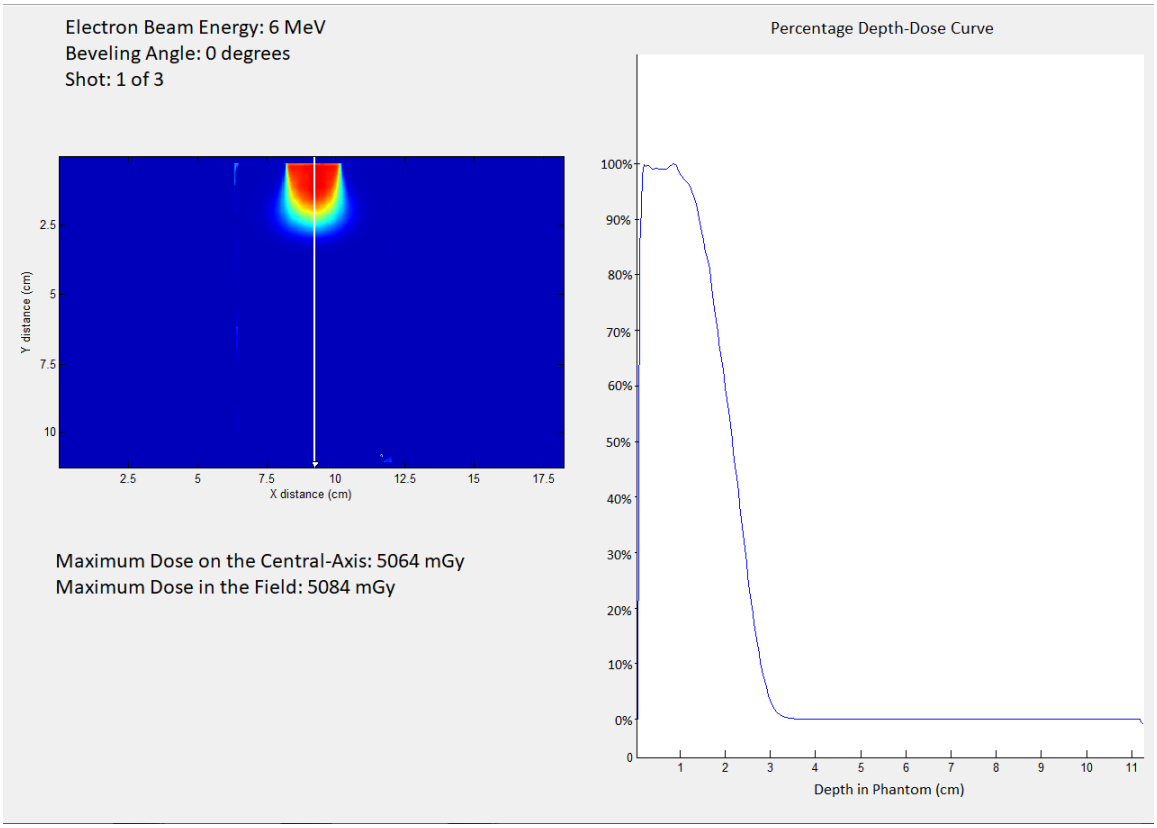

Figure 66. Central-Axis Percentage Depth-Dose Curve for the 0 degree cut out shot with a 6 MeV Electron Beam from the Reproducibility Study (Shot: 1 of 3)

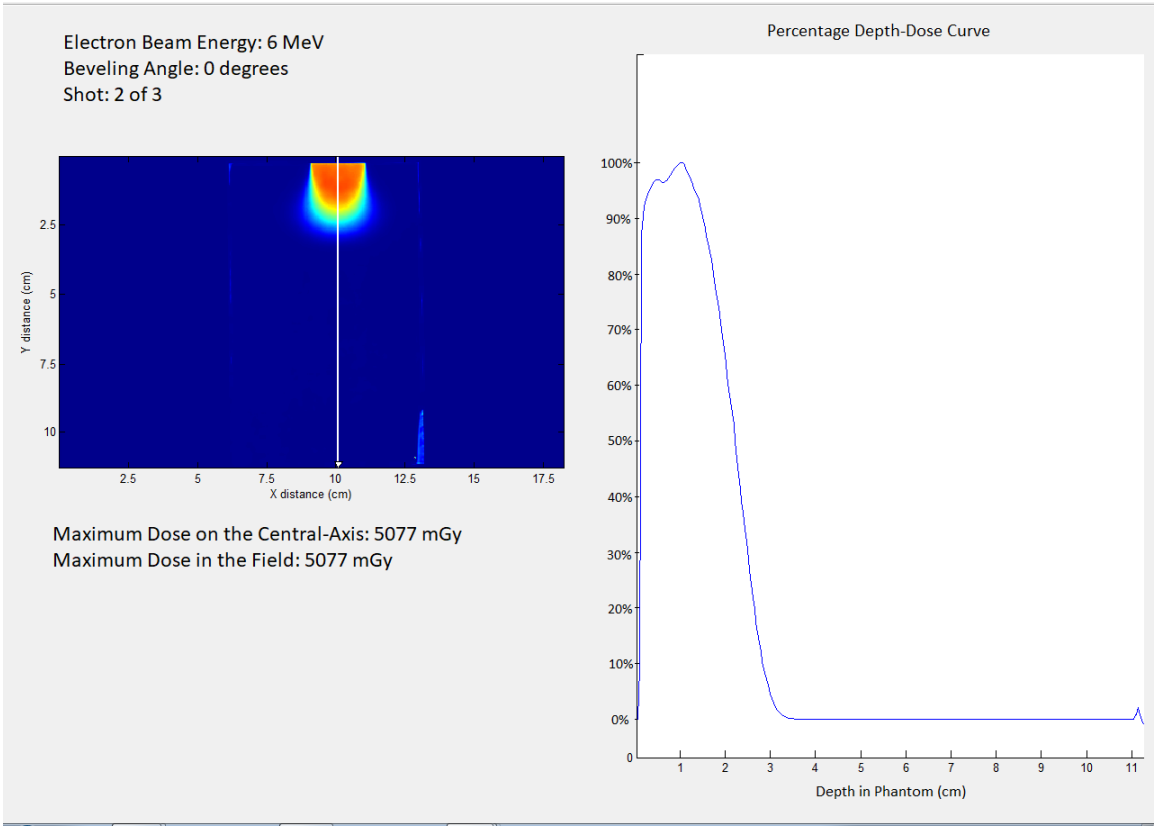

Figure 67. Central-Axis Percentage Depth-Dose Curve for the 0 degree cut out shot with a 6 MeV Electron Beam from the Reproducibility Study (Shot: 2 of 3)

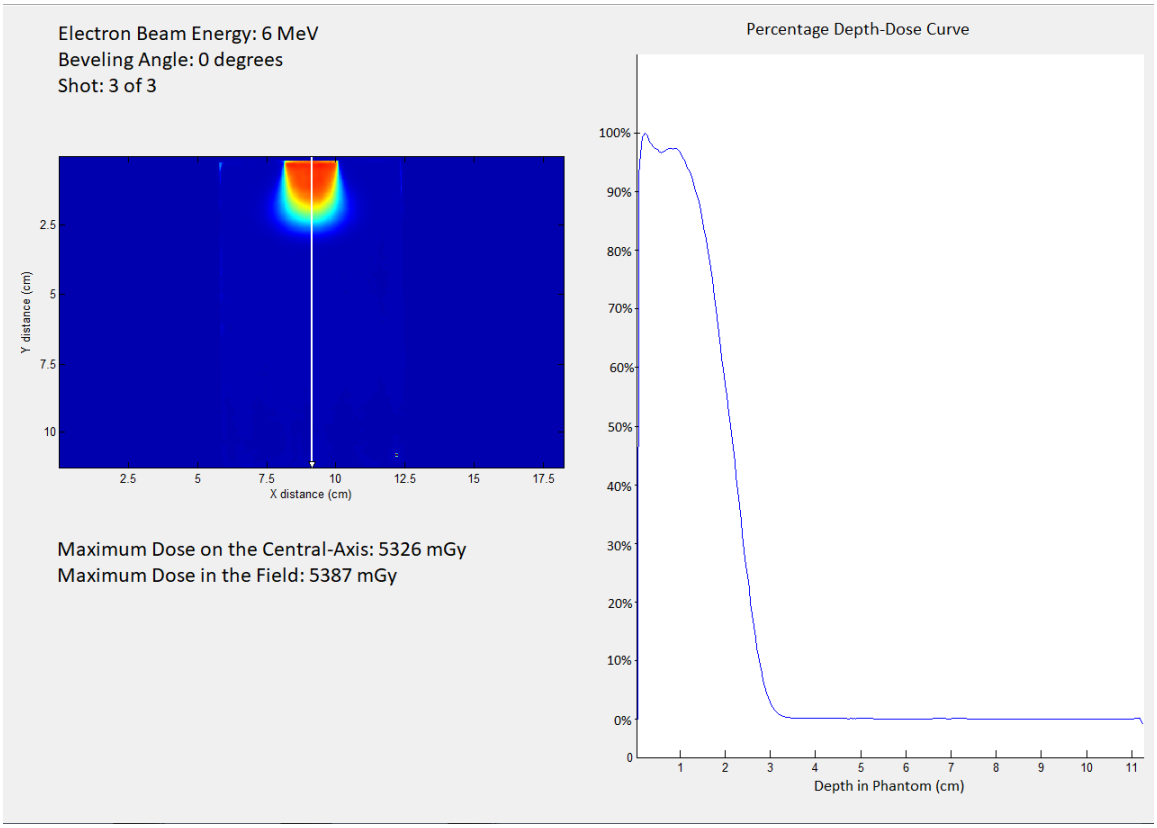

Figure 68. Central-Axis Percentage Depth-Dose Curve for the 0 degree cut out shot with a 6 MeV Electron Beam from the Reproducibility Study (Shot: 3 of 3)

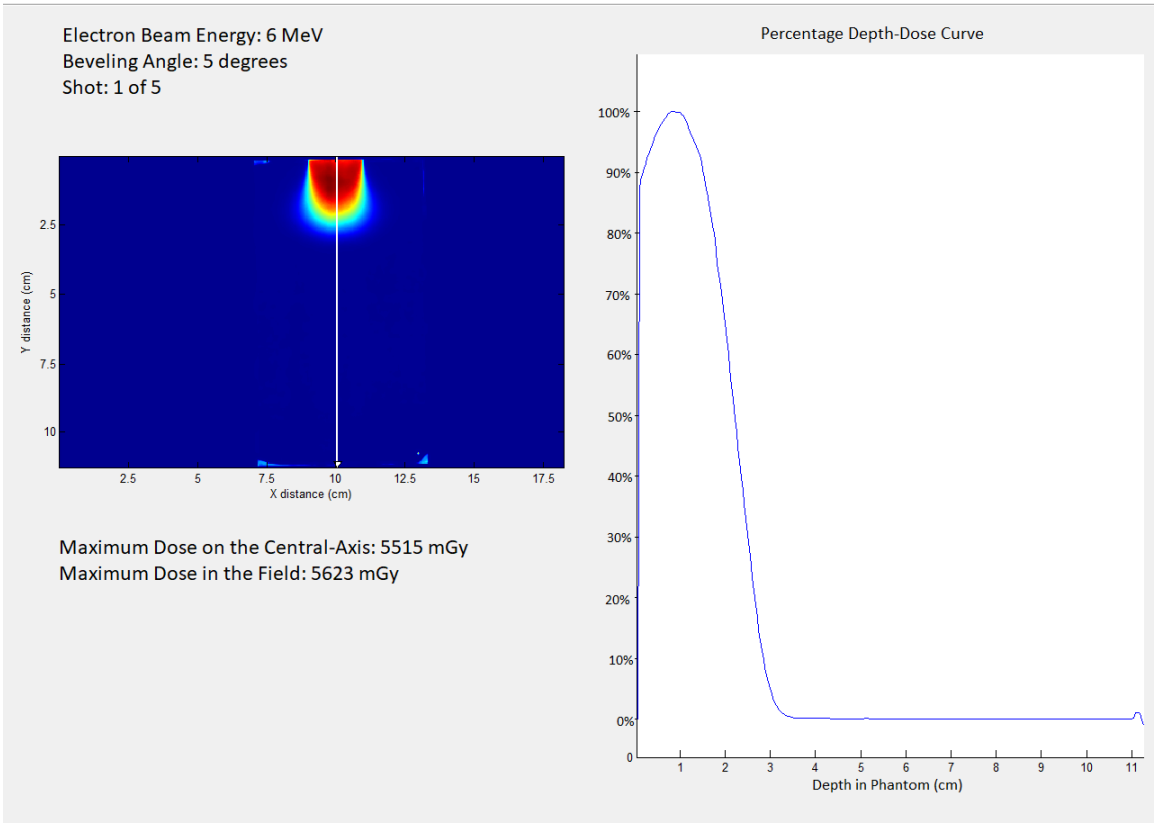

Figure 69. Central-Axis Percentage Depth-Dose Curve for the 5 degree cut out shot with a 6 MeV Electron Beam from the Reproducibility Study (Shot: 1 of 5)

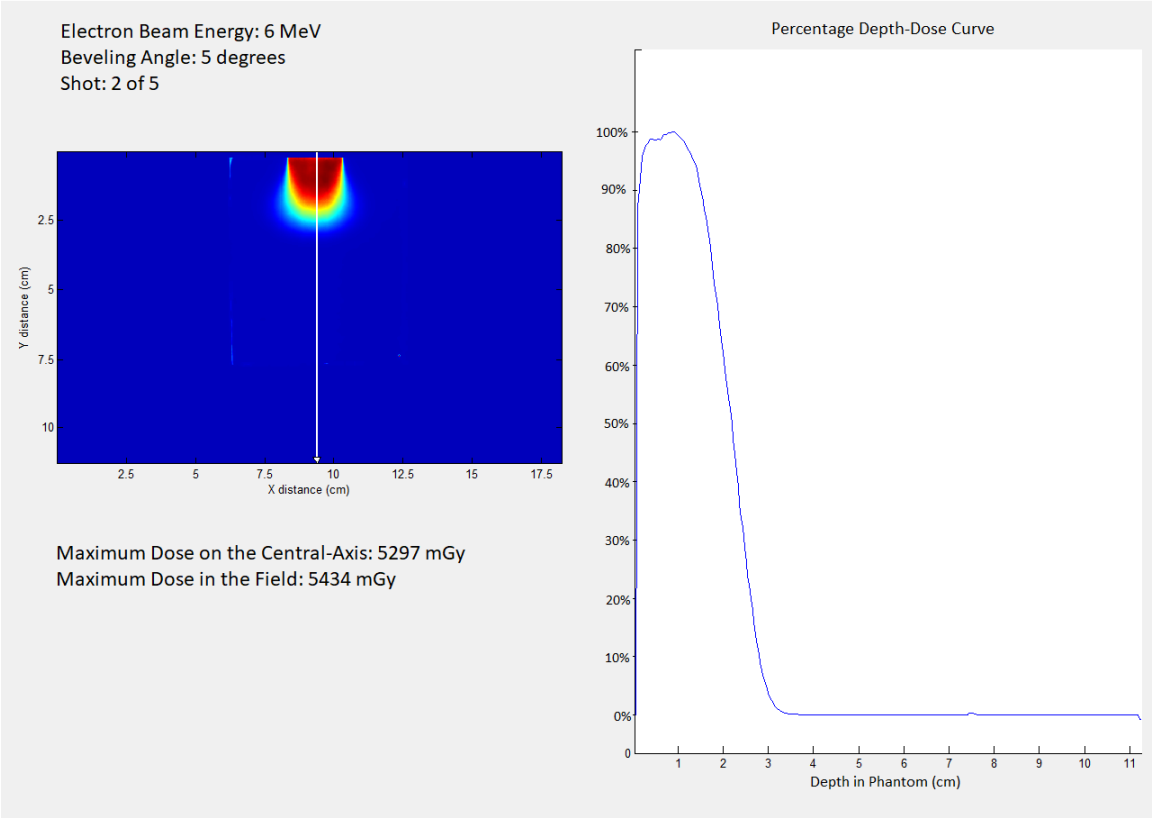

Figure 70. Central-Axis Percentage Depth-Dose Curve for the 5 degree cut out shot with a 6 MeV Electron Beam from the Reproducibility Study (Shot: 2 of 5)

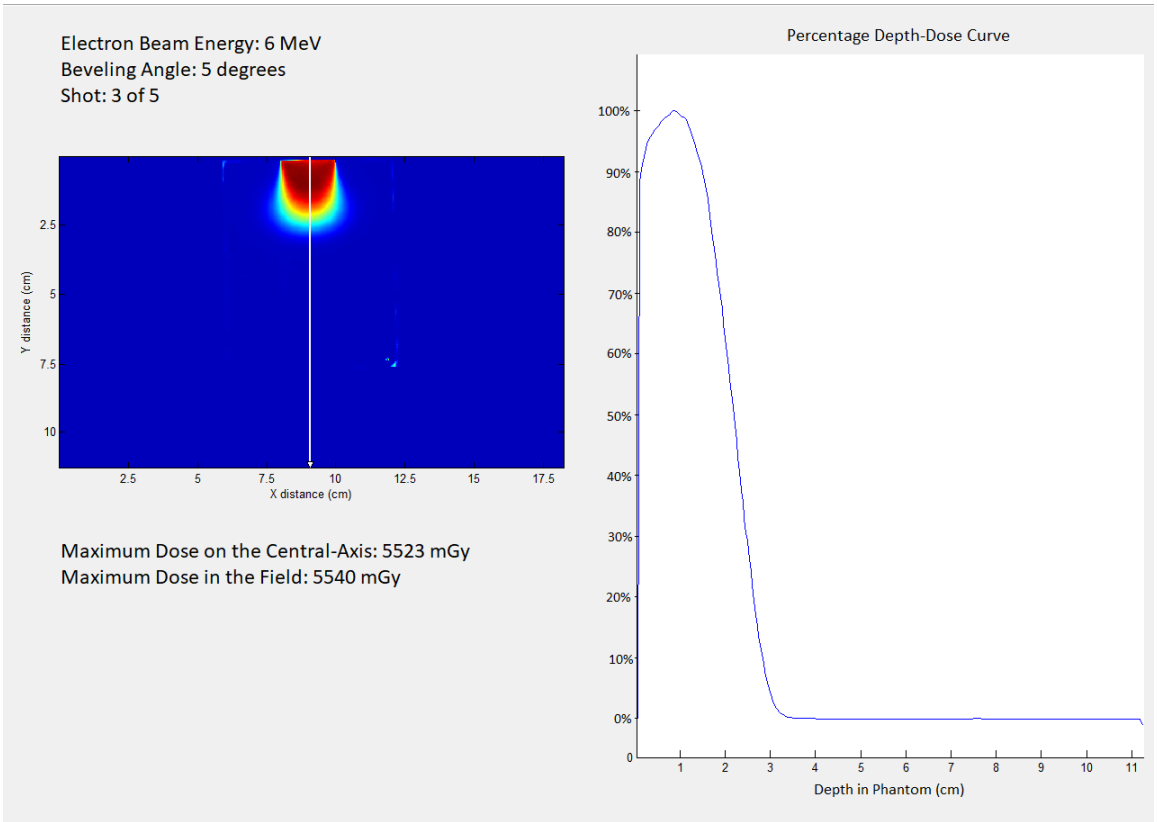

Figure 71. Central-Axis Percentage Depth-Dose Curve for the 5 degree cut out shot with a 6 MeV Electron Beam from the Reproducibility Study (Shot: 3 of 5)

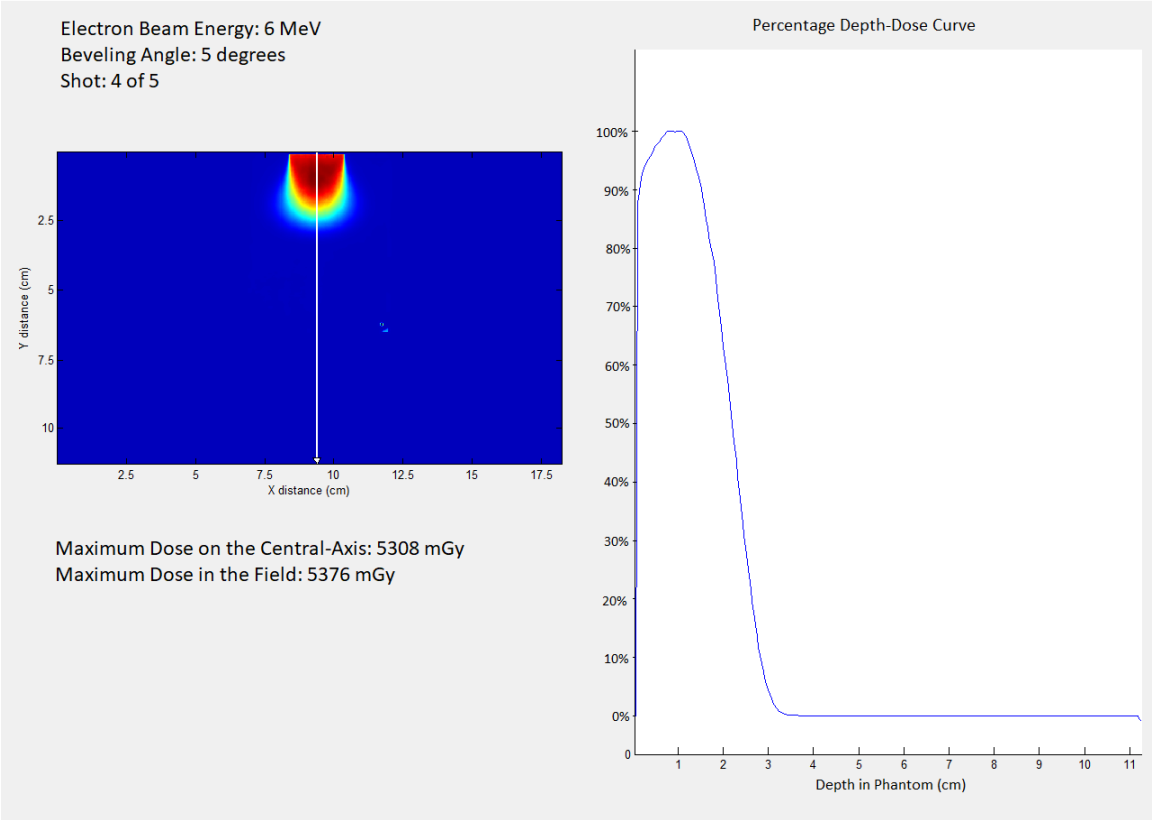

Figure 72. Central-Axis Percentage Depth-Dose Curve for the 5 degree cut out shot with a 6 MeV Electron Beam from the Reproducibility Study (Shot: 4 of 5)

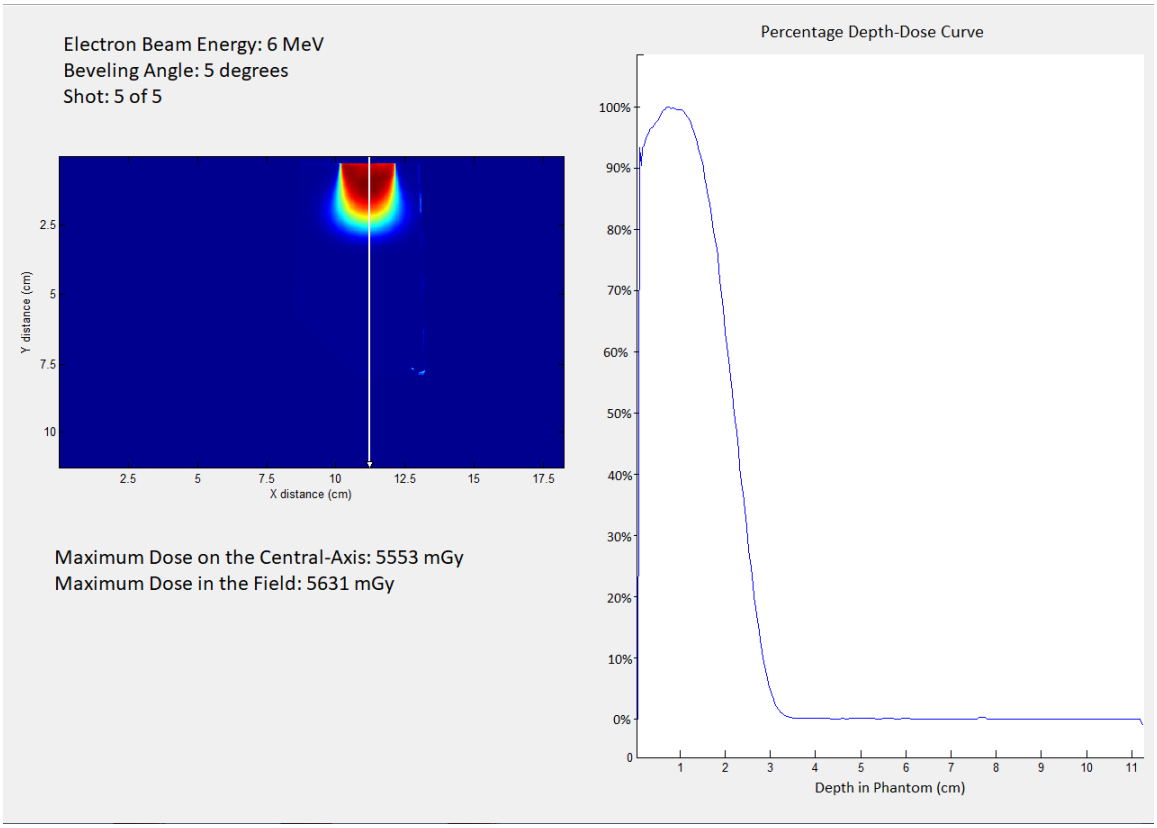

Figure 73. Central-Axis Percentage Depth-Dose Curve for the 5 degree cut out shot with a 6 MeV Electron Beam from the Reproducibility Study (Shot: 5 of 5)

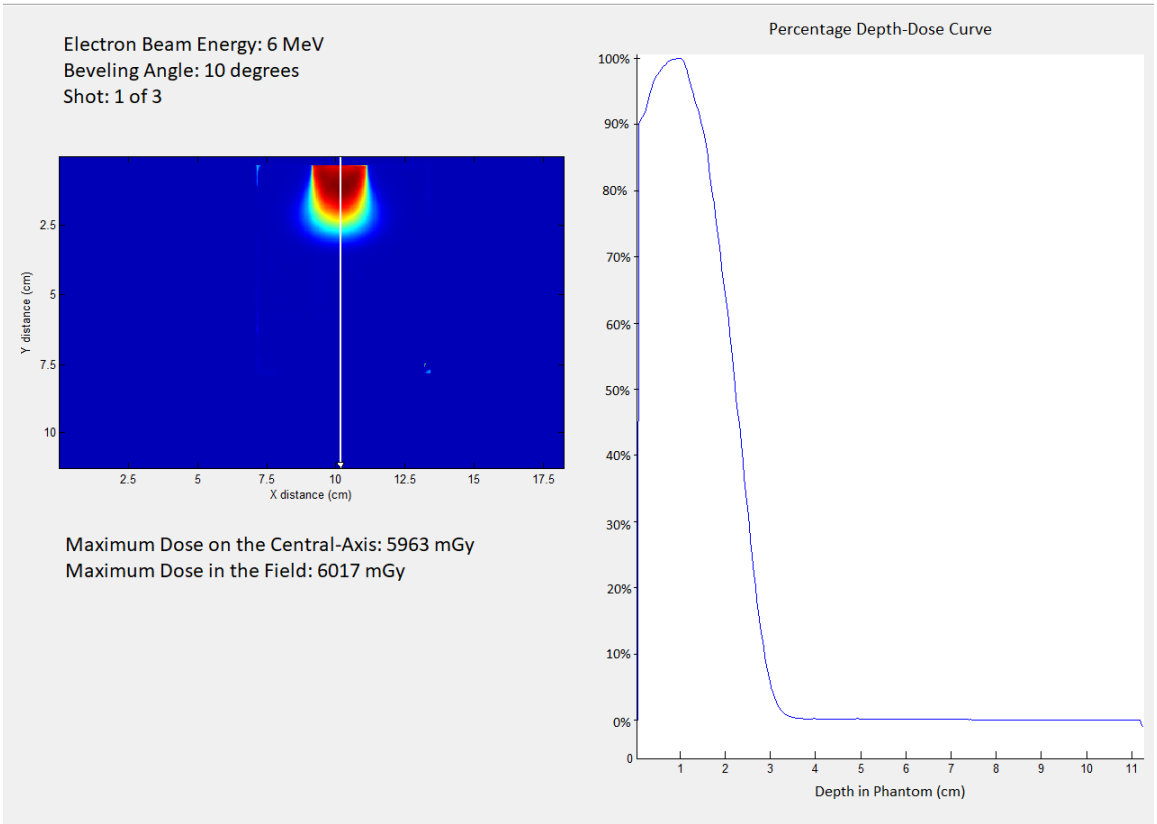

Figure 74. Central-Axis Percentage Depth-Dose Curve for the 10 degree cut out shot with a 6 MeV Electron Beam from the Reproducibility Study (Shot: 1 of 3)

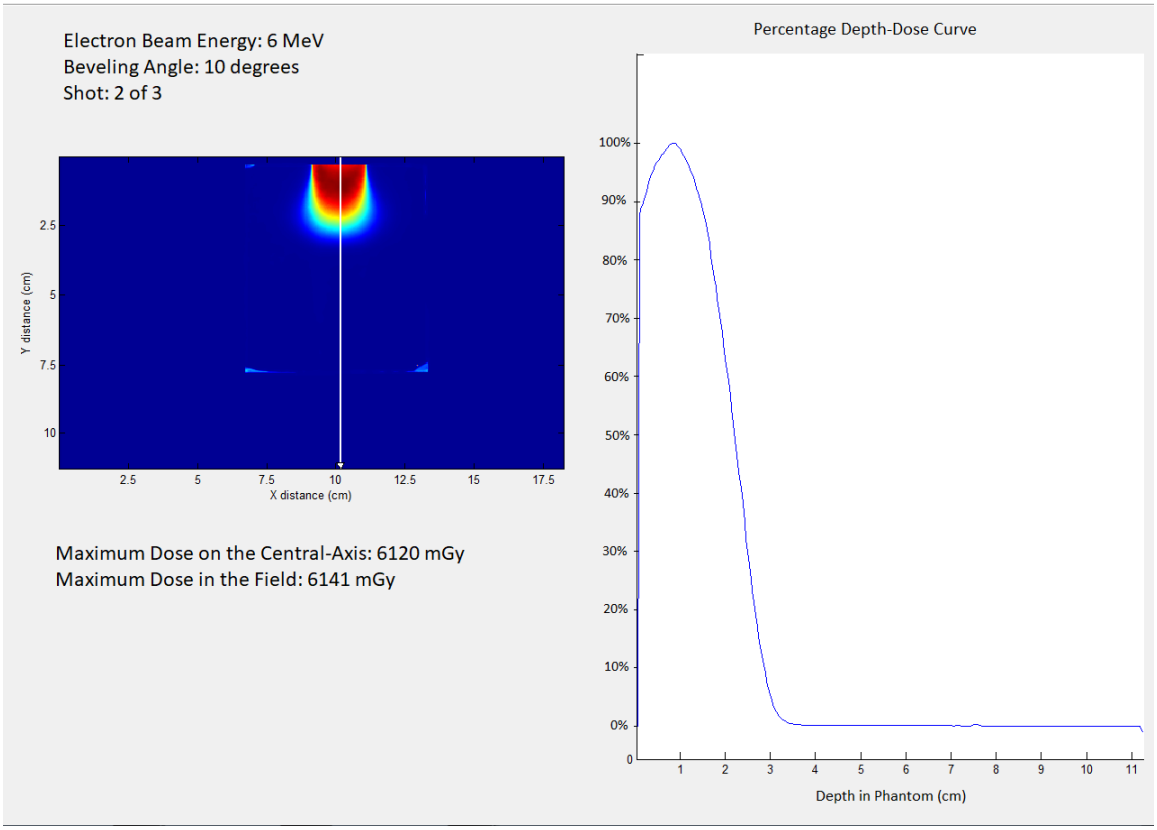

Figure 75. Central-Axis Percentage Depth-Dose Curve for the 10 degree cut out shot with a 6 MeV Electron Beam from the Reproducibility Study (Shot: 2 of 3)

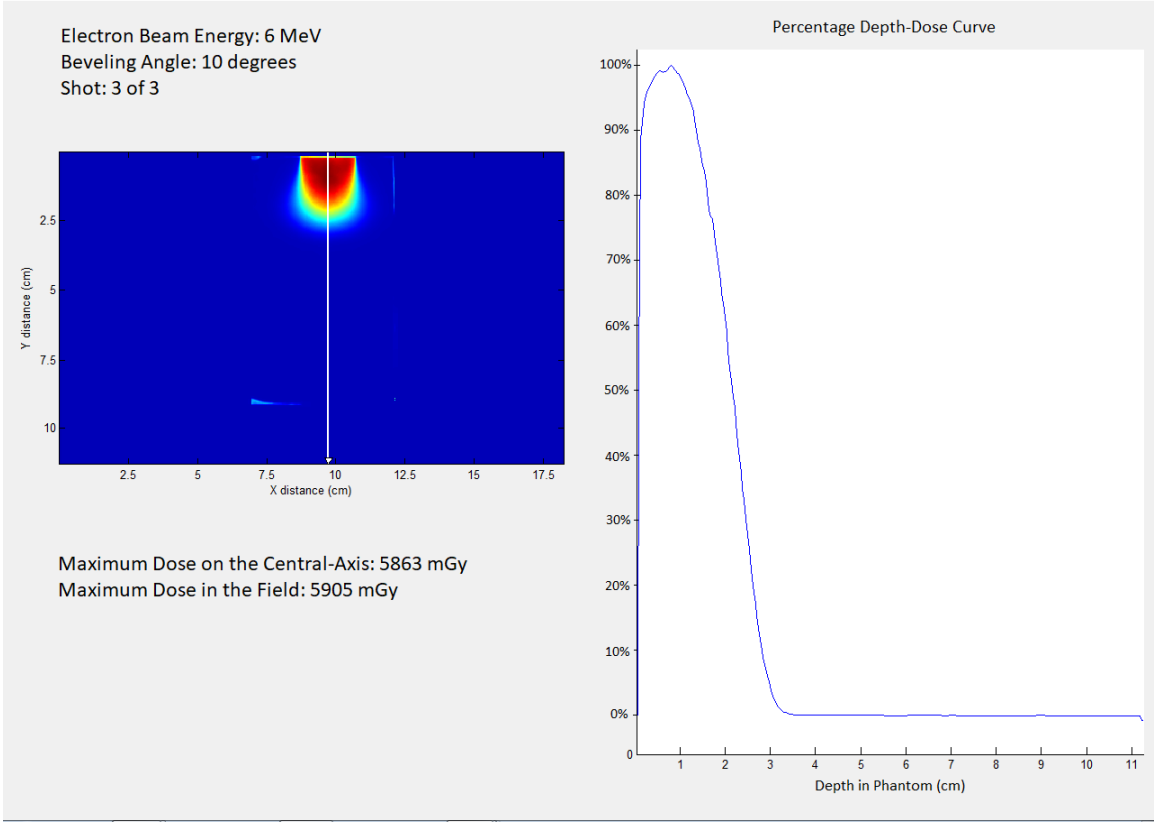

Figure 76. Central-Axis Percentage Depth-Dose Curve for the 10 degree cut out shot with a 6 MeV Electron Beam from the Reproducibility Study (Shot: 3 of 3)

Appendix C

Appendix C contains the diameter of the prescription field, or 90% maximum line, as a function of depth in water equivalent material. These have been calculated for the 6 MeV fields with 17.5 and 22.5 degree beveling angles. The 6 MeV shot of the 20 degree cut out contain major artifacts and could not be calculated. The 25 and 30 degree cut outs shot with the 6 MeV electron beam had a prescription region too thin for calculation. The same was true for the 8 MeV shots with beveling angles greater than 20 degrees.

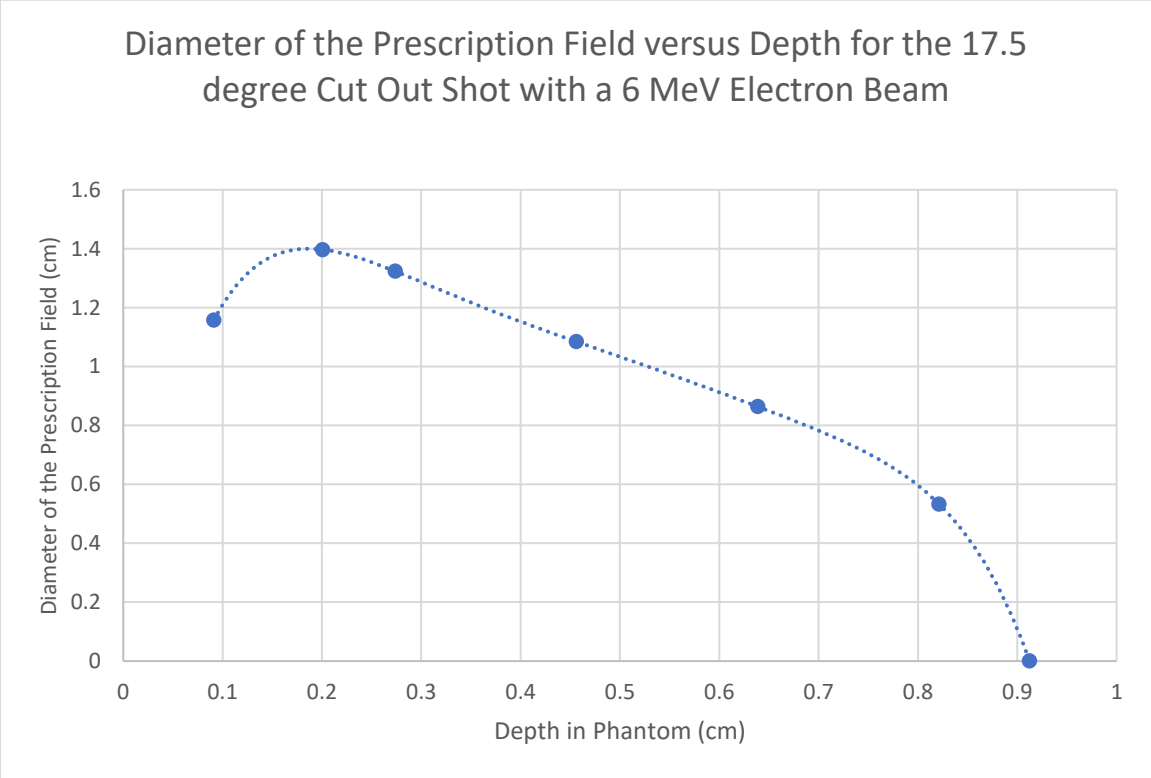

Figure 77. Diameter of the Prescription Field as a Function of Depth for the 17.5 Degree Cut Out shot with a 6 MeV Electron Beam

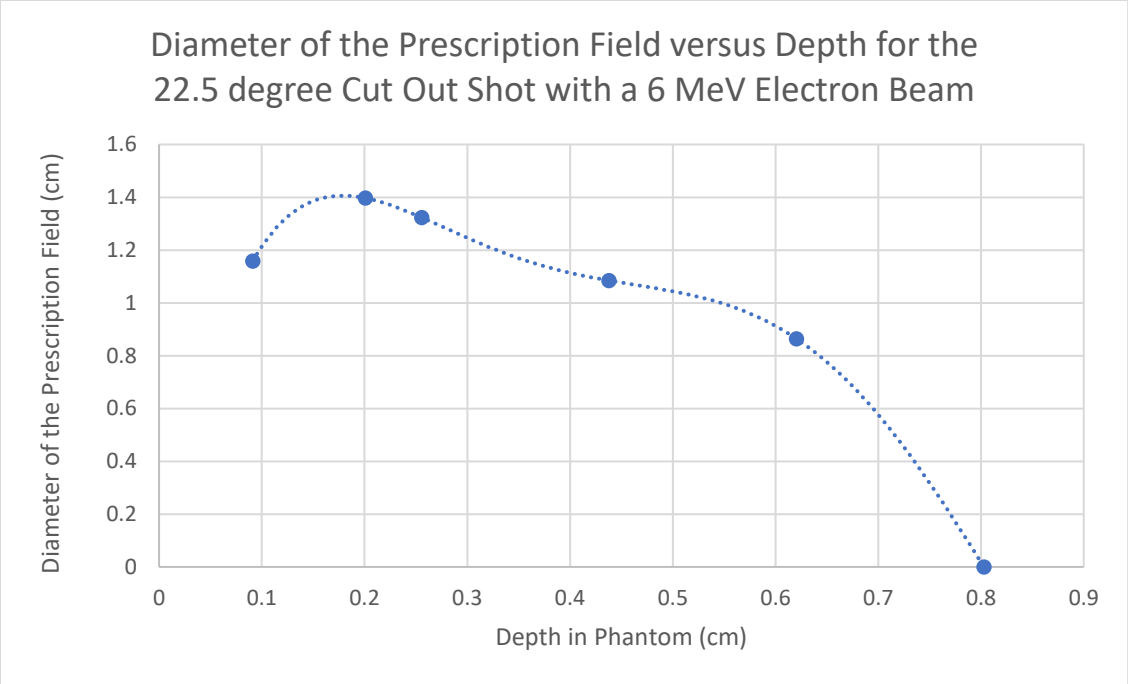

Figure 78. Diameter of the Prescription Field as a Function of Depth for the 22.5 Degree Cut Out shot with a 6 MeV Electron Beam

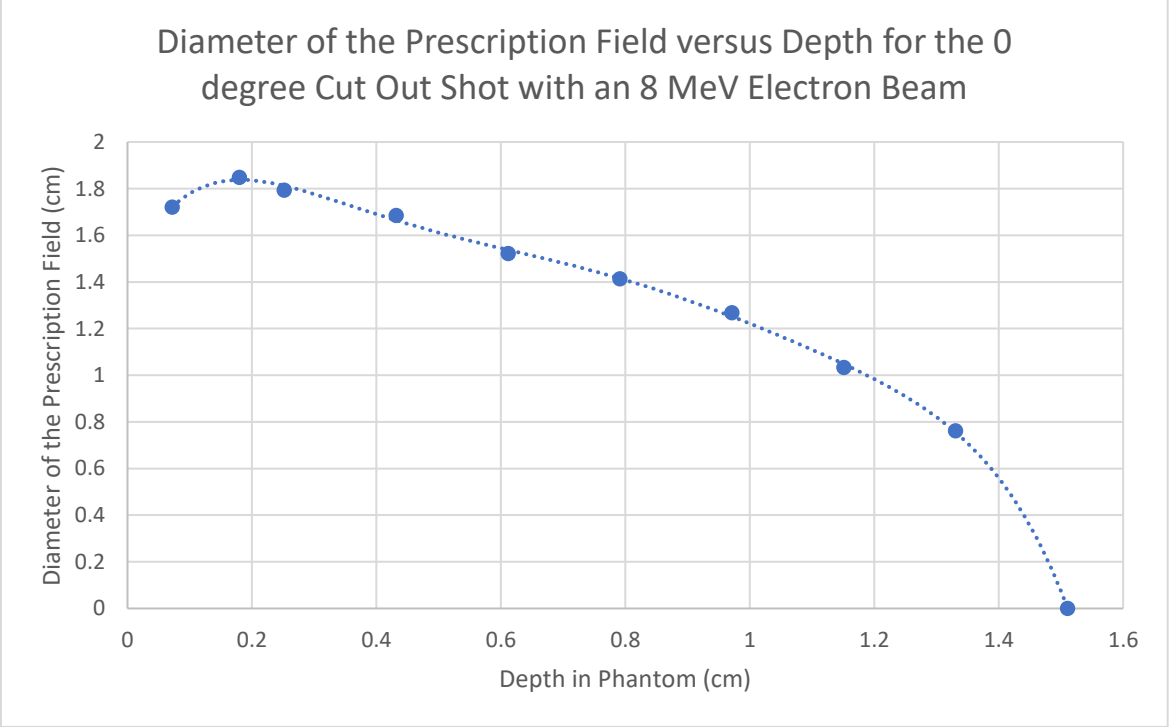

Figure 79. Diameter of the Prescription Field as a Function of Depth for the 0 Degree Cut Out shot with an 8 MeV Electron Beam

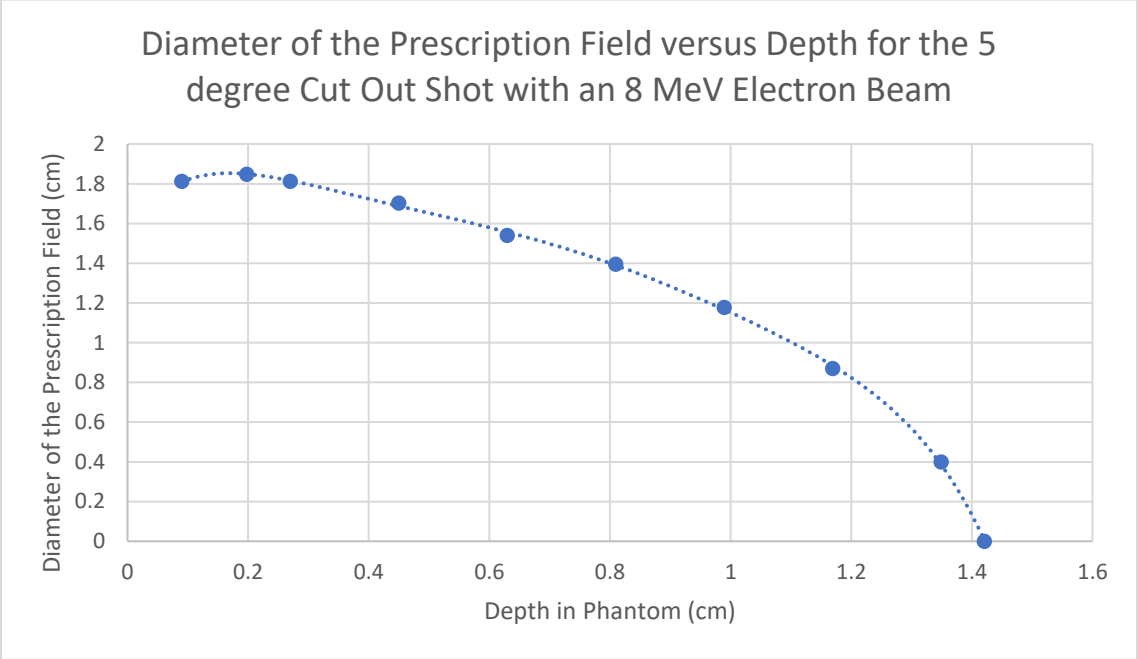

Figure 80. Diameter of the Prescription Field as a Function of Depth for the 5 Degree Cut Out shot with an 8 MeV Electron Beam

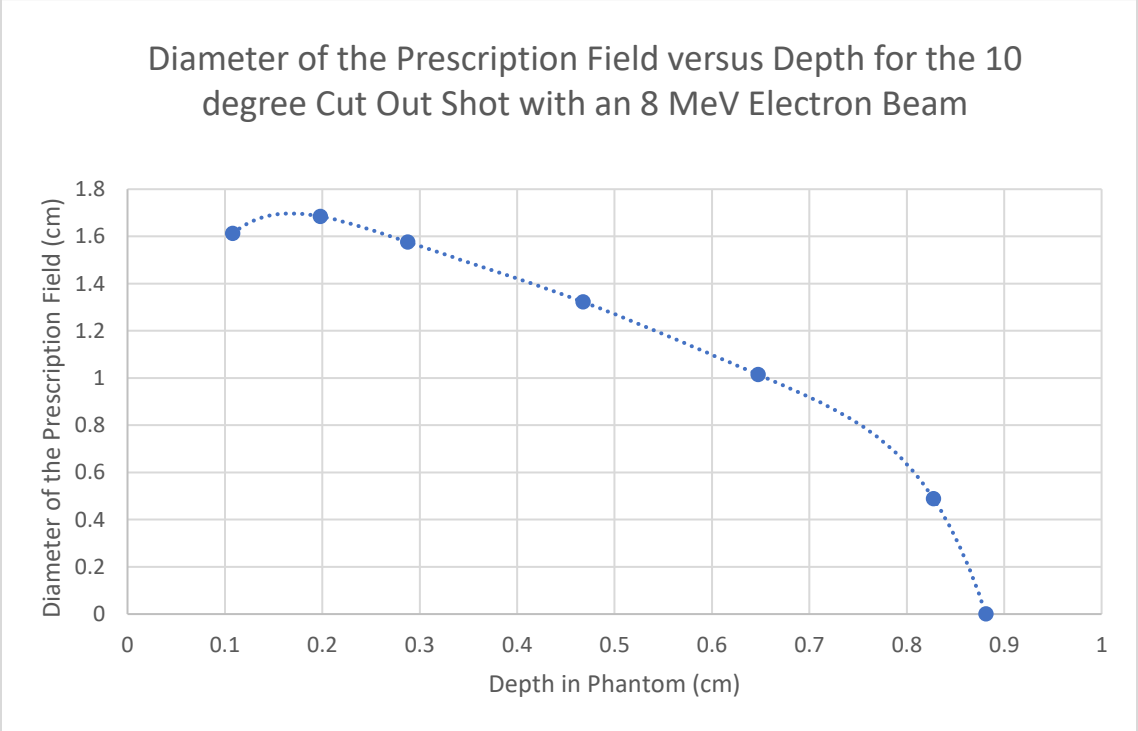

Figure 81. Diameter of the Prescription Field as a Function of Depth for the 10 Degree Cut Out Shot with an 8 MeV Electron Beam

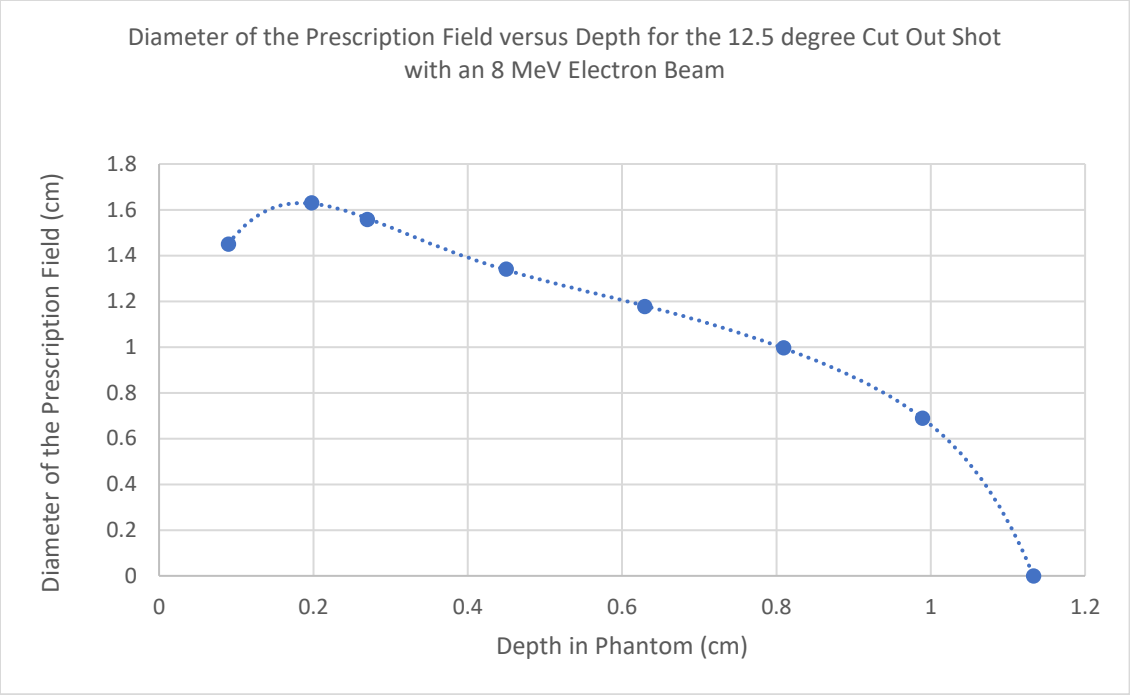

Figure 82. Diameter of the Prescription Field as a Function of Depth for the 12.5 Degree Cut Out Shot with an 8 MeV Electron Beam

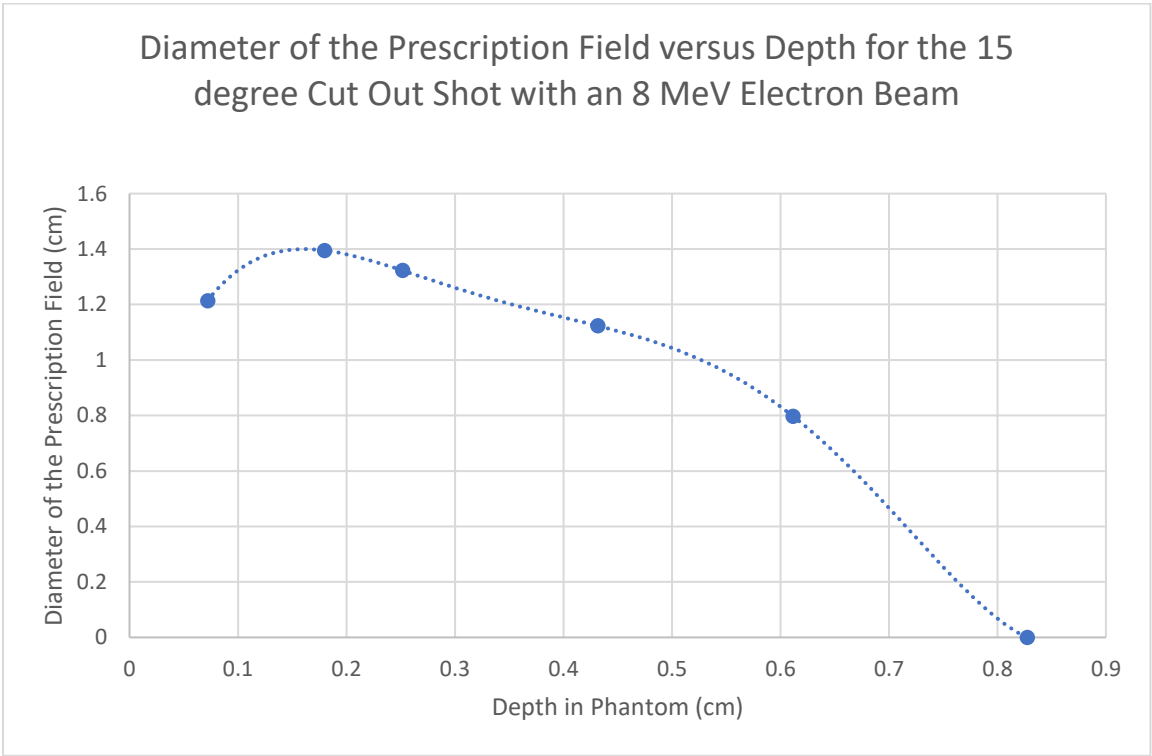

Figure 83. Diameter of the Prescription Field as a Function of Depth for the 15 Degree Cut Out Shot with an 8 MeV Electron Beam

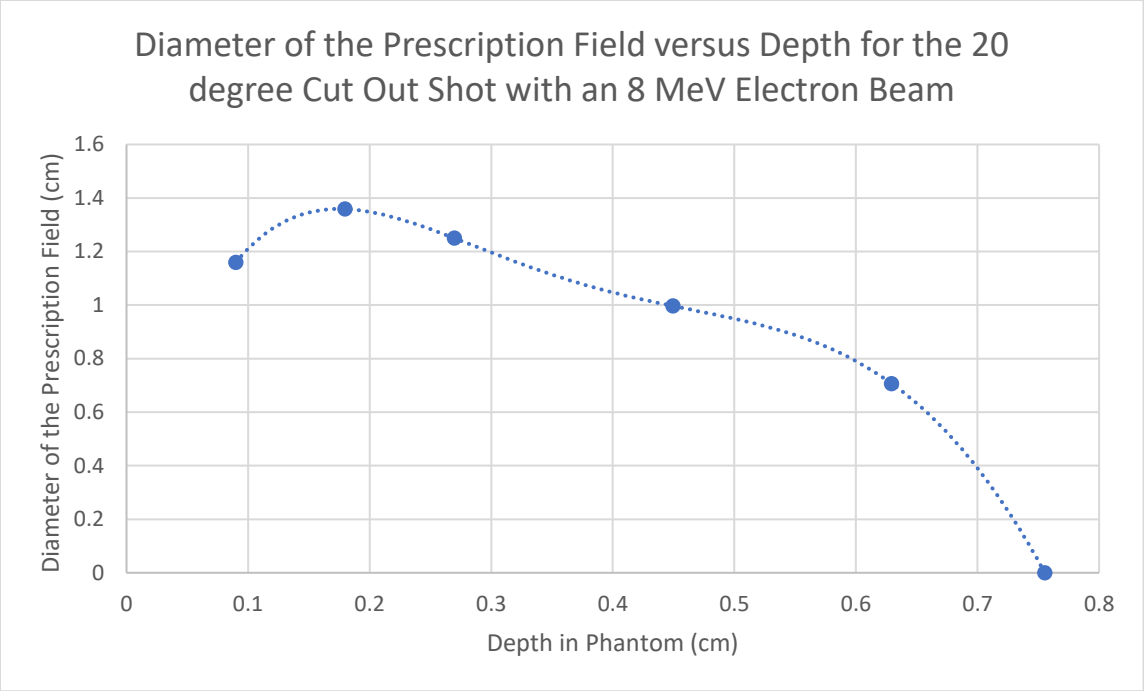

Figure 84. Diameter of the Prescription Field as a Function of Depth for the 20 Degree Cut Out Shot with an 8 MeV Electron Beam